Design and Fabrication of a Label-free LC3 Immunosensor towards the Estimation of Autophagy Flux

by

Ruan de Jager

Thesis presented in partial fulfilment of the requirements for the degree of Master of Engineering (Electronic) in the Faculty of Engineering at Stellenbosch University

Supervisor: Prof. W.J. Perold

Co-supervisor: Prof. B. Loos

March 2021

Declaration

By submitting this thesis electronically, I declare that the entirety of the work contained therein is my own, original work, that I am the sole author thereof (save to the extent explicitly otherwise stated), that reproduction and publication thereof by Stellenbosch University will not infringe any third party rights and that I have not previously in its entirety or in part submitted it for obtaining any qualification.

Date: 2020/11/21 .....

Abstract

Design and Fabrication of a Label-free LC3 Immunosensor towards the Estimation of Autophagy Flux

R.G. de Jager

Department of Electrical and Electronical Engineering,
University of Stellenbosch,
Private Bag X1, Matieland 7602, South Africa.

Thesis: MEng (E)

December 2021

In 2016 professor Yoshinori Oshumi proved that autophagy is dysfunctional in neurodegenerative diseases such as Alzheimer's, enhanced in various cancers and progressively declining in ageing. Autophagy also relates to metabolic disorder, infectious and general degenerative diseases, and is a critical factor in the development of diseases relating to an increase in cancer risk. The ability to monitor autophagy has become key interest in the bio-tech industry and is also an excellent indication of a person's overall health, however to monitor and determine autophagy flux remains a challenge.

LC3 protein is a proven biomarker that directly relates to the rate of autophagic activity and accumulates as autophagosomes are formed. With an increase and decrease in the rate of autophagy the concentration of LC3 levels will alternate and is an excellent estimate towards determining autophagy flux.

For this project different biosensing techniques were explored for LC3 detection with an electrochemical biosensor chosen to be most applicable due to its robustness and selectivity towards proteins. The goal towards a proof of concept utilised commercially manufactured carbon nanofibre screen printed electrodes by Dropsens that were modified in development of an immunosensor. For antibody crosslinking, the sensors were electrografted using a diazonium salt mixture to form carboxyl support groups followed by the activation of these groups using EDC/NHS activation chemistry. The antibody bindings were verified with fluorescent microscopy by attaching a secondary antibody. Square wave voltammetry was use as method of detection due to its simplicity as well as the method generating absolute data for comparison. All square wave voltammetry experiments were executed in 5 mM ferricyanide redox couple.

The functionality of the sensors were tested by performing a full scale test over a wide range of different protein concentrations. The work done was successful towards a proof of concept sensor for LC3 detection, with an increase in protein bindings observed over the tested range and space for optimisation to increase sensitivity and accuracy.

Uittreksel

Ontwerp van 'n LC3-II Immunosensor in die rigting van 'n Autofagie Vloed Lesing

("Design and Fabrication of a Label-free LC3 Immunosensor towards the Estimation of Autophagy Flux")

R.G. de Jager

Departement Elektries en Elektronies Ingenieurswese,
Universiteit van Stellenbosch,
Privaatsak X1, Matieland 7602, Suid Afrika.

Tesis: MIng (E)

Desember 2021

In 2016 het professor Yoshinori Oshumi bewys dat autofagie disfunksioneel in neurodegeneratiewe siektes is soos byvoorbeeld Alzheimer's, versterk is in 'n verskeindenheid kankers en geleidelik afnemend in veroudering is. Autofagie het ook verband met metaboliese agteruitgang en aansteeklik asook algehele degeneratiewe siektes, en speel 'n kritiese rol in die ontwikkeling van siektes wat in verband met kanker risiko is. Die bepaling en monitering van autofagie se aanvraag het vermeerder maar bly tans 'n groot uitdaging.

LC3 proteïn is 'n bewysde biomerker vir autofagie en staan in direkte verband met autofagie vloed waar die versameling van die proteïn verwys na die ontwikkeling van 'n outofagosome. 'n Vermeerdering en vermindering in autofagie vloed sal 'n verhoging en verlaaging in LC3 voortbring.

'n Elektrochemiese biosensor was mees van toepasing op gevolg van die literatuur studie omdat dit robuust en selektief op proteïne is. Die hoof konsep begrip is bewys deur gebruik te maak van kommersiele vervaardigde koolstof nanovesel elektrodes en dit deur prosesse te plaas namens die ontwikkeling van 'n immunosensor. Vir teenligaampie kruis koppeling was die sensors ge-electrograft met 'n diazonium sout mengsel om karboksiele groepe te vorm en is geaktiveer deur gebruik te maak van EDC/NHS kruis koppeling chemie. Fluoresserende mikroskopie was gebruik om die bindings te verifieer deur 'n sekondêre teenligaampie te bind. Blok golf voltammetrie was gebruik as die hoof metings metode en is uitgevoer in 5 mM ferricyanide.

Die sensor se funksionaliteit was getoets deur 'n volskaalse toets uit te voer en sy werking oor a wye spektrum van konsentrasies se evalueer. Die ontwikkeling van 'n bewys van konsep begrip was suksesvol waar 'n vermeerdering in konsentrasie waargeneem is op die geproduseerde data, met baie spasie vir optimeering om die sensor se sensitiwiteit en akuraatheid te verbeter.

Acknowledgements

I would like to express my sincere gratitude towards...

God, for in Him I find all my strength.

My Mom, Dad and Brother for making it all possible as well as their relentless motivation.

My second family, the du Plessis', for all their support and kindness.

Prof Perold and Prof Loos for their guidance as supervisors.

Dr. André du Toit for his assistance in the lab and sharing his physiological knowledge.

All my friends for believing in me.

Contents

List of Figures

List of Tables

Nomenclature

Constants

$\pi =$ 3.141592654
F = 96485.33289
R = 8.3144598

Variables

V_{cell}	Cell potential	[V]
V_w	Working electrode potential	[V]
V_r	Reference electrode potential	[V]
V_i	Input voltage	[V]
I_{cell}	Cell current	[A]
E	Applied cell potential	[V]
E^0	Standard potential	[V]
E_{pa}	Anodic peak potential	[V]
E_{pc}	Cathodic peak potential	[V]
$E^{0,}$	Formal potential	[V]
Δi_p	Differential peak current	[A]
t_p	Pulse width	[s]
f	Frequency	[Hz]

Abbreviations

Atg	Autophagy related protein
LC3	Microtubule-associated proteins 1A/1B light chain 3B
SWV	Square wave voltammetry
CV	Cyclic voltammetry
ELISA	Enzyme-linked immunosorbent assay
EIS	Microtubule-associated proteins 1A/1B light chain 3B
WE	Working electrode
RE	Reference electrode
CE	Counter electrode
PBS	Phosphate buffer saline
SMN	Survival motor neuron
CNF	Carbon nanofibre
NHS	N-hydroxysuccinimide
EDC	N-(3-Dimethylaminopropyl)-N-ethylcarbodiimide hydrochloride
Tris	Tris(hydroxymethyl)aminomethane
GPHOX	Graphene oxide

Chapter 1

Introduction

1.1 Background

The discovery of the intracellular protein degradation process termed 'Autophagy' (Greek, self-eating) has gained tremendous attention in the biomedical research arena, which was crowned by the Nobel Prize awarded to Prof Yoshinori Oshumi, Tokyo University, Japan, 2016 [1]. It has now become clear that autophagy is dysfunctional in neurodegenerative diseases, such as Alzheimer's disease, strongly enhanced in many cancers, and progressively declining in ageing [2; 3].

Autophagy advances the strength of cells and is crucial for the development, separation, and maintenance of cell function and for the host safeguard against pathogens. Deregulation of autophagy is connected to the vulnerability of different issues including degenerative diseases, metabolic disorder, ageing, infectious diseases, and cancer. Autophagic activity becomes a critical factor in the development and movement of diseases relating to increased cancer risk as well as in separate stages of cancer [4].

Given that cancer is an intricate process and autophagy applies its effects in numerous manners, the job of autophagy in tumorigenesis is setting subordinate. As a cytoprotective endurance pathway, autophagy prevents chronic tissue damage that can prompt cancer growth commencement and progression. In this setting, incitement or reclamation of autophagy may prevent disease. Conversely, when cancer growth begins, numerous disease cells enhance basal autophagy and uses autophagy to improve and get by in the hostile tumour microenvironment. These discoveries uncovered the idea that aggressive cancers can be dependent on autophagy for survival [4]. In this setting, autophagy hindrance is a restorative strategy for established cancers.

Due to the increased usage of biometric devices such as smart watches people have become more aware of their overall health. These devices are capable of reading a myriad of different biometrics which through advanced models can estimate various health statistics. Monitoring one's health statistics has become more popular as it helps improve fitness, monitor stress, manage sleep and knowing how to balance your active lifestyle and diet. The autophagic process removes damaged cells in order to regenerate newer healthier cells. Autophagy is an evolutionary self-preservation mechanism through which the body can remove the dysfunctional cells and recycle parts of them toward cellular repair and cleaning [5]. Therefore autophagic flux is an excellent indicator of your overall health

and the possibility of a frequent measurement will contribute tremendously towards a health and recovery report.

However, the major challenge remains in the research and clinical arena alike, to measure this process accurately. The basis for measuring autophagosome flux based on fluorescence imaging techniques had been previously established by Loos and Hofmeyr [6] and filed for protection in 2016. However, a device that is able to measure and sense autophagic activity (flux) does not exist.

In 2016/17, our group, together with Prof Loos and Hofmeyr, developed the first Autophagy sensor prototype (South African provisional patent (2018/04374)), a completely novel approach to, in a highly sensitive manner, detect an autophagy flux related key protein. However, in order to assess autophagic activity, multiple selective proteins have to be detected creating a signature for autophagic activity.

1.2 Motivation and Approach

Continuous research on autophagy keeps discovering more physiological processes and systems that relates to autophagic flux activity increasing the demand for a device that can actively screen and monitor the process. An autophagic flux reading can inform specialists about activity in physiological processes which the data can be used for a variety of applications. Some of them could be to develop personalised medication, monitoring cancer and neurodegenerative diseases and an overall health indication.

The uniqueness of our approach is based on the very different and cross-disciplinary approach that enables to quantify and measure a dynamic process, based on a single measurement point, using a flux response protein signature that is electronically detected and converted to an (numerically reported) activity status. This approach is based on the combination of metabolic control analysis (JH Hofmeyr), fluorescence live cell quantitative imaging (B Loos) and electro-textile based biosensors (WJ Perold). Key proteins that the project envisages to detect, have already been identified. Hence, the design of a sensor that can detect and integrate multiple resistance readouts forms part of this project.

Here we aim to move the technology to a fully functional, tested and applied device consisting of

i optimized hardware and sensing electronics, implemented with remaining flux signature proteins

ii optimized software algorithms to interpret and translate the protein signature into autophagic activity,

iii optimized miniaturized design with a sensor cartridge exchange unit that is ready for the market to operate as versatile point of care device.

The deliverable is an autophagometer/biosensor that provides a numerical flux value output that informs the pharmaceutical, health-care and research environment with a standardized autophagic flux measuring solution. Devices for a pharmaceutical industry market as well as point of care miniaturised instruments are envisaged as end goal deliverables.

The autophagometer/autophagy flux biosensor device has significant impact on parameters that contribute to economic impact, competitiveness of biomedical/pharmaceutical/health care industrial sectors as well as major social impact: Due to the three large but related industries (health sector, biomedical and pharmaceutical industry) that would be primary user of the device, major impact on GDP growth and job creation is enabled. The device, using nano-sensor based technology with a software component impacts positively on capacity building and knowledge base.

1.3 Project Scope

The project scope was to use a biomarker that relates to the autophagic process and develop a biosensor for marker detection towards the estimation of autophagy flux. An appropriate biomarker was provided by the physiology department of Stellenbosch University with the goal to detect it in a complex physiological solution such as plasma extracted from whole blood. Theory states that an increase in autophagy flux will result in an increased accumulation of biomarker levels. The developed biosensor should ultimately be a disposable sensor that plugs into an electronic device that performs measurements to determine autophagy flux levels. The measuring device should produce data that a developed software algorithm processes to extract relevant information to identify marker concentration. The final goal of the sensor is to be a mobile complete device capable of being autophagy estimation in under resourced environments.

1.4 Thesis Outline

This thesis explores two main concepts towards marker detection namely the methods of modification for biosensor development as well as methods of performing measurements on the developed biosensor.

The complex process of autophagy is studied first to understand the physiological working of different intricate mechanisms to allow the use of efficient methods during sensor development. The chosen biomarker was reviewed to gain knowledge on its role in the autophagic system to determine how the detection of markers can be utilised towards an autophagy flux reading. Current methods for determining autophagy flux are explored and compared to show the need of a robust point-of-care device. Furthermore various different biosensing techniques are studied to determine which would suite the detection of an autophagic biomarker best and fits the requirements specified. The study takes a look at different biosensing methods, measurement techniques as well as measuring devices. A potentiostat is required for performing voltammetric modification and measurements, where to different industry grade commercial potentiostats are studied and compared to show how the device's specifications would effect the electronic sensing system. Based on the literature review a sensing technique is chosen as well as an accompanying measuring technique. The literature review was followed by a detailed discussion of the methodology for sensor development. It explains how the sensors were characterised, modified and verified with an in depth discussion on the results found as well as the interoperation thereof. The success of the developed biosensor is discussed in the last chapter as well as recommendation for improvement and further development.

Chapter 2

Literature Study

An extensive literature study was done to recall the research done in the field of autophagy and its far-reaching fields. The discussion would be on the content gathered regarding this topic as well as recommended methods of determining autophagic flux. The method analysed for determining autophagy flux builds on prior scientific research.

Neurodegenerative diseases such as Alzheimer's, Parkinson's and cancer occurs more often and there is therefore a need to develop technologies to target this tragic health problem in a world with an ageing population. Neurodegeneration results in impaired autophagy in humans with no means at this point in time to quantitatively analyse this crucial system and substances that are known to regulate autophagy cannot be accurately screened.

Currently no technology exists that can adequately measure autophagic flux. The purpose of this research is aiming towards developing a technology that utilises specific proteins to quantify autophagic flux data through the use of sensing hardware and software analyses.

2.1 Autophagy

Autophagy is an exceptionally powerful metabolic process whereby a cell digests parts of itself, thus the origin of its name autophagy from the Greek auto meaning 'self' and phagen meaning to 'eat'[6]. The autophagic process is an evolutionary procedure where cytoplasmic material is engulfed in a double membrane vesicle which when fusing with a lysosome initiates cellular degradation [7].

Autophagy is a standard physiological process which is responsible for cellular protein degradation in the body. This process is responsible for the recycling of damaged and old cellular components and is crucial for functionality [3]. It gets rid of potentially harmful protein material and replacing it with new and alternative types which can possibly change the cell characteristics. From metabolic disturbances and organism development to reparation of damaged cell and tissues all continually occurring in living organisms as the dynamic shifting of cells takes place. Knowledge on autophagy has revealed relation to a wide range of fields including immune response, neurodegeneration, cancer, human ageing, cardiomyopathy and atherosclerosis [3; 7].

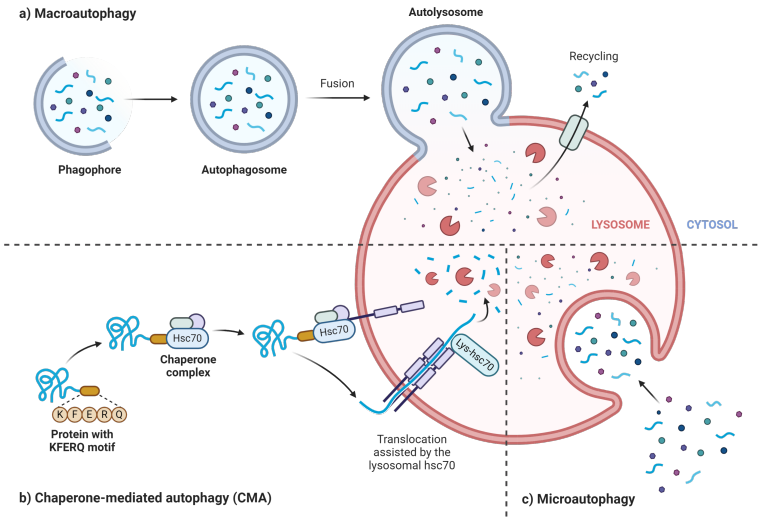

Figure 2.1: Schematic representation of the complete autophagic process [9]

With autophagy linking to these popular fields, it since has received a well known focus in science and medicine. Various clinical trials [8] have already shown some results using autophagic inducers which ramps up excitement towards the possibilities of autophagic control. As our knowledge about autophagy expands it has shown that in order to utilize this highly dynamic metabolic process thoroughly, it is important determine the rate at which this process takes place also known as autophagy flux.

2.1.1 Autophagy Machinery

Autophagy is split into three main types of categories as shown in Figure 2.1 and is classified as macro, micro, and chaperone-mediated autophagy (CMA), with macro autophagy the category of interest it being the biggest of the groups. Autophagy-related (Atg) proteins also classified as key proteins play an important role in the autophagic cycle and are present during the formation and regulation of autophagosomes as well as subsequent events during the cycle. An autophagosome is a double membrane cell that engulfs the cellular material to be degraded by autophagy, the core machinery proteins that relates to the formation of the spherical cell along with other autophagy-related proteins will be discussed in the following sections.

2.1.1.1 Autophagy-related Proteins

With macro-autophagy, from now on known as autophagy, the category of interest it will be discussed and broken into multiple steps. The initiation of the autophagic system starts with the identification of the cellular material then inducing an elongation of the phagophore (double membrane enclosing to encapsulate cytoplasmic components). The autophagosome which forms due to the completion of the phagosome elongation, then fuses with a lysosome inducing the cellular degradation process. Several key proteins (Atg) relate to the regulation and formation of autophagosomes and are specific to their function in each step.

For autophagy to adapt to intracellular and extracellular stress an efficient system is required. A central regulator of autophagy mTOR is a mammalian target of rapamycin.

The binding affinity of Atg1-Atg13 and Atg17 kinase complex are increased in single-celled microorganisms due to the activation of Atg1 as a result of inhibition of Tor by rapamycin intervention or nutrient deprivation [10]. The activation of Atg1 stimulates the formation of Atg1-Atg13-Atg17 scaffold proteins as well as subsequent recruitment of other autophagy related proteins to the phagophore assembly site (PAS) to initiate autophagosome formation. Thus, Atg1 is crucial in autophagy induction [11].

The primary role of autophagy is the bulk degradation of cytoplasmic proteins consisting mostly of older, aged and damaged cellular material. It however also targets specific organelles which is mediated through specific protein receptors. This selection allows the recognition of target cargo for focused degradation. The basic similarities between the pattern of yeast Atg19 and C-terminal recommends that p62 is an Atg19 analogue. It goes about as a receptor for organelles or ubiquitinated proteins in higher eukaryotes [10]. p62 thus assumes a significant part in encouraging the process of selective clearance of ubiquitinated substrates and aggregate-prone proteins in autophagy. The binding of both mono or poly-ubiquitinated proteins to microtubule-associated protein 1 light chain 3 (LC3) is also facilitated by p62 [12]. This results in the engulfment and degradation of the autophagic cargo.

2.1.1.2 Autophagosome Formation

The move into the molecular environment of autophagy began with the recognition of the AuTophaGy-related (ATG) genes. Up untill today 30 ATG genes have been identified through independent genetic screens in yeast model systems. These ATG genes are involved in various subtypes of macro-autophagy including starvation-induced autophagy, the cytoplasm-to-vacuole targeting (Cvt) pathway and pexophagy. Many of the genes have known orthologues in other eukaryotes[13].

A specific subtype of ATG genes plays a key role in autophagosome formation and is necessary for autophagosome formation in all subtypes. The corresponding gene products are referred to as the ‘core’ autophagy machinery. Three major functional groups comprise the core machinery: (1) Atg9 and its cycling system including Atg9, the Atg1 kinase complex (Atg1 and Atg13), Atg2 and Atg18; (2) the phosphatidylinositol 3-OH kinase (PI(3)K) complex (vacuolar protein sorting (Vps)34, Vps15, Atg6(Vps30) and Atg14); (3) the ubiquitin-like protein (Ubl) system, which includes two Ubl proteins (Atg8 and Atg12), an activating enzyme (Atg7), two analogues of ubiquitin- conjugating enzymes (Atg10 and Atg3), an Atg8 modifying protease (Atg4), the protein target of Atg12 attachment (Atg5) and Atg16 [13].

In addition PtdIns3K complex is involved in the recruitment of ubiquitin-like (Ubl) conjugation systems, Atg12-Atg5-Atg16 and LC3 (also known as mAtg8). At the phagophore construction site proteins accumulate to assist in the enlargement of the developing autophagosome and the extension of the autophagosomal membrane. The phagophore assembly site (PAS) is the projected site for autophagosome formation. The PAS can be defined as a composite of the elongating membrane known as the phagophore and core machinery proteins, with the exact conformation of depending on the stage of autophagosome formation. The combined actions of the core machinery at the PAS advances to the enlargement and metamorphosis of the phagophore into an autophagosome. Dur-

ing this process most core machinery proteins are excluded from the complete spherical membrane, with some being relocated to peripheral sites except for Atg8 [14].

2.1.1.3 Vesicle Fusion and Autophagosome Breakdown

Once the autophagosome has fully developed, Atg4 is used to split LC3-II from the outermost membrane and discharge it into the cytosol. Subsequently the Atg12-Atg5-Atg16 complex is released into the cytosol after formation of the autophagosome is complete. Meanwhile, a substantial measure of Atg8-PE remains in the completed autophagosome during its movement to the lysosome. After fusion between the lysosome and autophagosome and the disintegration of the remaining single-membrane cell wall that encapsulates the cargo, the accumulation of Atg8 is released into the lysosome lumen and degraded. Alternative methods of action have been recommended but it is possible that Ubl proteins have a function in phagophore expansion. The degraded cargo which consists mostly of amino acids, are transferred to the cytoplasm where during periods of starvation it can be utilised for protein synthesis and nutrients.[10]

2.1.2 Autophagy Flux

Flux refers to the rate of flow through a surface or substance where autophagic flux can be characterised as the rate of autophagic activity pointing to the rate of forming autophagosomes. A relative change in activity degradation will result in a relative change in the respective rate of degradation. There is a collection of techniques used most often by systems to determine autophagic degradation activity, such as western blot analysis for specific key proteins, transmission electron microscopy, and fluorescence microscopy. These methods produce critical data that uncovers the molecular regulation of autophagic machinery and are highly valued in the analyses of the autophagic pathway. In all 3 approaches assessment of the existence of autophagosomes is the determining component of autophagic activity regardless the usage of appropriate inhibitors. Subsequent to the commencing of the autophagic pathway, the cytosolic, proteolytically processed form of MAP1LC3/LC3 (microtubule-associated protein 1 light chain 3), termed LC3-I, is modified with lipid extensions to form LC3-phosphatidylethanolamine, LC3-II, which is specifically sent to to the phagophore membrane [15]. During the completion of each phase of autophagosome maturation, the LC3-II on the outer surface is separated through disunion, whereas the LC3-II that is present within the internal spherical membrane remains associated with the realised autophagosome. The concentration of LC3-II therefore corresponds well with autophagosome quantification [15].

The autophagic system can be expressed as a multistep pathway where the quantitative measure of cellular material flowing along this route is defined as the flux, the rate of flow in steady state through this pathway. *Flux as the rate of flow along the pathway* is a term in line with metabolic studies where it refers to the rate of flow of metabolite along a metabolic pathway.

Each step in this pathway relates to a certain rate v, which is quantified by the number of units processed per cell per time unit. For example where the lysosome fuses with the autophagosome and the rate is characterised as v_2, the rate could either be the number of autophagolysosomes produced or autophagosomes consumed per time unit.

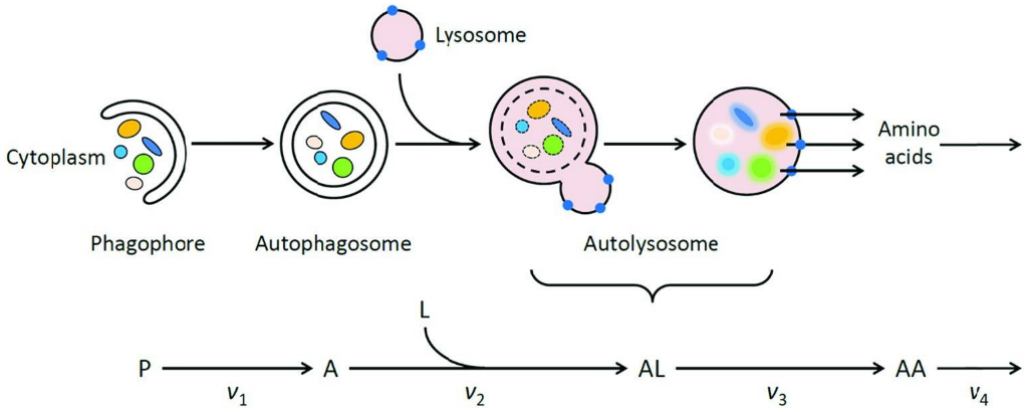

Figure 2.2: Schematic and reaction network representation of the autophagic process. P=phagophore, A=autophagosome, L=lysosome, AL=autophagolysosome, AA=amino acids [15]

$$v_2 = \frac{-dn_A}{dt} = \frac{-dn_L}{dt} = \frac{dn_{AL}}{dt} \tag{2.1}$$

where n_A, n_L and n_{AL} are the total individual entities per cell. The total autophagosomes and lysosomes are consumed in step 2, thus the negative signs for n_A and n_L in (2.1) ensures a positive rate for v_2.

The rate at which the entities change are expressed by the following differential equations:

$$\frac{dn_P}{dt} = -v_1, \frac{dn_L}{dt} = -v_2, \frac{dn_A}{dt} = v_1 - v_2, \frac{dn_{AL}}{dt} = v_2 - v_3, \frac{dn_{AA}}{dt} = v_3 - v_4, \tag{2.2}$$

In order for the system to be in steady state the entities that are entirely consumed or produced could be regarded as constant at the time of the experiment. Thus at steady state the entities A, AL and AA which are variable entities are zero implying they remain constant over time.

$$\frac{dn_A}{dt} = \frac{dn_{AL}}{dt} = \frac{dn_{AA}}{dt} = 0 \tag{2.3}$$

The individual steps are thus numerically equal, $(v_1 = v_2 = v_3 = v_4 = J)$ implying a linear pathway for steady state. The rate at any individual step at steady state is therefore equal to the steady state flux J. By blocking one of the steps like step 2 for instance completely, a quantification of the autophagosome flux can be measured by determining the initial rate of autophagosome accumulation.

2.1.3 Existing Autophagy Measuring Techniques

The precise measurement of autophagic activity is an ever progressing demand as well as understanding into its function in biological processes, and remains a huge challenge to this day. Measuring autophagic flux in a robust, well-quantified and delicate manner is still a tremendous challenge despite technological advances on screening of the molecular aspects of the autophagic machinery. Found in this section are research methods where an abstract framework is identified for defining and measuring autophagosome flux at

single-cell level. The theoretical framework of metabolic control analysis is what the idea discussed is based upon and differentiates between the route along which there is a flow of cellular mass and the quantitative measure of this flow.

2.1.3.1 Biochemical Detection of LC3-II

The detection of LC3-II by biochemical methods is possible through a technique called western blotting [16]. Western blotting for endogenous LC3, also known as immunoblotting, is one of the few methods using a reporter assay that can reliably monitor the autophagosome formation, degradation and recycling process. However, this method of immunoblotting brings forth 2 underlying challenges: Firstly, the number of autophagosomes are indirectly assessed, supported by the existence of LC3-II in the lysate of a complete cell accumulation. Secondly, high background increases the difficulty of accurately assessing miniscule changes in LC3 protein levels and remains a small technical challenge. Also, and more problematic, a western blot does not measure rate.

The concomitant use of substances like bafilomycin A1, or combinations of leupeptin and pepstatin, is the method used to prevent the fusion of lysosomes, and can only indicate an increase or decrease in autophagosome formation through an increase in LC3-II immunoblot signals [17]. This method only measures whether flux is occurring, increasing or decreasing, and unless the signal is documented over time during treament to stop lysosome fusion it can not indicate the rate. Thus based on a single time stamp only the flux cannot be determined, and this method called a "autophagic flux assay," only indicates LC3 accumulation.

2.1.3.2 Transmission Electron Microscopy

Microscopy techniques enables the identification of individual autophagosomes allowing an absolute and quantitative assessment of their existence. An important method for confirming the state and presence of autopgagosomes, lysosomes, autolysosomes as well as endosomes, is known as transmission electron microscopy (TEM) and provides us with highly resolved ultrastructural information. The structural assessment of the intraorganellar signal generated by TEM within autophagosomes is possible solely based on electron density, homogeneity, and ultrastructure. Through this the discovery of Huntington disease is possible for example, which causes cargo recognition impairment, by revealing details about the nature of autophagy targets e.g. pathology, mitophagy or lipophagy and bulk cytoplasm [18].

In addition extremely powerful methods for extracting quantitative structural data for example autophagosomal diameter or percentage of area occupied have been developed. However, requirements for TEM processing involves fixation and embedding of the sample in order for time-lapse analysis to be possible thus making it less suitable and extremely difficult for measuring the rate of flow, hence autophagic flux. For this to be possible various tissue samples need to be collected at different time stamps at the moment of treatment intervention without the accompanying use of lysosomal protease activator at saturated concentrations. This is an extremely expensive, labor and time intensive path and would still not allow for direct quantification of active turnover.

Moreover, to accurately assess the intracellular autophagosome group size a three-dimensional image analysis tool would be required. Since TEM-based image analysis only provides an incomplete reflection of the autophagosome pool it is restricted to data solely derived from a single focal plane. TEM can thus indicate whether there is change as well as if the change is significant when analysing number of autophagosomes. Again it does not quantify the rate of change and is incapable of providing quantifiable flux, and also not able to recognise if the system is at steady state. TEM acquisition and analysis also does not provide information as to whether the system is at steady state. Thus the data on intracellular architecture and organellar ultrastructure of autophagosomes has no value towards the estimation of autophagic flux.

2.1.3.3 Light Microscopy

Fluorescence microscopy uses fluorescent tags to the molecules as markers of interest enabling detection. A specific wave length (200 - 500 nm) excites the markers which in turn emits a fluorescent signal [19]. Previously researched autophagy related proteins can be assessed for analysing autophagic activity and requires substantially less expertise than electron microscopy [20]. A green fluorescence protein (GFP) is typically used to tag LC3 protein in autophagy research.

Fluorescence or confocal microscopy is the foundation on which light microscopy techniques are built upon and fulfils the requirements needed for quantitative flux analysis as it allows measuring rate. Fluorescent microscopy allows the visualisation of the LC3 cell structures and is an extremely valuable tool as it can quantify participating entities such as the total autophagosome count in a single cell. It is necessary that when performing fluorescent microscopy the test is performed over time as the autophagosomal pool alone does not describe autophagy flux but the rate of entity turnover is required. The fluorescent signal can quantify LC3-positive structures, and by completely blocking a step in its pathway the rate of accumulation could be assessed accurately at a single-cell level.

A possible method of quantifying autophagic activity is by expressing GFP-LC3 assessed by fluorescent activation, then plotting the geometric mean on an intensity histogram normalised to its control signal of any given cell population. Using big data, the large number of cells provide desirable statistical power usually requiring a minimum of 10 000 entities. The possibility of using this method to determine the rate of LC3 accumulation is there, it is mostly used to determine whether autophagic flux is occurring and whether it is increasing or decreasing.

Fluorescent microscopy enables imaging through a whole cell allowing the total acquisition of the autophagosomal pool, thus a method to quantify the total puncta is required to assess the pool size. Software known as WatershedCounting3D has the exact function of automatic puncta counting and is perfect for quantifying the autophagosomal pool. The software's assessment returns the average number and total area of GFP-LC3 puncta per cell, where the percentage change in GFP-LC3 puncta is usually how autophagic activity is expressed. The induction of autophagy could result in an increase in autophagosomes and impaired lysosome fusion, these crucial aspects are deceptive of this approach and not currently well dressed. Another potential difficulty although there are steps to reduces this, is when over/co-expressed to aggregate-prone proteins LC3 is known to accumulate and the assemblage could be mistaken for autophagosomes.

2.2 Biosensors

A biosensor is a sensor with the capability of detecting the presence of some biological matter. It is an analytical device that utilises a physiochemical detector in combination with a biological component enabling the device to 'sense' biological molecules and living organisms when the sensor are exposed to them. Some sensors can detect merely the presence of a certain biological components and some are able to quantitatively assess the detail in a physiological process. The quantitative data is usually by means of an electrical signal transferred and processed to determine the concentration of a specific bio-element [21; 22].

These type of sensors would be extremely advantageous in rural areas where medical care is not easily accessible and would enable high level diagnostics at in very remote areas. The goal of these sensors is to have them be extremely user friendly, as small as possible, robust, multifunctional and sensitive but most importantly, cost effective [23]. Biosensors is a broad field with a myriad of techniques and approaches but the in depth discussion of them is beyond the scope of this thesis, with some of them being piezoelectrical, optical, gravimetric, pyroelectric and electrochemical. Electrochemical will be the focus in this project since it covers all the specifications mentioned and the fabrication is relatively simplex [24].

2.2.1 Biosensor Fundamentals

A biosensor typically has the following building blocks:

1. Bio-receptor
2. Transducer
3. Signal amplification
4. Signal processing
5. Data analysis

The bio-receptor is responsible for the detection of the target analyte and consists of the bio-recognition elements for identification purposes. The bio-receptor is typically located at the sensor's transducer where an electrical signal will be generated as the receptor picks up the presence of a target molecule and can be in the form of antibodies which is most common for electrochemical biosensors. Enzymes, microorganisms and nucleic acid is also capable of acting as bio-receptors. The generated signal then passes through analogue circuitry for signal amplification and processing, to be interpreted at the circuit output by means of data analysis algorithms [22; 25]. The recognition event differs for different biosensors and have an effect on the analyte by means of exothermic reactions, movement of electrons and the release of gases like hydrogen and oxygen for example [26]. Figure 2.3 shows a typical biosensor model.

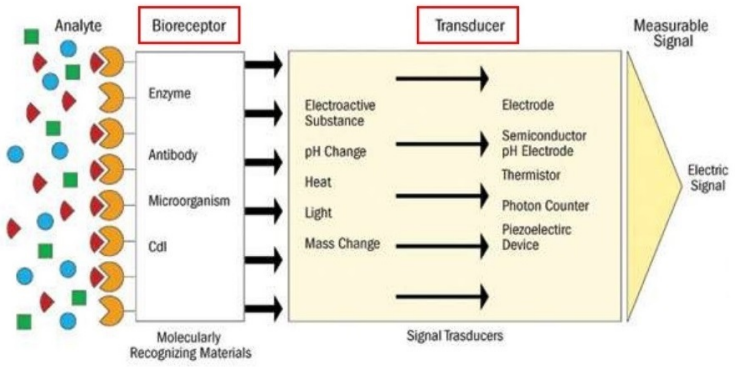

Figure 2.3: Schematic of a typical biosensor showing the fundamental components it is comprised of [27]

2.2.2 Electrochemical Biosensors

The purpose of a biosensor is the transform a bio-recognition event into an electrical signal. Electrochemical biosensors have the capability of detecting highly specific elements very sensitively which is why such a transducer is appealing [28]. A chemical change occurs at the transducer that is dependant on the analyte concentration which is the result of the bio-element and bio-receptor undergoing a binding reaction. The change in chemistry ultimately results in a change in the electrical signal generated by the transducer. Biocatalytic devices and affinity sensors are the two main types of electrochemical biosensors, where the first utilises enzymes and the latter uses antibodies and nucleic acids. Upon recognition of the target analyte an enzyme will release an electroactive species with an example of such a biocatalytic device the well known blood glucose monitoring device that patients of diabetes make use of. When immobilisation of antibodies onto the sensor surface is executed the bio-receptor can bind with specific analytes and is then known to be an affinity biosensor. Selective enzyme are difficult to find and not widely available for most target analytes thus affinity sensors are the more common choice [28].

Electrochemical biosensing consists of a multitude of different techniques with three main categories, voltammetric, potentiometric and impedimetric sensors [29]. A technique that utilises transistors is also favourable with charge accumulating at the gate of the transistor with the gate containing the bio-receptor that converts the chemical change to a current, and known as the field-effect technique [24; 30; 31]. The different techniques are unique in its advantages as electrochemical biosensors with all having trade-offs in terms of simplicity of fabrication, detection sensitivity, robustness and miniaturisation, featuring certain drawback as it excels in specific areas. Electrochemical impedance spectroscopy (EIS) is the backbone of impedimetric biosensors and extracts information by measuring the complex impedance of a cell. A small sinusoidal waveform is induced onto the transducer surface and measures the exiting waveform to determine the resistive and capacitive elements of the cell. This method requires sophisticated electronics capable of detecting in and out of phase current which is a complicated task [32; 33; 34]. Potentiometric sensors operates by measuring the voltage change over a cell while assuming no current is flowing through the cell but they are slow in response and sensitive to environmental noise resulting in inaccurate readings [29]. Voltammetric sensors are the most attractive due to its sensitivity and overall simplicity, and operates by applying a specific potential

waveform and measuring the resulting current [35; 36; 37]. Due to previously reported success as well as the simplicity and cost-effectiveness thereof, Voltammetric techniques will be further discussed. Section 2.3 goes into depth on the theory and application of voltammetric techniques in electrochemistry.

2.2.2.1 Voltammetric Biosensor

Electrochemical biosensors usually consists of three electrodes known as the working, counter and reference electrodes. In some cases electrochemical sensors only require two electrodes to be in contact with the solution where the reference and counter electrode is short circuited. The working electrode (WE) serves as the sensor's transducer and is usually a redox conductive material. All modification is exerted onto the working electrode and is the site where the bio-recognition event takes place. The role of the reference electrode (RE) is to maintain a constant stable potential and is mostly made of silver of silver chloride, although when pure silver is used it tends to oxidise and contaminate the voltammetric readings. The counter electrode (CE) is usually of the same material as the working electrode and also requires to be conductive in a redox solution as it establishes a current path between itself and the working electrode [28]. Discussion on the materials used follows in Section 2.2.3.2.

An applied voltage over the working and reference electrodes produces a redox current that originates at the working electrode due to the oxidation and reduction of the electrolytic solution. This principle of voltammetric biosensors is dependent on the concentration of the electrolytic solution and, results in a change in current flow as the concentration varies due to a change in available ions [29]. In order for current to flow in the redox species the applied potential is required to be in the redox potential range. Square wave voltammetry (SWV), cylclic voltammetry (CV) and differential pulse voltammetry (DPV) all operate by means of an applied potential and measuring the resulting current, whereafter the data is visualised on a voltammogram (plot of the applied voltage versus measured current) [35]. The different techniques are unique in the parameters of the applied waveforms, except for amperometry that is the plot of measure current over time.

An early example of amperommetry is the monitoring of glucose oxidising in the presence of glucose oxidase (GOx) [38], and is an amperometric biosensor that measures the flow of current while maintaining a constant potential. The reaction is shown as,

$$\text{glucose} + \text{O}_2 \xrightarrow{\text{GOx}} \text{D}-\text{gluconic acid} + \text{H}_2\text{O}_2 \tag{2.4}$$

where glucose acts as the reaction's analyte with the product being H_2O_2 and O_2 the substrate. The current is produced by the oxidation of hydrogen peroxide at the electrode surface as shown in Figure 2.4, which is proportional to the amount of glucose in the sample.

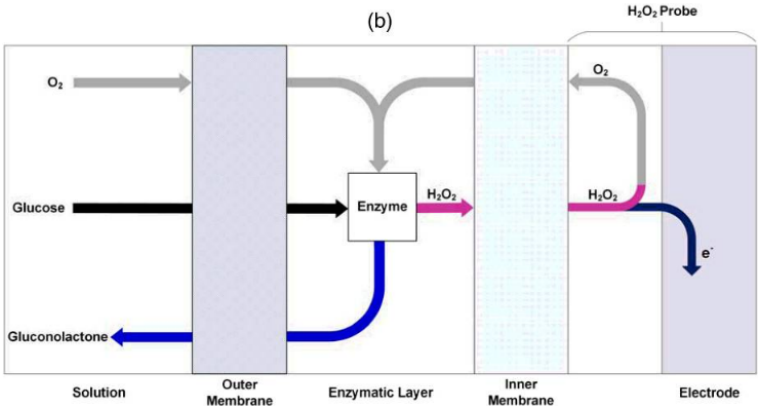

Figure 2.4: Diagram of a first-generation amperometric biosensor for glucose detection [38]

The range of oxidation and reduction potentials required for first generation amperiommetry can be varied by the use of redox mediator which in turn increases the electron transfer capabilities [29]. Kuek Lawrence et al. used a ferrocene monocarboxylic acid mediator [39] to carry electrons from the GOx to the electrode surface in development of an amperometric biosensor that is paper based, with Figure 2.5 showing the fabrication method. Instead of hydrogen peroxide ferrocene is then reduced, generating an electrical signal as it undergoes re-oxidation [40].

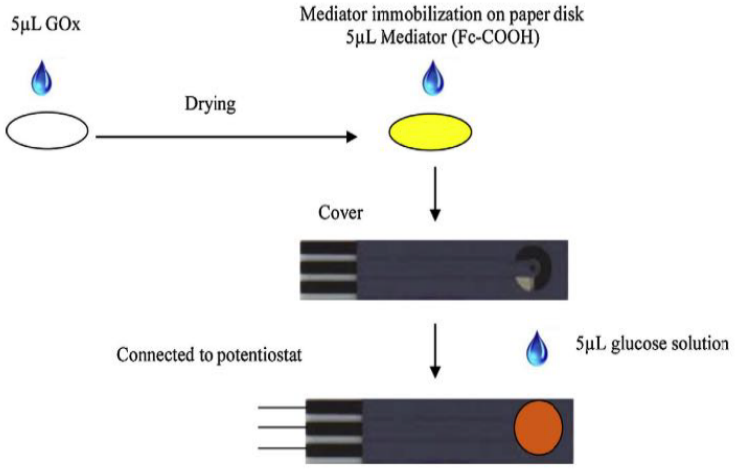

Figure 2.5: Diagram showing fabrication method of a ferrocene monocarboxylic acid mediator glucose biosensor [39]

Dropcasting was used to absorb GOx on paper and air dried. The optimal redox potentials and pH was determined beforehand conducting experiments to optimise the sensitivity of the sensor. After adding the mediator to the paper it was carefully place onto the carbon screen printed electrode. By monitoring the current the voltage that will yield the largest oxidation current was chosen with the biosensor operating between 0 and 0.5 V. The experiments were executed in 0.1 M PBS of pH 7.0, which is identified as the optimal pH level for the behaviour of the mediator. A detection limit of 0.18 mM is achieved in the range of 1 to 5 mM glucose and also resulted in a 2% degradation over a 4 month period still being able to detect glucose levels in soft drinks comparable to

industry standard tests. This sensor is proof that a low-cost simplex sensor like this could show promise in the industry of food processing control.

Cyclic voltammetry (CV) is a voltammetry method used for gathering information on the electrochemical window of a reaction and presents data such as the potential range of the reaction as well as the reaction rate [24]. The voltage over a cell is swept to and from two specified potentials at a specific scan rate. Scanning towards a positive potential the species R undergoes oxidation shown in (2.5).

$$\mathrm{R} \rightleftharpoons \mathrm{O} + \mathrm{ne}^- \tag{2.5}$$

As the sweep reaches a predetermined switching potential the the cell is scanned in the reverse direction whereas the species O undergoes reduction and is reduced back to R [41].

$$\mathrm{O} + \mathrm{ne}^- \rightleftharpoons \mathrm{R} \tag{2.6}$$

Scanning the potential in both directions enables us to analyse the electrochemical behaviour inside a cell being an advantage over other voltammetry techniques as it yields valuable information of the reaction on the electrode surface. Figure 2.6 shows the waveform of a single CV cycle in an arbitrary redox solution and its corresponding current response.

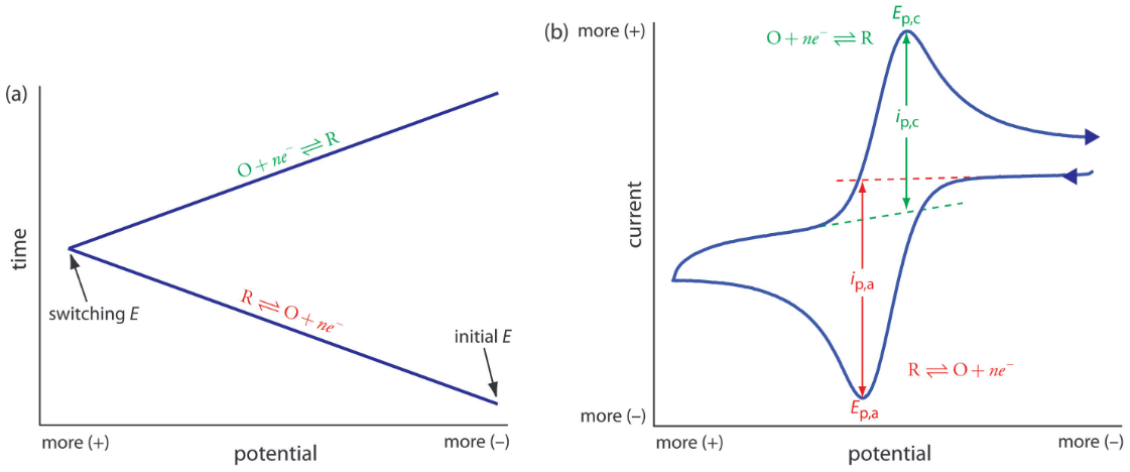

Figure 2.6: Diagram for cyclic voltammetry details. a) Plot fo applied potential over time as the cell is swept from a more negative potential towards a more positive potential and *vica versa* as it reaches the switching potential. b) the resulting current signal corresponding with the applied waveform of a). [41]

With cyclic voltammetry producing data on the behaviour of an electrochemical reaction, it is often used for monitoring electrode modification. It can also be used for sensing purposes but since the resulting current waveform is complex it is difficult to extract absolute values and is thus less common. The voltammogram in Figure 2.7 reported by Kuek Lawrence et al. is the waveform produced by CV as the electrodes undergo modification with the tests executed between stages. It can be seen that PBS (black) has no contribution, the mediator (red) induces some redox reaction and the ferrocene

mono-carboxylic acid mediator (blue) with a significantly unregulated redox reaction due to the enzyme dependent oxidation of glucose [42].

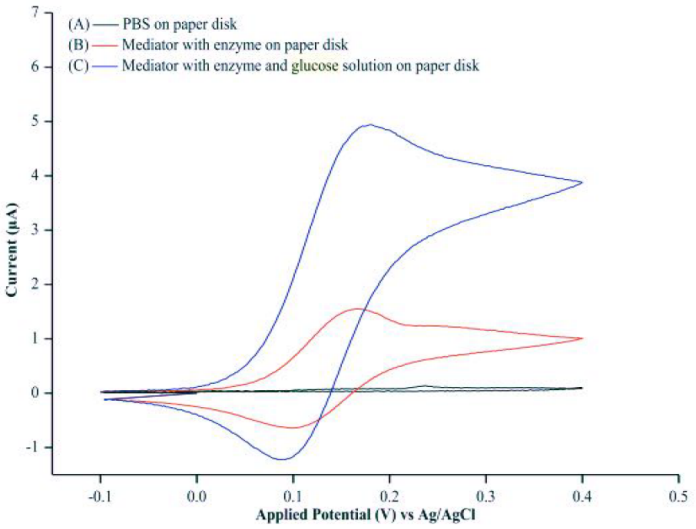

Figure 2.7: Graph of GOx immobilised onto a paper disk [39]

Apart from the monitoring of electrochemical cells and reactions, cyclic voltammetry can also be used as a method of modification. Eissa et al. demonstrates the modification of the working electrode by creating carboxylic moieties as diazonium salt is reduced onto the electrode surface [43]. The experiment present the results of how different carbon based screen printed electrodes perform after a cyclic scan from 0.2 to -0.6 V and back to 0.2 V at a scan rate of 100 mV/s. The cyclic voltammetry in carboxyphenyl diazonium salt solution is known as electrografting with Figure 2.8 showing the voltammogram of the modification process.

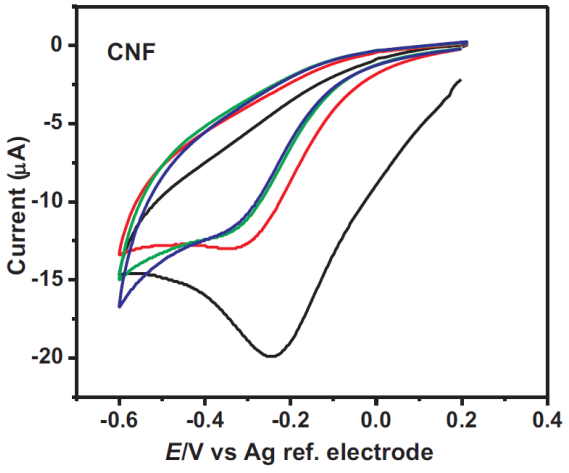

Figure 2.8: Voltammogram of successive cycles of electrografting in diazonium salt solution [43]

The first cycle displays a strong irreversible reduction peak current at -0.25 V decreasing bit by bit after every successive cycle. The initial electron transfer between the working electrode and the diazonium salt results in the reduction peak and diminishes as

more carboxylic groups are grafted onto the electrode surface, causing a drop in electron transfer efficiency. The biosensor for detection of survival motor neuron protein by Eissa et al. was further developed by means of square wave voltammetry.

Square wave voltammetry (SWV) has become a popular method in electrochemical methods in recent years where multiple papers [43; 44; 45; 46] have proved its success in the field of biomarker detection. SWV is based on the principle of a square wave superimposed onto a staircase waveform as shown in a) in Figure 2.9, with b) the resulting current. The current is sampled at the end of each pulse indicated by the black squares where the sampled current at 1 is subtracted from the current at 2 resulting in the voltammogram in b). This differs from differential pulse voltammetry where the sample is taken at the beginning of each pulse.

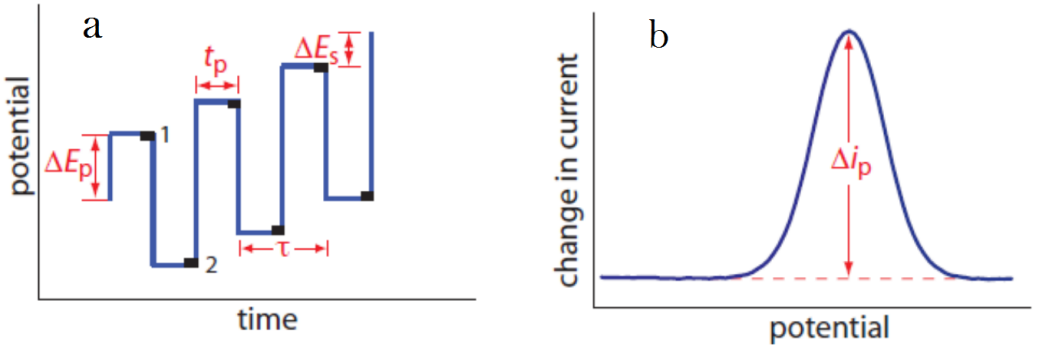

Figure 2.9: Figure to display the principle of operation of square wave voltammetry. a) graph of the applied waveform with ΔE_p the fixed pulse potential, t_p the pulse time, τ the cycle time and ΔE_s the fixed change in potential per cycle b) Graph of the resulting current measured (1-2) with Δi_p the relative change in peak current [41]

In the development of a biosensor for detection of survival motor neuron protein by Eissa et al. different materials was exploited for screen printed electrodes where the carbon nanofibre sensors were reported to have the most responsive platform. The high sensitivity of the electrodes are due to the greater surface area and the fibres also have a high degree of selectivity. After electrografting with diazonium salt as shown in Figure 2.8, the carboxyl groups were activated by using EDC/NHS activation chemistry which is required for antibody attachment. The square wave voltammetry experiments with parameters at a scan range of 0.3 to -0.4 V at 125 mV/s, 25 Hz, pulse amplitude 20 mV and 5 mV step potential, were conducted in a 5 mM potassium ferricyanide ($[Fe(CN)_6]^{3-/4-}$) redox species prepared in 10 mM PBS, pH 7.4. Different concentrations of SMN protein were detected by measureing the relative change in peak current as shown in Figure 2.10, showing how the peak is increased as more protein is bound to the working electrode. Due to a positively charged SMN protein and the experiments performed at a pH of 7.4 the SMN protein will attract the redox anions, and with its isoelectric point at 8 an increase in electron transfer efficiency is experienced yielding an increase in reduction peak current. A linear response from 1.0 pg/ml to 100 ng/ml is reported with a 0.75 pg/ml detection limit. Tests conducted with whole blood and diluted with lysine buffer showed a 91 to 95% SMN protein recovery rate, proving the SMN detection capability in whole blood.

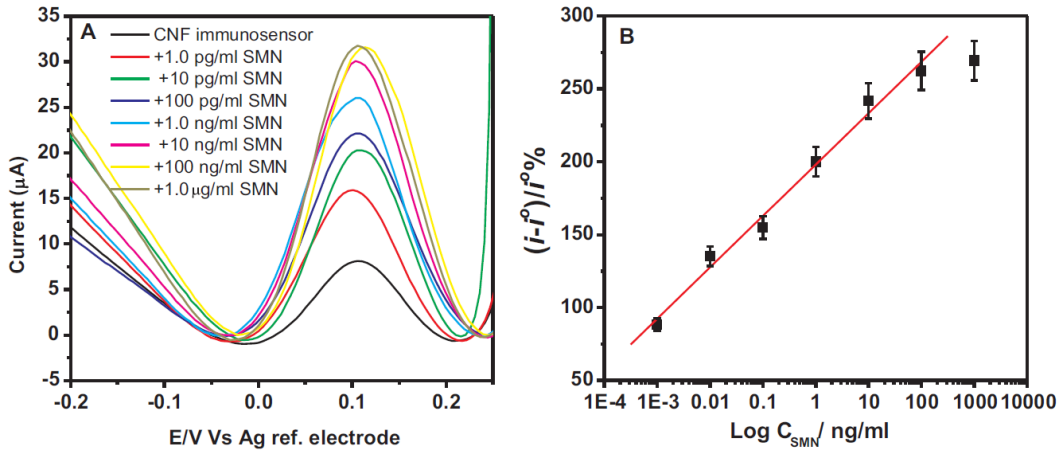

Figure 2.10: a) Square wave voltammetry results of different SMN protein concentrations b) Calibration curve based on the change of square wave voltammetry peak currents [43]

Li et al. demonstrates that electron transfer capability can also be decreased by the blocking effect. Without the use of an amplification or fluorescent marker, the "label-free" angiogenin biosensor utilises an anti-angiogenin-aptamer capture molecule as a bio-receptor, immobilised onto a gold electrode. The functionality of the aptesensor is presented on the left of Figure 2.11 showing how the gold working electrode repels redox anions due to its negatively charged phosphate backbones [47]. An EIS measurement verified an increase in the charge transfer resistance due to the surface modification, thus with a higher concentration of angiogenin the more the redox peak is supressed showed on the right of 2.11.

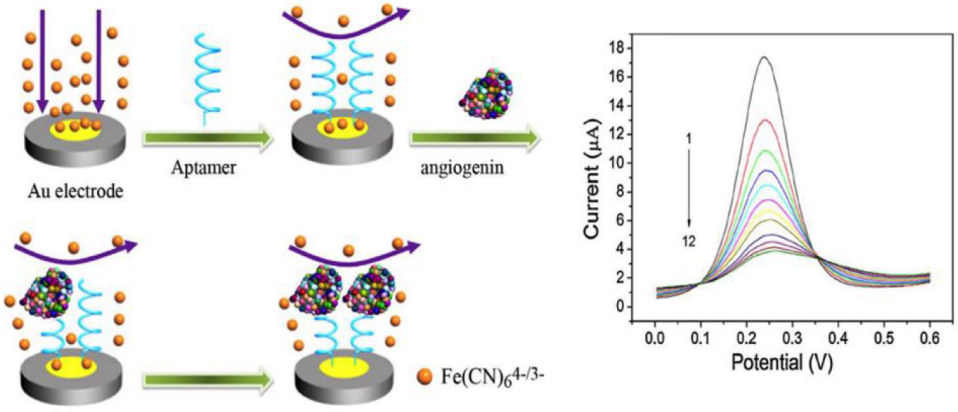

Figure 2.11: Diagram of a biosensor for detection of angiogenin using aptemers for bio-detection (left) and the resulting square wave voltammetry response for different concentrations (right) [47]

After experimenting with different measuring techniques, it was reported by Li et al. that square wave voltammetry was the most repeatable and sensitive compared to other voltammetry techniques such as electrochemical impedance spectroscopy and cyclic voltammetry. A linear detection range of 0.01 nM to 30 nM was reported for the detection of angiogenin in a sample with a 1 pM detection limit. A comparison between a commercial human angiogenin assay and the aptesensor was made by using samples from lung

cancer patients, and showed to give an accuracy of 92 to 104%. The accuracy percentage was determined by taking the ratio between the aptesensor's measure concentration and that of the immunoassay confirming that the aptesensor is capable of detection of complex biological samples. The disadvantage of aptamers though is that is is very fragile and unstable making it very difficult to fabricate such a sensor.

Voltammetric biosensors are popular due to its simplicity, robustness, simplex fabrication methods, it is easily characterisable and produces in depth electrochemical reaction behaviour data and is clear why it is a common choice. There are however trade-offs to different voltammetry techniques such as amperometry that has very low detection limits due to negligible charging currents and thus are simple and robust, but very little target proteins have enzymes to associate with it with the capability of oxidation and reduction in a redox solution [28; 48]. Cyclic voltammetry is uncommon for being a measure of detecting the presence of a target molecule but is a key method in the modification of sensors towards detection such a modifying the working electrode through electrografting and is also the means of sensor characterisation. The sweeping voltage though produces charging currents that are difficult to analyse and does not yield absolute values thus complicated to assess. Square wave voltammetry generates a peak current which is a direct result of change on the working electrode making it ideal for a target detection test. It is sensitive and reliable making it a popular technique in biosensing [44].

2.2.2.2 Impedimetric Biosensor

Electrochemical impedance spectroscopy (EIS) is the basis of an impedimetric biosensor with the test delivering depth detail into different dimensions of a cell. The popularity of EIS is increasing due to its proven sensitivity, being able to assess a myriad of dynamics in chemical and physical properties. Due to its multi-dimensional analysis the monitoring of bio-recognition events are extremely attractive with the potential to pick up the slightest of change in cellular behaviour of several catalization reactions with enzymes [49].

The electrical real impedance of a cell, which is also known as the resistance of an electrical component, is the measure of opposition for current to flow through the component when a voltage is applied. If the component facilitates capacitance then the component has both resistive and capacitive impedance known as complex impedance with the real component being resistive and the imaginary capacitive, with the imaginary part caused by an electrical phase shift. The complex impedance of a cell is measured by generating a small sinusoidal signal and applying it to the cell while sweeping through a range of frequencies. The resulting current as well as the phase shift is measured to determine the complex impedance of the cell. The frequency spectrum is utilised enabling the test to pick up complex changes in cell chemistry as binding between enzymes and antibodies takes place. Combination of data plots between complex impedance and frequency yields in depth data relating towards electron transfer processes at the electrode surface as well as valuable information on the double layer capacitance formation due to the diffusion transport of the species in the redox solution. Electrochemical impedance spectroscopy can be used in the modelling of electrical equivalent circuits providing absolute data on the behaviour of cell change [38]. Figure 2.12 shows the resulting experimental data obtained from performing EIS.

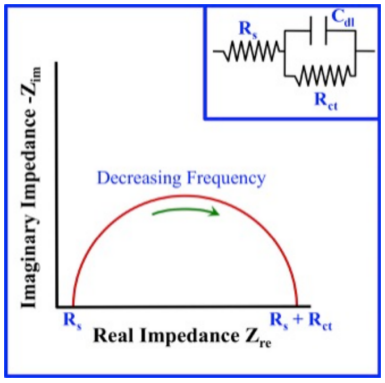

Figure 2.12: Diagram showing the resulting data generated from an EIS scan and the cells equivalent circuit with R_s the solution resistance and R_{ct} the charge transfer resistance [50]

An obstruction present in the analyte when the target molecule is bound to the electrode surface is measured as the impedance between the two redox probes changes and is known to be a Faradaic process. A non-Faradaic process is the result of the double layer capacitance as it changes due to target molecule binding and is in the form of charging currents. Capacitive sensors like IDE's (interdigitated electrodes) for example, experience a change in capacitance after sensor modification and identifies as non-Faradaic electrochemical impedance spectroscopy [38].

2.2.3 Biosensor Components

This section looks at the specific building blocks towards a biosensor and the components it consists of. Important topic ie. immobilisation strategies for binding the bio-recognition element to the transducer is discussed as well as common materials used in the transducer fabrication.

2.2.3.1 Bio-recognition & Immobilisation Strategies

Biological and physiological processes relate to very specific biomolecules and are associated with particular characteristics, proteins and cells that solely identifies with this process. These biomolecules are known as biomarkers, a marker that identifies with a certain process and can be accurately measured and are captured by the bio-recognition element such as enzymes, antibodies and whole cells [51; 24]. Detection of a biomarker in a sample could indicate that the process it relates to is active where the biomarker concentration will determine the degree of this process. A biosensor consists of a bio-recognition element immobilised onto it and is able to indicate if a certain biological process is underway as well as the intensity of this process as the concentration of biomarkers are higher.

Aptamers comes in two forms known as single stranded DNA (deoxyribonucleic acid) and RNA (ribonucleic acid) and are sensitive, stable and highly specific nucleic acids [52]. Aptamers are attractive for fabricating biosensors due to modification methods not greatly influencing its ability to bind to a specific target and can easily and cost effectively be synthesized with chemical tags, and have being successfully used in the detection of biomarkers towards cancer and a number of foodborne pathogens [47; 53; 54; 55; 56]. Enzymes are known to have biocatalytic activity and are highly specific consisting of amino

acids that catalyze biochemical reactions and are widely used detection in electrochemistry with these type of biosensors being relatively cheap, provides fast results and are reusable. Some drawbacks though, is that the enzyme layer loses its activity and thus needs to be sporadically regenerated and to limit interference from unwanted reactions in the same redox potential range redox permeable membranes are to be employed. Despite these disadvantages they still excel for use in biosensors and are popular for its use in glucose monitoring in patients of diabetes [28; 48; 57; 58] as well as the detection of l-lactate [59] and cholesterol [60; 61]. Cultured cells and live cell lines are utilised in whole-cell based biosensors and immobilised onto the transducer which can then detect a change on the transducer surface as these cells respond or grow. These cells are very dependant on environmental factors, thus such biosensors are still enclosed in laboratories to control these factors but are able to provide very complex functional data and by using organic electrochemical transistors the study of these cells are possible [30; 31; 62].

With antigens as biomarkers, antibodies have shown to be great recognition elements being highly specific and is the principle behind affinity based biosensors. Antibodies are of importance as they create a platform of sensitivity to proteins on the transducer surface with the level of sensitivity on immobilisation orientation, method, and the blocking of bindings to non-specific species. The antibody structure is shown in Figure 2.13 consisting of two light- and two heavy chain with constant and variable regions. "Fc" identified the non-antigen binding fragment and "Fab" the antigen binding fragment.

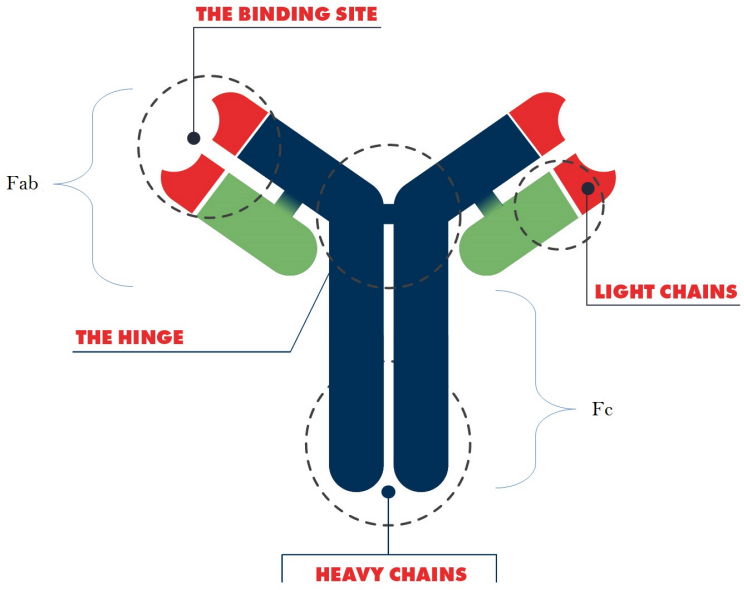

Figure 2.13: Diagram showing the structure of an antibody [63]

When antibodies are immobilised the orientation is of high importance. For interaction with the analyte careful immobilisation is required with techniques to control the antibody orientation by interaction with the antibody molecule and numerous reactive groups on a solid surface, ensuring that the binding ability is not compromised. There is a possibility of saturating the transducer surface by "coating" it with multiple layers, resulting in the antibodies to not function effectively and leads to steric hindrance. Biotin-streptavidin linkage, covalent binding and adsorption to a conductive surface are all

methods for antibody immobilisation [28; 64]. Affinity immobilisation methods a surface of high affinity is provided as with biotin-streptavidin linkages a high affinity of biotinylated biomolecules are present. Effective orientation of the antibodies on streptavidin functionalized surfaces is allowed as the biotin molecule is attached to the "Fc" region. A very specific surface is required for this method as well as an antibody with a biotin tag which is not always widely available, but apart from this it is a relatively simplex method of immobilisation. The absorption methods leads to sporadic orientation of antibodies as numerous functional groups react with each other, but is a simplistic method that enables surface functionalisation for antibodies through van der Waals and electrostatic forces [65].

Covalent bonding between the functional groups on a transducer surface and an antibody is preferred due to the reusability factor it gains as well as enabling the sensors to be stored for longer periods without losing efficiency. Through covalent immobilisation of antibodies with functional groups highly reactive chemicals are required which can cause the loss of antibodies as well as decrease the binding capacity of antibodies, also causing time delays as a result of tedious extra modification steps [66]. Glycomoiety coupling, thiol coupling and amine coupling are three methods by which covalent immobilisation is possible as shown in Figure 2.14. Glycomoiety coupling uses amine groups present on the sensor surface linking to active diol groups on the antibody's "Fc" region that is created while executing this method. Through the reduction of disulphide groups (-S-S-), a binding between one of these active groups and a thiol group present on the antibody is required which will form sulfhydryl-reactive groups (-SH). A thiol-disulphide exchange will occur as one of these active disulphide groups on the sensor is in the presence of a sulfhydryl-reactive group. With only a few sulfhydryl groups available on the protein the orientation of the antibodies become a controlling factor and the binding efficiency could be increased [66; 65].

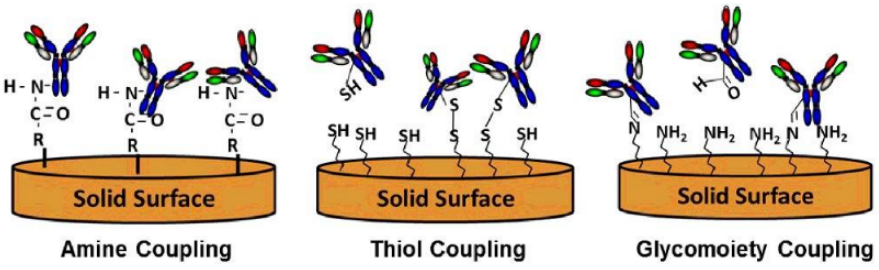

Figure 2.14: Diagram showing various covalent immobilisation techniques [65]

Electrografting as discussed in Section 2.2.2.1 is an electrochemical method where a diazonium salt solution is grafted onto the transducer surface [67]. The grafting process is executed by using a potentiostat and performing a cyclic voltammetry scan and sweeping a potential over the created electrochemical cell. The cathode of the experiment is set up to be the transducer material, then by taking diazonium salt and dissolving it in an electrolytic medium the diazonium salt solution is reduced onto the substrate surface set up as the cathode and known to be the working electrode. The range of the voltage sweep is chosen to be in the range of diazonium salt's voltammetric peak where after a specified amount of sweeping cycles a washing step is performed to remove any access salts and unbound materials [68; 69].

Bio-receptor based assays for receptor immobilisation is not limited to only antibodies with electrografting functional groups onto the electrode surface a respected technique with successfully reported results [70]. Corgier et al. [71] reported conjugating diazonium salt to graphite electrodes after immunoglobulin G (IgG) antibodies was bound to 4-carboxymethylaniline with the sequence given in Figure 2.15.

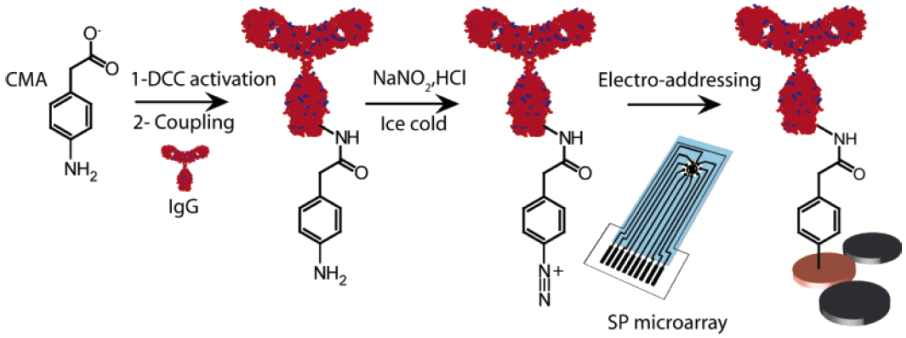

Figure 2.15: Diagram showing the sequence of electrode surface modification of a graphite substrate by Corgier et al. [71]

Eissa et al. also used electrografting by reducing diazonium salt onto the working electrode in the modification towards biosensor development for detecting SMN protein. Eissa et al. reported to have first modified the electrode surface after electrografting prior to the immobilisation of the SMN protein which differs from the method reported by Corgier et al. EDC (1-ethyl-3-(3-dimethylaminopropyl) carbodiimide hydrochloride) and NHS (N-hydroxysuccinimidyl-4-azidosalicylic acid) was used as an activation buffer bore immobilisation and is known as EDC/NHS activation chemistry. The different methods of modification by Eissa et al. in Figure 2.16 can be compared to that of Corgier et al. in Figure 2.15

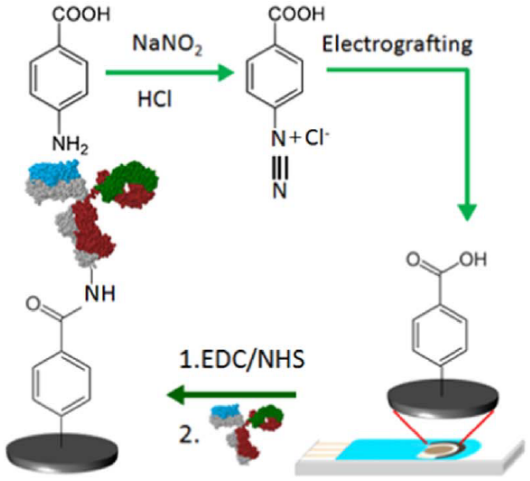

Figure 2.16: Diagram showing the sequence of electrode surface modification by Eissa et al. [43]

Three electrode SPE's (screen printed electrode) were used by Eissa et al. [43] to demonstrate the success of their modification on the working electrode with al sensors being carbon based. The performance of six different materials were explored being single-

and multi-walled carbon nanotubes, graphene, graphene oxide, carbon screen printed and carbon nanofibres, with the counter electrode consisting of the same materials and and a silver chloride reference electrode. The reference electrode creates a stable potential point not affected by its environment and small disturbances [72]. Eissa et al. [43] reduced diazonium salt onto the working electrodes through cyclic voltammetry as a functionalisation step with parameters as -0.6 V to 0.2 V potential range at a scan rate of 100 mV/s.

A potentiostat was used for performing cyclic voltammetry scans. Figure 2.17 shows the voltammograms of successive cycles of the electroreduction of 4-carboxylpenyl diazonium salt onto different substrate materials.

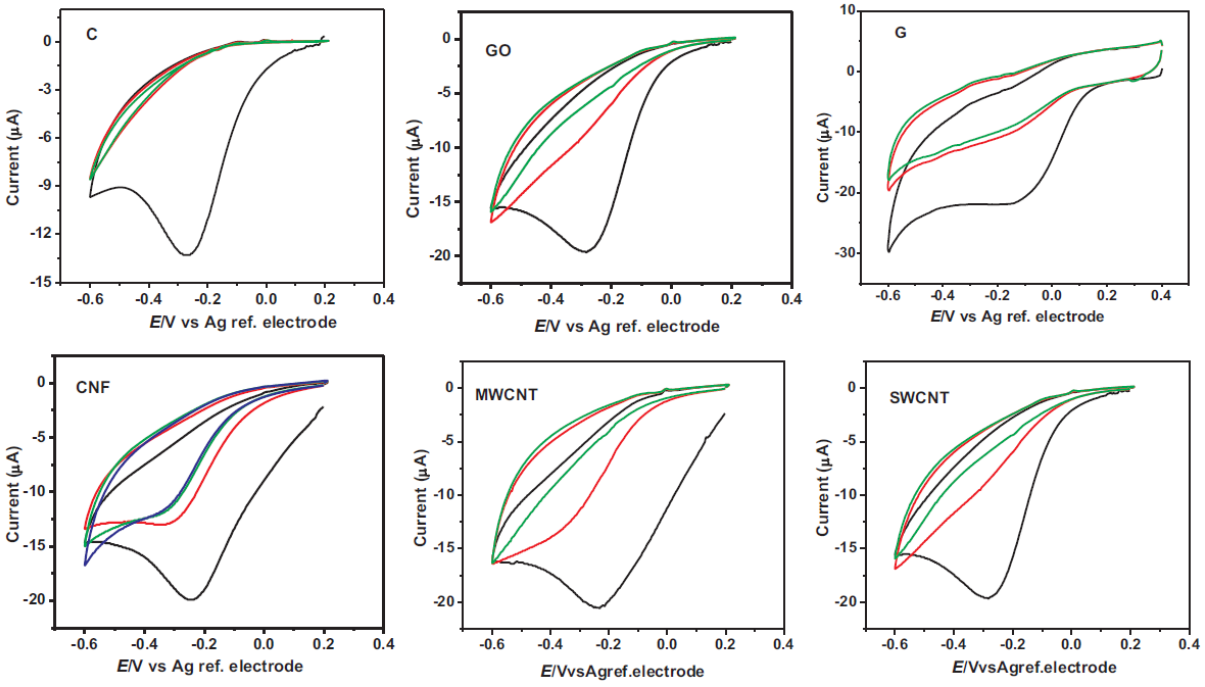

Figure 2.17: Diagram showing CV voltammograms with successive cycles of electrografting on different transducer materials [43]

2.2.3.2 Transducer

The material used to fabricate the sensor's transducer is largely dependant on the type of biosensor. Examples of transducer materials are quartz crystal microbalance sensors that uses gold [73; 74; 75], polystyrene sulfonate for organic electrochemical transistors [30; 31; 76; 77], and gold-coated glass for optical biosensors based on surface plasmon resonance [78; 79; 80; 81]. Some sensor make use of a hybrid between materials to combine their advantages such as graphene oxide and gold-nanoparticle modified graphene towards fabrication of an impedance sensor [82; 83]. The requirement for electrochemical biosensors is the ability for current to flow thus any type of conductive polymer is accepted, with the specific polymer depending on the specificity and sensitivity of the sensor. The material is chosen based on cost, stability, biocompatibility, conductivity and modification simplicity such as the presence of functional groups for crosslinking purposes.

Figure 2.18 shows the molecular structure of graphene oxide that consists of a multitude of oxygen containing groups on the outer edges of its flakes, as well as the basal

planes and is in its whole a single atomic layer material. Its significant surface area make for effective protein immobilisation, by using the EDC/NHS crosslinking protocol the functional carboxylic groups (-COOH) makes for ideal immobilisation [84].

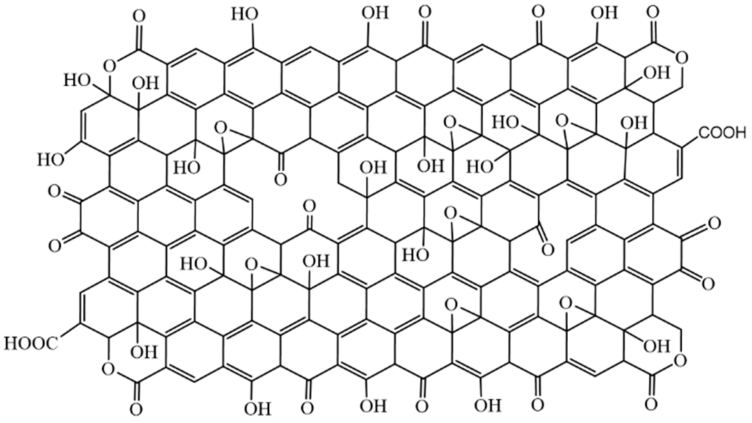

Figure 2.18: Chemical structure of graphene oxide [85]

By creating smaller changes at the electrode surface the sensitivity of the biosensor is increased. This is done by lowering the charge transfer resistance of a standard glassy carbon electrode by modifying it with graphene oxide, and literature reporting the execution of a dropcasting step as modification [53; 84; 86; 87].

Carbon nanofibres, due to its orientation has an exceptionally high surface area causes it to be highly conductive and sensitive, and is an excellent substrate for transducers in electrochemical biosensors. The fibres in the form of nanotubes, are folded and stacked to form graphene layered cylindrical structures through using a technique called catalytic chemical vapour deposition [88]. The fibres are grown on a substrate by applying high temperatures to gas-phase molecules causing it to decompose. Figure 2.19 is a picture of carbon nanofibres taken by an electron microscope where multiple and individual fibres can be seen.

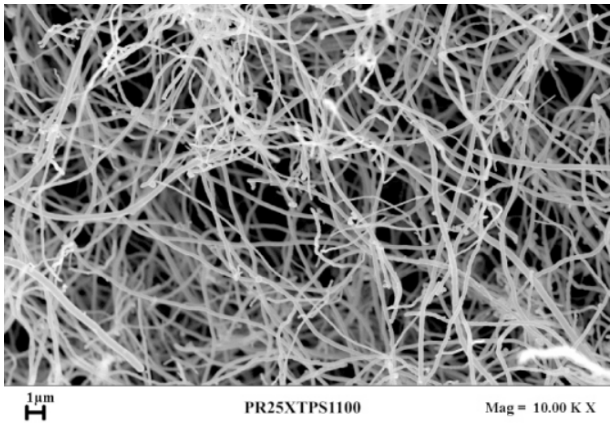

Figure 2.19: Picture of a CNF sheet taken by an electron microscope [88]

The fibres consists of oxygen containing groups capable of modification to form functional groups without compromising the structural integrity of the material. The large surface area creates an immobilisation matrix for antibodies to bind to. With the plane

defects of its outer walls contributing to high electron transfer in an redox species along with its great surface-to-volume ratio this material is the prime transducer substrate.

The manufacturing of screen printed electrodes has recently become quite popular as it is an excellent starting point of building a sensor proof of concept, and there exist companies that supply them commercially. A company such as Dropsens provides various different screen printed electrode of which you can customise the combination of materials with the three electrode SPE's having dimensions of 3.4 x 1.0 x 0.05 cm. The carbon based SPE's consists of a ceramic base substrate with a carbon counter and working electrode, and features a silver reference electrode. Dropsens provides a cable that connects to a potentiostat where the sensor could plug in to as you would a UBS into a computer. It comes at relatively cheap price of R100 and operates in small sample solutions of 50 µl. Figure 2.20 shows a carbon nanofibre screen printed electrode from Dropsens, Spain.

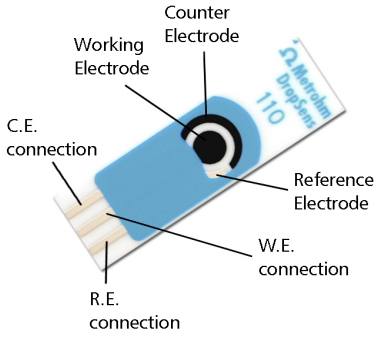

Figure 2.20: Carbon nanofibre screen printed electrode from Dropsens, Spain, showing the sensor layout and configuration [89]

2.2.4 Research Based Autophagy Flux Biosensors

Physiological processes are complex procedures and are typically a changing state, making information in an absolute measurement of the biology very limited. Therefore monitoring the dynamic process of autophagy and determining the rate at which it occurs remains a great challenge. An absolute measurement could indicate if autophagy is occurring but biosensors are not yet intelligent enough to understand the increase and decrease thereof, with the development of such biosensors for monitoring the different forms of autophagy still underway. Techniques do exist for determining autophagy flux by chemically probing a sample to modulate the process enabling us to measure the dynamic process, but requires great form of experience and an in depth physiological knowledge [13].

Biosensing and monitoring of the autophagic process has two main approaches to consider as shown in Figure 2.21 with examples of these approaches previously reported in literature [13]. The first of the two categories is an extensive process by monitoring the behaviour and activity of autophagy as primary molecules are modified which changes the autophagic mechanism, and assessing the molecular activity. The second approach would be to monitor the "path" of target molecules by following them to determine the accumulation of these target molecules as they are delivered in each phase of autophagy, such as autophagosome/ lysosome fusion for example to facilitate a specific target molecule as a biomarker.

With the approach of monitoring a specific target molecule it is essential to be able to tag or clearly identify the molecule in order to follow its "path" and determine its fate. Through the use of electron microscopy the visualisation of mitochondria and intracellular pathogens is possible and by assessing their staining patterns generated the process is analysable, or detection by fluorescent microscopy subsequent to labelling the target molecules with the appropriate dyes [13]. By genetically binding fluorescent markers with target proteins it greatly expands the possibilities for monitoring autophagy as the delivery of certain target molecules can be properly traced. The presence of fluorescent protein markers are capable of detection even in the degradation of organelles as they are highly stable proteins persisting in their fluorescent form [90]. Western blots follows the binding of fusions such as fluorescent markers and displays the relative change in sizes of these fusions produced by degradation. In some cases the target delivery to the autophagosome could be followed by assessing enzymatic activity [13; 90], with a focus gaining on the labelling of target molecules to be followed as new forms of selective autophagy is reported.

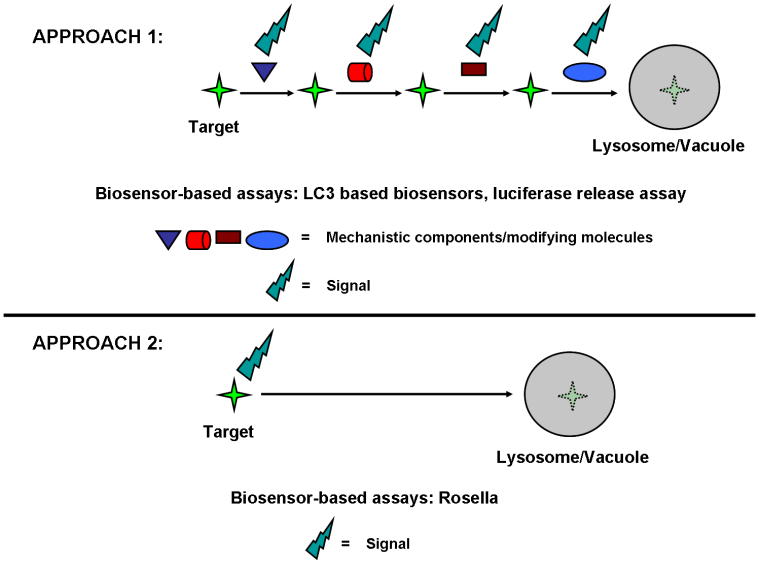

Figure 2.21: Approaches for monitoring autophagy. 1) Tracing key molecules in the pathway like LC3 for example 2) Continually sensing reports on the target material in the environment of the biosensor [91]

2.2.4.1 Fluorescence-based biosensors for monitoring live autophagy in cells

The measuring and monitoring of autophagy flux in live cells, organs and tissues has spiked an interest in researchers and is resulting in fast technological advancement towards developing a high level measuring system. Recent development has shown success in the monitoring of autophagy in a living organism but the measurement for a specific form and application thereof is not yet available [13].

Research-based biosensors for the detection of autophagic flux within a living organism has been developed and is discussed in the next two sections. The monitoring is executed by means of fluorescent markers to determine the autophagic pathways as these markers emit light detectable through certain microscopy techniques. The first method explained in Section 2.2.4.2 covers the detection of Atg4b (autophagin) and Atg8 (LC3), key proteins

relating to the activation of specific processes in autophagy, and the second discussed in Section 2.2.4.3 operates by directly labelling autophagic cargo such as the cell nucleus.

2.2.4.2 LC3

Fluorescent microscopy reveals as autophagy is initiated the LC3-I protein with a green fluorescent protein (GFP) tag gets converting to LC3-II with the emitting fluorescent puncta relating to the formation of the phagophore, with the total puncta accumulated as the measure of the degree of the autophagic process [92; 13]. The autophagosome fuses with a lysosome which is the degradative organelle. Just before fusion with the degradative lysosome the autophagin removes GFP-LC3 from the surface of the autophagosome, with GFP-LC3 still at the inside of the membrane emitting fluorescence up until autophagolysosome degradation.

The accumulation of fluorescent puncta is graphically displayed, and to determine autophagic flux each fluorescent emitter needs to be accounted for. This is extremely time consuming and without the proper expertise an accurate interpretation is not possible. A method called fluorescence activated cell sorting (FACS) isa method used to analyse fluorescence over on a time dependant manner enabling the monitoring of autophagy in living organisms [93].

To enable the environment of the modification probe to be monitored a method reported in literature is deployed where a red fluorescent protein (mRFP) and a green fluorescent protein (EGFP) is fused to LC3 in parallel [94; 13]. The characteristics of the fluorescent proteins differs by emission as the pH changes, with the green fluorescent protein mostly suppressed and the red highly emitting because of the acidity of the lysosome lumen. The tandem fusion called tfLC3, now exhibits the estimation of autophagy induction as well as flux through its compartments without the need of chemical inhibitors and inducers [94].

2.2.4.3 Rosella: A Biosensor for Selective Autophagy

As interest is peaking among researchers about the understanding of the different selective forms of autophagy and the rate at which cargo degrades, and more approaches are extensively studied to monitor this process and looking at individual cargo that may provide in depth detail on the behaviour of this process [95; 96]. Existing methods of estimating autophagy flux as discussed in Section 2.2.4.2 requires the probing of the autophagic process in combination to various steps to extract information on a certain phase in the autophagy pathway, but a different approach can reveal the exact delivery of the target molecules to the lysosome as in Figure 2.21. A genetically encoded dual colour-emission biosensor called Rosella, fuses a fast-maturing variant of the red fluorescent protein DsRed.T3, with a green fluorescent protein, pHluorin, which are both pH sensitive variants of these proteins and is shown in Figure 2.22 A [91; 97]. Specifics about the cargo being delivered to the lysosome is now available and are tied to cellular components or bound to an individual protein and most crucial, Rosella yields data on the environment of the biosensor as in Figure 2.22 B [91; 97].

Specific cargo such as mitochondria, cytosol and the nucleus have been proved as traceable by Rosella and serves as a biosensor for estimating the degradation of autophagy

in yeast cells [91; 98; 99], through FACS analysis in fluorescent microscopy. The findings presented by Devenish et al. and Rosada et al. is extended by studying the reorganisation of the nuclear membrane, and it is proved that the Rosella biosensor can successfully monitor selective- and non-selective autophagy specifically in mammalian cells.

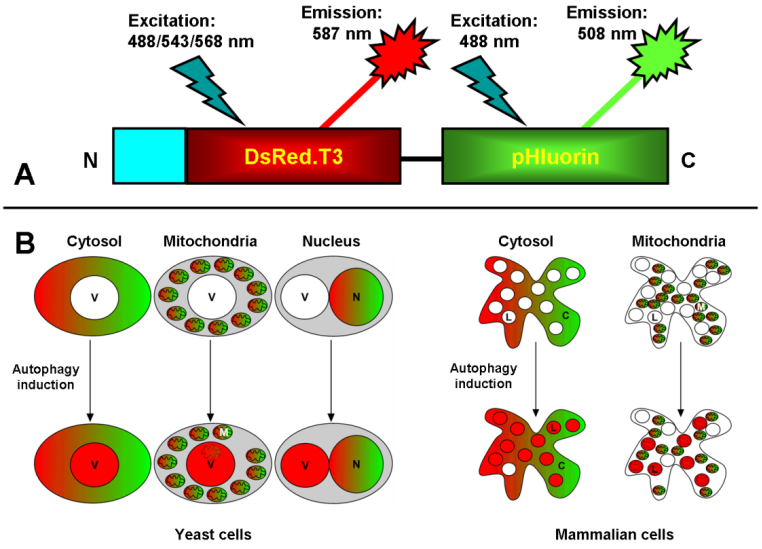

Figure 2.22: The monitoring of autophagy by using the Rosella biosensor A) A simple schematic of Rosella B) Shows how Rosella can be used to trace target material and monitor delivery of the cytosol [91]

2.3 Electrochemical Study

This section covers the theory behind electrochemical methods and the behaviour of electrons as they flow through various chemical compounds. The study distinguishes between the flow of electrons during an electrochemical reaction and reversely the reactions caused by electron flow, and explains the electrochemistry taking place on a biosensor. An electrochemical biosensor is viewed as an electrochemical cell and described with a mathematical model, with the behaviour of electrons and their transfer kinetics discussed as it is subjected to voltammetric methods. The theory of cyclic and square wave voltammetry is also expanded from Section 2.2.2.1 providing more in depth detail on the reactions taking place.

2.3.1 Electron Kinetics and The Electrochemical Cell

Electrochemistry consists of electrodes dispersed in a ionic conductor with some electrical characteristics, undergoing a reaction induced by an electrical charge and monitoring the flow of electrons passing through the conductor. This project focuses on assessing the electron flow, hence current, passing through an electrolytic medium by means of electrodes namely the working, counter and reference electrode. The reaction between the electrolyte and the three electrodes is studied and the theory of the effect of subjecting it to various voltammetric methods.

The electrochemical cell works on the principle of current flowing through the electrolytic medium it is immersed in by means of an applied potential over the cell's elec-

trodes, with the behaviour of electron flow depending on the characteristics of the ionic conductor together with the composition of the electrode materials. Different voltammetric methods provide diverse potential characteristics suited for specific applications, resulting in changing currents which produce valuable information on the detail of the chemistry inside the reaction and the electrode surfaces. EIS is a voltammetric method that provides complex detail of an electrochemical cell of which the data could be used to create a model of the cell as discussed in Section 2.2.2.2. The data gathered by EIS can indicate a change on the electrode surface interface and yield information on charge transfer and solution resistance as well as changes in the cell's capacitance [38]. As the binding of target molecules take place the characteristics of the cell is changed, and by fitting the EIS data to an equivalent circuit of the cell the change in resistance and capacitance could be monitored. The Randle's equivalent circuit is a popular equivalent model of an electrochemical cell and is shown in Figure 2.23.

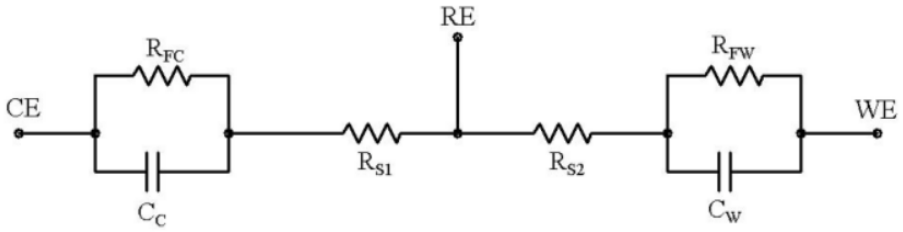

Figure 2.23: The Randle's equivalent circuit of a three electrode electrochemical cell [100]

Both electrodes consist of a parallel circuit with a double layer capacitance C_C and C_W that is caused by both the electrode capacitance and and electron charge distributed near the electrode surface. The electron charge distribution is dependant on the concentration of the electrolyte, with a higher concentration the result will be more ions in the solution and impact the current flow as a potential is applied. With more ions in the solution the electrode voltage would result in greater electrostatic forces causes an increase in electron flow. The non-faradaic current flows whether or not the redox active species is present and effectively causes cell capacitance, which is directly proportional to the scan rate explaining why cyclic voltammetry is ineffective for biosensing characterisation. The cell capacitance is minimised for biosensors, with the focus on small changes in the current the non-faradaic current provokes noise into the measurement and is undesirable. R_{FC} and R_{FW} is the charge transfer resistance and dependant on the concentration of the electrolytic species, electrode material and applied voltage. It is the resistance of electron flow caused by the ability of the electrodes to transfer ions to and from the electrolyte and could be infinite if no redox active species is present. R_{S1} and R_{S2} is the measure of solution conductivity.

In an electrochemical cell consisting of three electrodes where the third is the reference, electron transfer occurs between the working and counter where the reference is used to maintain a stable potential and to monitor the voltage on the working electrode placing it in close proximity. The material of the counter electrode is chosen such that the ions flowing from the counter to the working electrode does not cause decomposition of the substance enabling a reaction with the working electrode. The monitoring of the working

electrode requires a potential independent of the current flowing and is done by adding the reference electrode that maintains a stable voltage with not current passing through it, thus the advantage of the three electrode system.

A potentiostatic device is capable of executing controlled experiments by applying specific potential waveform and monitoring the resulting current produced by the cell, and is usually capable of a wide range of potentiostatic techniques. The basic configuration of an electrochemical experiment is shown in Figure 2.24

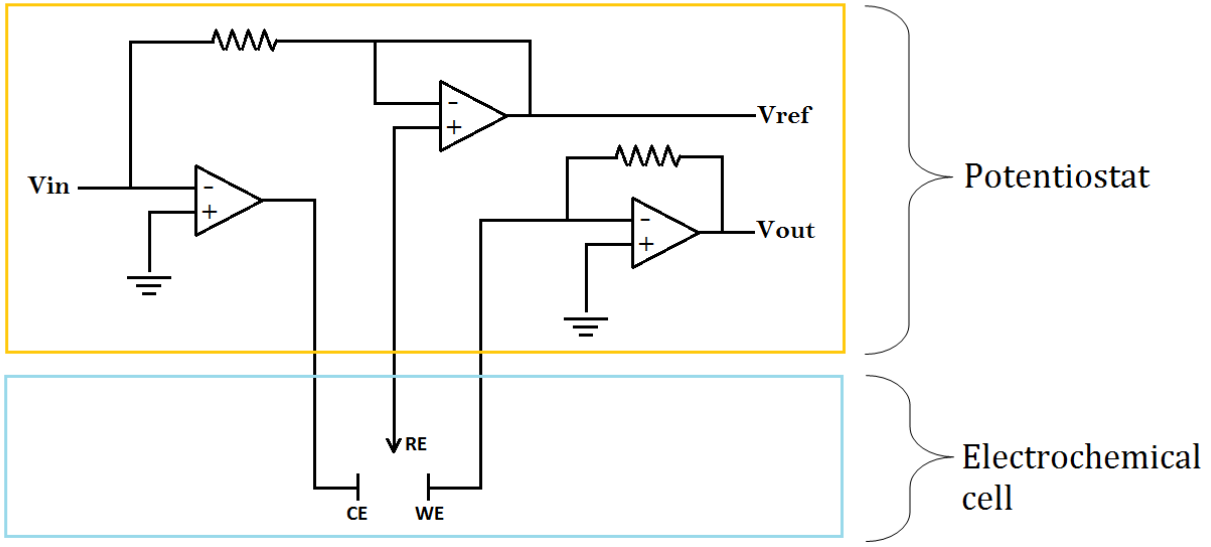

Figure 2.24: Typical configuration of an electrochemical setup

2.3.2 The Nernst Equation

A voltammetric practical guide written by Elgrishi et al. [101] explains how cyclic voltammetry relates to the Nernst equation and can also be found in an electrochemistry textbook written by Belding et al. [102]. Bard and Faulkner covers how square wave voltammetry in another book handling on electrochemical methods [103]. Since the component of interest when using electrochemical biosensors is the faradaic current, to focus on the electron transfer the parameters of the voltammetry methods such as scan rate are chosen to minimise the capacitive non-faradaic currents. The Nernst equation is used to describe the diffusion rate and state the behaviour of the electron transfer kinetics by,

$$\begin{aligned} E &= E^0 + \frac{RT}{nF} \ln \frac{[Ox]}{[Red]} \\ E - E^0 &= \frac{RT}{F} \ln \frac{[Ox]}{[Red]}, \end{aligned} \tag{2.7}$$

with E as the electrochemical cell potential, [Ox] is the concentration of the oxidized form, and [Red] is the concentration of the reduced form, F is Faraday's constant, R is the universal gas constant, T is the temperature, E^0 the standard potential of the oxidized and reduced forms at equilibrium, and the total number of electrons. The formal potential can be experimentally measured and is halfway between the peak reduction and oxidation potentials, and is only the case for reversible redox couples meaning reduction as well as

oxidation is possible at the working electrode. For the transfer reaction explaining only the movement of a single electron the standard potential would be replaced by the formal potential and the total amount of electrons n, would be replaced by a 1. To calculate the formal potential we use,

$$E^0 = \frac{E_{pa} + E_{pc}}{2}, \tag{2.8}$$

where E_{pa} refers to the voltage reached relating to the peak anodic current generated as the result of an oxidation reaction, and reverse the E_{pc} refers to the voltage reached relating to the peak cathodic current generated as the result of a reduction reaction. Equation (2.7) shows that it is required for the working electrode to be in close proximity of the redox active species and and is able to predict change in the species' concentration as behaviour of the applied voltage changes which is also true for the reverse. At the initial point of the experiment where only the oxidised form of the species is present reduction would occur when the applied voltage is less that the formal potential, oxidation of the reduced species if it is above the formal potential and lastly no change in concentration with the applied voltage equal to he formal potential. The voltammogram of the execution of cyclic voltammetry clearly visualises the reaction and is shown in Figure 2.25 to demonstrate.

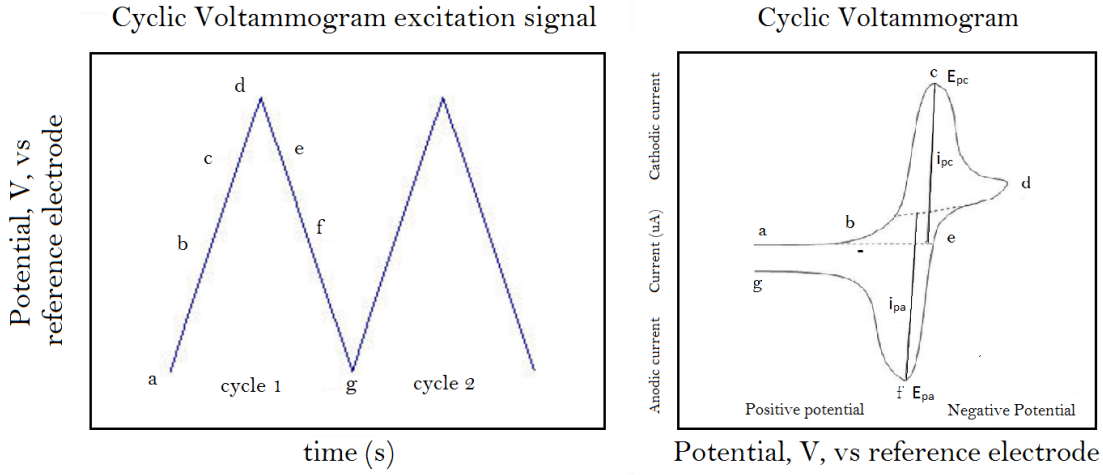

Figure 2.25: Voltammograms of the excitation signal (left) and resulting current (right) of a typical cyclic voltammetry scan [104]

A voltage sweep is performed with successive cycles of this sweep looking like the triangular waveform produced on the left. A cathodic scan is executed by sweeping the voltage from a) to d) in the more negative direction and results in the reduction of the redox active species which is why is it also referred to as the reduction or cathodic current, and peaks at E_{pc} located at c) relating to its cathodic current i_{pc}. As the scan reaches a switching potential the sweep is reverse sweeping towards a more positive potential from d) to g) known as the anodic scan resulting in the oxidation of the species as predicted by (2.7) with the relating current known as the anodic current, and peaks at E_{pa} located at f) relating to its anodic current i_{pa}.

When assessing voltammograms a few key things are to be considered namely the relativeness of the peak currents, the fact that the test does not have to start with the cathodic scan, the maximum point of the faradaic currents and lastly conventions. When

looking at the peak currents is is necessary to take into account that the currents do not start at zero and thus the peaks cannot be measured from zero, but measured relatively from the signal's baseline. In Figure 2.25 the dotted lines on the voltammogram on the right are the two peaks' baselines and is the result of capacitance in the cell or other redox potentials in the scan range of the experiment causing non-faradaic current flow. The reverse current from d) to g) is also dependent on the switching potential with the baselines dependent on the scan rate as well as the effective reversibility of the electroactive species. A perfectly reversable electroactive species which satisfied the Nernst equation can reduce voltammogram baselines.

The initial potential of the cyclic scan largely depends in which form the electroactive species is before the experiment starts, and will also the determine the scan direction with it not always being true that a cathodic initial sweep is possible. If the redox species is in its oxidised form then it will require the scan to start far positive scanning towards a negative potential to enable the sweep to reduce the species, and vice versa, if the redox species is in its reduced form it will require the scan to start far negative scanning towards a positive potential to enable the sweep to oxidise the species. In some experiments the species is prepared to contain both the oxidised and reduced species in equal concentrations allowing the system to start in any position and a current will be produced in any scan direction.

While observing faradaic currents it is clear that a sweep in the negative direction will result in a reduction of the electroactive species taking place at the working electrode. However, due to the current reaching a diffusion limit it is not possible for it to increase above or below the reduction and oxidation potentials as the diffusion of the oxidised species on the electrode surface is diminished as the result to the reduced form's build-up. Thus with the rate of diffusion decreasing the current is also decreased from c) to d) as the excitation signal goes further negative. Lastly the convention when looking at voltammograms for cyclic voltammetry in this project will be the IUPAC convention with an example of the voltammogram in Figure 2.6, and the second convention being its mirror.

There are numerous variables to take into account when performing these experiments, many of which are uncontrollable and can greatly influence the system. Thus performing multiple iterations of each experiment is required in order to perfect the test and make sure the scanned signal is stable. The controllable variables such as supporting electroactive redox species as well as the electrode material are factors that the electrochemical window depends on and should be predetermined in order to make sure that the combination of electrode and electrolyte is redox inert. To make sure no external aspects are influencing the system a background scan is conducted using cyclic voltammetry which will determine the non-faradaic current in the supporting electrolyte, with factors such as bubbles on the electrode surface can play a major role. A washing step is performed with the liquid of use for each experiment before use to remove these bubbles and make sure the are no external resistance in the redox active species. These are all required steps before using the electrode setup as a biosensing technique and although CV yield valuable information about the redox species, a more sensitive and advanced method such as square wave voltammetry is utilised.

SWV is a well-known technique, falling in the category of pulse voltammetry and is

capable of picking up small changes on electrode surface by simply evaluating an absolute value is produces. Similar to CV it also sweeps linearly to and from a potential range but instead, pulses along this path and "walks" only in one direction. The principle of SWV as shown in Figure 2.26 is base on a typical square wave superimposed on a staircase signal.

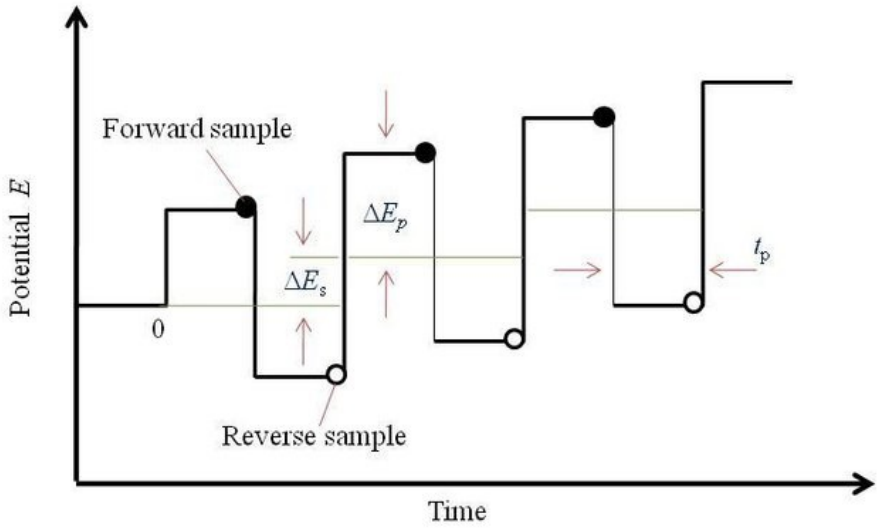

Figure 2.26: Square wave voltammetry excitation signal [105]

Where ΔE_p is the amplitude of the square wave, ΔE_s the step height, t_p the pulse width, and the forward and reverse current sample points denoted by the solid and blank dots, with the resulting current being the reverse current sample subtracted from the forward current sample. For SWV each pulse cycle has conditions that are complex causal functions [103]. There exists links of the electrode surface between the mechanisms as well as kinetics making them depend on previous cycles, making it increasingly more complex to theoretically calculate the peak current response due to the diffusion layer close to the electrode not being renewed at the start of each measurement. When calculating the peak current and assuming that only the oxidised is available, it results in,

$$\Delta i_p = \frac{nFA\sqrt{D_O}C_O^*}{\sqrt{\pi t_p}}\Delta\Psi_p, \tag{2.9}$$

with the differential peak current as Δi_p, Faraday's constant as F, the surface area of the working electrode as A, the oxidised species' diffusivity as D_O, the oxidised species' concentration as C_O, the pulse width t_p, and Δ a dimensionless constant. The amounts of electrons transferred due to square wave voltammetry parameters relates to the dimensionless constant Δ and due to removing capacitive currents the method becomes more responsive than CV, and is its primary advantage. Looking at (2.9) it is clear that the faradaic current decays at a rate that is inversely proportional to the square root of time whereas the non-faradaic capacitive currents decays exponentially which is the result of sampling the current at the end of the pulse [44].

2.4 Potentiostatic Devices

A potentiostat is an electrical device capable of performing complex electrochemical techniques by using different signal excitation methods and applying them onto electrochemical cells via three electrodes. Typical potentiostats that are used to characterize and analyse electrochemical cells as well as biosensors are usually bench top systems of high functionality capable of performing a myriad different experimental methods. They are extremely expensive making them illogical to use for biosensor testing and characterisation as they are confined to specialised laboratories and usually requires a high level of expertise to operate. Electrochemical biosensing is becoming more popular which led to more portable and affordable potentiostatic devices been developed to overcome these problems, where this section will discuss the various available commercial as well as research based potentiostat devices for electrochemical and biosensing applications. Three commercial potentiostats are reviewed namely the Palmsens 4, the Gamry Interface 1010T and the 910 PStat mini, and are all from companies that specialise in electrochemical instrumentation, as well as three research based devices called the Dstat [106], dual-microprocessor potentiostat [107], and Universal Wireless Electrochemical Detector (UWED) [108].

2.4.1 Principle of Operation

The fundamental operation of a potentiostat is that after applying a very specific excitation waveform the resulting current can be accurately measured and the applied potential accurately monitored relative to a stable and fixed potential. In the basic two electrode configuration as shown in Figure 2.27 A) the current that flows through the working electrode is measured while the potential is monitored over the working and counter electrode. In A) the cell is not subdivided and the experiment considers the whole cell whereas the point of interest lies only at the reaction on the working electrode and thus adds variables that might contaminate the results [109]. The problem this creates is not only added factors to the equation of this experiment, but results in poor potential control of the working electrode as the current passing through the counter electrode [103] causes a very volatile reference point of measuring the working electrode potential thus leading to inadequate interfacial potential control during the execution of the specified waveform.

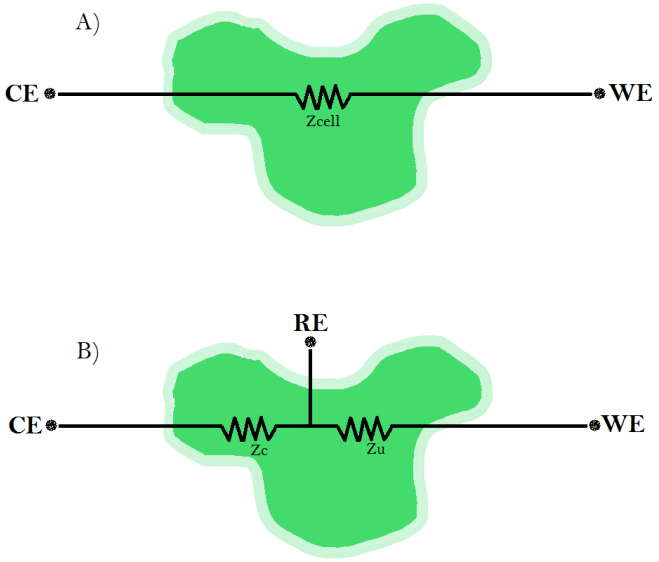

Figure 2.27: A typical model of an arbitrary electrochemical cell in two different configurations **A)** represents the cell in a two electrode configuration and **B)** shows the configuration of a three electrode cell featuring an added reference electrode.

To overcome the problem of insufficient potential control, the counter electrode is split into two so that there exists an electrode designated for the monitoring of the applied potential. This electrode is known as the reference electrode and due to its role as reference point for aiding in the monitoring of the applied potential it requires to be extremely stable and fixed at a known value. The working electrode is also kept at a fixed and known potential and with the changing current flowing from the counter to the working electrode the potential over the reference and working electrode can be closely controlled, creating a half-cell and ultimately removing one half by means of the potential control which places focus on the working electrode. The potential control results in the potentiostat applying a specific potential on the counter electrode with the final potential measured across the reference and working electrodes to be exactly that requested by the user. The reference electrode is implemented as such the no current can flow through it making sure that there is no uncompensated potential difference over Zu, and allows the counter electrode to supply enough current to compensate for the voltage drop across Zc which takes into account the solution resistance as well as the reaction at the half-cell. Figure 2.28 shows the potentiostatic model of an electrical equivalent circuit with the electrochemical cell connected to it. The potential of the cell will be the working versus the reference electrode potential, and assuming this configuration to be true in the this project the resulting current flows into the working electrode [110].

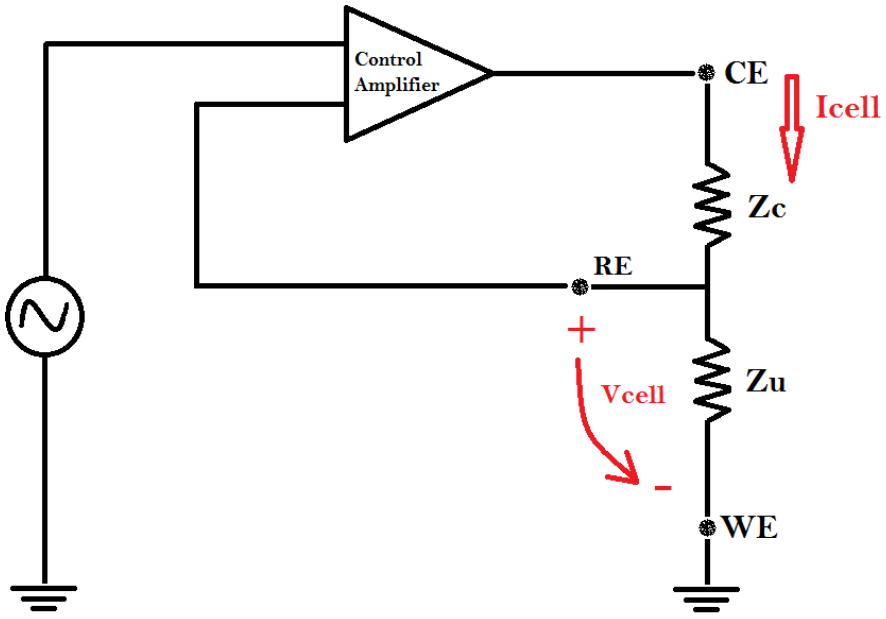

Figure 2.28: Simplified potentiostatic electrical equivalent circuit in a three electrode configuration

With he amplifier adding a gain factor to the difference of the input terminals with,

$$\begin{aligned} V_o &= A(V_+ - V_-) \\ &= A(V_i - V_r) \end{aligned} \tag{2.10}$$

with the output of the amplifier denoted as Vo and the gain factor known as A, with no current flowing through the reference electrode due to its almost infinite input resistance. The current flowing through the cell can be described as,

$$I_{cell} = \frac{V_o}{Z_c + Z_u} \tag{2.11}$$

and,

$$I_{cell} = \frac{V_r}{Z_u} \tag{2.12}$$

with the cell current as I_{cell} , the uncompensated and compensated impedance as Z_u and z_c. Taking (2.11) and (2.12) and combining them forms,

$$\begin{aligned} \frac{V_o}{Z_c + Z_u} &= \frac{V_r}{Z_u} \\ V_r &= \frac{V_o}{Z_c + Z_u} \\ V_r &= \beta V_o \end{aligned} \tag{2.13}$$

where the feedback signal is denoted as β. Taking (2.10) and (2.13) in combination gives,

$$\begin{aligned} V_r &= \beta A(V_i - V_r) \\ V_r &= \beta A V_i - \beta A V_r \\ \frac{V_r}{V_i} &= \frac{\beta A}{1 + \beta A} \\ &= \frac{1}{\frac{1}{\beta A} + 1} \end{aligned} \tag{2.14}$$

with the gain A large enough to discard the one and (2.14) simplifying to

$$V_r = V_i \tag{2.15}$$

proving that the control amplifier operates to maintain the voltage over to working and reference electrode, having it be equal to the input voltage. Figure 2.29 shows an extended version of the circuit in Figure 2.28 featuring a current sensing circuit to convert the current flow to a relating measurable voltage produced over R_f. The working electrode is kept at ground so that,

$$\begin{aligned} V_{cell} &= V_w - V_r \\ &= 0 - V_i \\ &= -V_i \end{aligned} \tag{2.16}$$

with the cell voltage as V_{cell}, potential at the working electrode V_w, potential at the reference electrode V_r, and the applied voltage waveform as V_i. The current is then measured to be,

$$\begin{aligned} V_{cell} &= -I_{cell} \times R_f \\ I_{cell} &= \frac{V_o}{R_f} \end{aligned} \tag{2.17}$$

where I_{cell} is the current flowing through the cell, R_f the feedback resister and V_{out} the voltage generated by the I-V converter and measured over the feedback resistor.

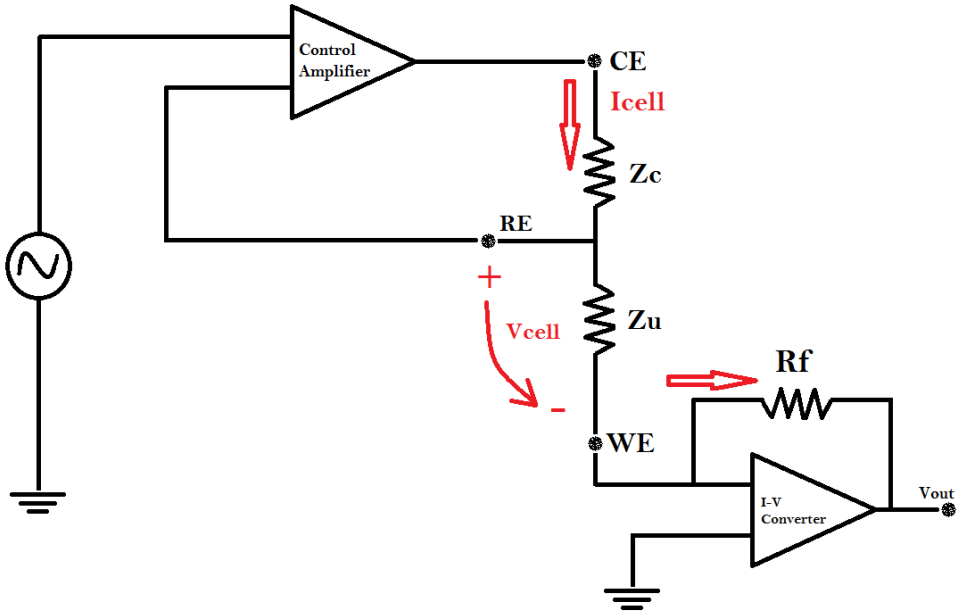

Figure 2.29: Extended simplified potentiostatic electrical equivalent circuit in a three electrode configuration with I-V converter

There are many different configurations of the circuitry that makes up a potentiostat, with each class yielding different ways of controlling the voltage across the electrodes. Each configuration is built to utilise a specific advantage but as more focus is put an a certain area other areas experience drawbacks which is the trade-off of analogue design, and is done by varying circuitry parameters and requirements. The purpose of a potentiostat is to control reactions taking place in an electrochemical cell which is possible due to electroactive species present in the solution, and is done by carefully controlling the cell voltage V_{cell}, forcing the electrochemical cell to undergo certain reactions and monitoring the electron charge transfer as a result of these reactions.

2.4.2 Commercial Potentiostatic Devices

Apart from the electrochemical cell in Figure 2.29 the circuitry forms part of a bigger system which is to be the potentiostat. Different potentiostats have different trade-offs with this section discussing the specifications of 5 potentiostats, where a comparison will be made based on their technical specifications and product reviews. Due to the nature of the experiments performed of this project the technical specifications does not have a great influence thus the main focus is placed on the cost of these systems. The devices chosen are the Palmsens 4 [111], Gamry Interface 1010T [112], PGSTAT 101 [113], μSTAT 200 [114], and the Dropstat [115].

A comparison is made by drawing up tables to summarise and compare their technical specifications where Table 2.1 refers to the voltage specifications of the device and Table 2.2 the current specifications.

After considering these tables it is concluded that the PGSTAT101 has the best voltage resolution throughout the devices, as well are the widest voltage range which is similar to that of the Palmsens 4, and is also the most accurate. A great advantage of the Gamry Interface 1010T is that it is capable of handling multichannel experiments enabling the

Potentiostat	**Voltage specifications**		
	Range	**Accuracy**	**Resolution**
Palmsens 4	$\pm 5V$, $\pm 10V$,	$\pm 1mV$ offset $\pm 0.1\%$	$12.5V$, $50V$, $200V$
Gamry Interface 1010T	$\pm 0.4V$, $\pm 1.6V$, $\pm 6.4V$	$\pm 1mV$ $\pm 0.2\%$ of setting	$75V$
PGSTAT 101	$\pm 10V$	$\pm 0.2\%$	$3\mu V$
μSTAT 200	$\pm 2V$	0.1%	$1mV$
Dropstat	$\pm 2V$	unavailable	$1mV$

Table 2.1: Table containing commercial potentiostats input voltage characteristics

Potentiostat	**Current specifications**		
	Range	**Accuracy**	**Resolution**
Palmsens 4	$100pA$ to $10mA$ (9 range settings)	0.1% $\pm 0.1\%$	0.0006%, $5fA$ for $100pA$
Gamry Interface 1010T	$\pm 100mA$ (6 range settings)	$\pm 5pA$ $\pm 0.3\%$ of setting	$\pm 5pA$ $\pm 0.3\%$ of setting
PGSTAT 101	$10nA$ to $10mA$	$\pm 0.2\%$	0.0006% of range setting
μSTAT 200	$1nA$ to $100\mu A$ (6 range settings)	unavailable	0.1%
Dropstat	$\pm 200\mu A$	unavailable	0.1%

Table 2.2: Table containing commercial potentiostats current characteristics

device to handle seamless data acquisition. The Palmsens 4 and the PGSTAT101 have the best potential ranges and the Dropsens devices are not well documented and features potential ranges 5 times less than its closest competitors.

The µStat is documented to be the most sensitive for measuring current. The Plamsens 4 is more accurate but the PGSTAT101 claims to have the best resolution. Most of these devices have their accuracy based on a specific current setting range where the current sensing circuitry is a determining factor, and is the ballpark current range is knoen the device can be focused on that range for a specific application. The more current ranges it is capable of the more functionality is has and is capable of handing more diverse experiments, with the Palmsens 4 at 9 current ranges. Changing the current range inherently switches between different current sensing resistors with the accuracy and resolution dependent on the technical specifications of the multiplexor circuit.

Most potentiostats are benchtop devices and are for use in specialised laboratory environments, and are usually not very portable. The consideration of weight and size is more applicable when looking at handheld devices which contains an internal battery

for the purpose o being portable. The Dropstat is a handheld device and the effect of its trade-offs can be witnessed in its specifications. However, the Palmsens 4 is not necessarily handheld but made portable with an internal battery, has Bluetooth functionality capable of executing experiments by smartphone and lastly, tops all devices in most specification categories. It weighs 500 grams which is relatively light to the devices in competition like the Interface 1010T at 2 kg, and the PGSTAT101 at 2.1 kg, and taking all into account it results in the best device in consideration.

2.4.3 Research Based Potentiostatic Devices

This section discusses the various potentiostatic devices developed for research purposes. The typical schematic is shown in Figure 2.30 as an extension to Figure 2.29 with the main components that makes up a potentiostat shown namely the input signal passing through a control amplifier to regulate the cell potential, a current sensing circuit to convert the cell current into a measurable format followed by a current coltage measurement.

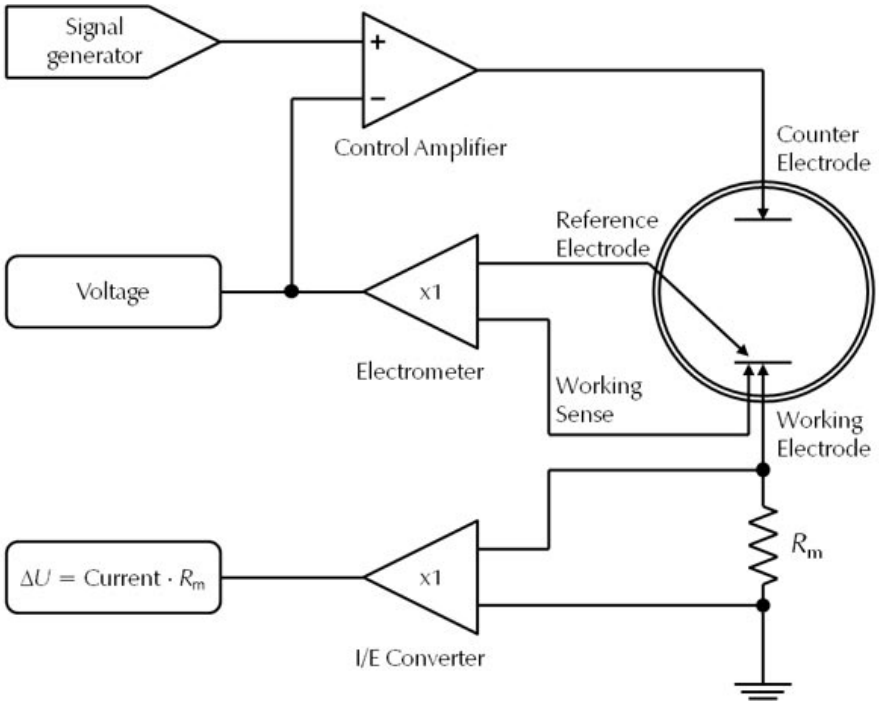

Figure 2.30: Simplified schematic of a typical potentiostat [116]

Figure 2.30 is only a basic representation of the fundamental components of a potentiostat with the accuracy, stability, resolutions and reliability of the measurements dependent on the more intricate details inside the components and is expressed in complex circuitry. The analogue circuitry handles the input and measured signals with the control and implementation executed by microcontrollers either communicating with personal computers or using its own built-in operation systems. The resolution of the system is largely dependent on the ability of the microcontrollers to generate analogue signals, hence the DAC's (digital to analogue converter) resolution and the measurement resolution dependent on the bit specification or the microcontroller's ADC's (analogue to digital converter). Advances in one aspect results in trade-offs in other with the following section considering 5 different research based potentiostats.

Dual Microprocessor Potentiostat

Huang et al. (2015) [107] reported in literature the development of a potentiostatic device utilising two different microprocessors to study the signal processing capabilities thereof. The processors worked in parallel and was used in conjunction with multiplexing resistors to select a current sensing range, with the one processor assigned for measuring and processing measurements and the other to generate the required excitation waveforms. Figure 2.31 shows the schematic circuit representation of this device.

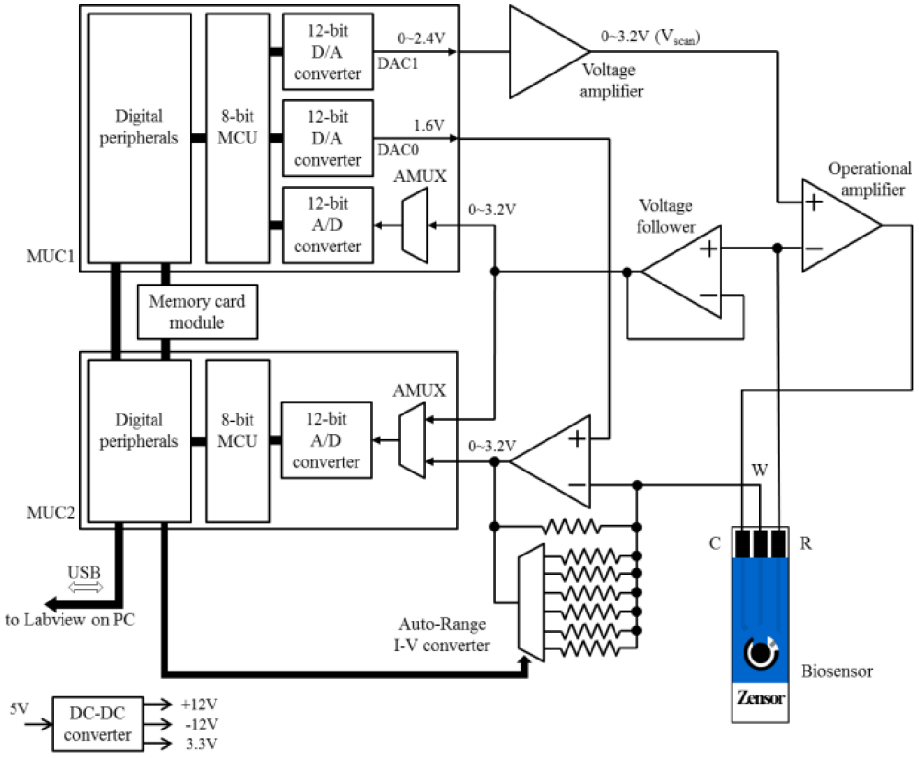

Figure 2. The circuit diagram of a portable potentiostat designed with dual-microprocessors.

Figure 2.31: Circuit diagram of a portable potentiostat using dual microprocessors [107]

Literature reported the developed device to have resulting specifications such as: A potential range of ±1.6 V with a resolution of 1 mV at a scan rate of 5 mV/s, and a current range from 16 to 160 mA at a resolution of 8 µA and 80 pA. All ADC's and DAC's have a 12-bit resolution using the C8051F005 microcontrollers with acceptable results when in comparison with commercial potentiostats.

Point-of-need Potentiostat

A research group in South Africa developed a potentiostatic device reported by Bezuidenhout et al. [117] by utilising an LMP91000 sensor by Texas Instruments [118]. The device operates by means of a voltage regulator controlling the upper and lower voltage range implemented by a microcontroller. The group utilised an Arduino Uno for control of the applied potential by taking the internal voltage supply of 5 V and using it as the source to set the reference voltage, making the device limited to a maximum potential range of 5 V up and down. To test the standard of the device its performance was compared to commercial potentiostats after executing experiments in 5 mM ferricyanide by means of cyclic voltammetry with 0.1 M KCl. The performance reference was based on the

repeatability of tests and analysing the average and standard deviation of 3 scan cycles using electrodes from Dropsens.

The group from the University of Pretoria developed the device with the LMP91000 sensor as the key component, being perfect for the application of a potentiostatic device due to its programmable analogue frontend. The accuracy of the device's current specifications is unknown as it is not well documented but features a current range from 5 to 750 µA and an applied potential resolution of 2%.

CheapStat

The main goal for the development of this potentiostat is to be cost effective, hence the name CheapStat by Rowe et al. [119], and comes from the motivation of being able to supply financially disadvantaged and underprivileged communities with a potentiostat for educational purposes. The hardware and software design was released as open source with the operation of various techniques such as cyclic, square wave and linear voltammetry tested. The confirmation of the device's functionality was done by analysing the response of cyclic voltammetry in an electrochemical setup using ferricyanide, as well as looking at its performance towards detecting the change in DNA sequence by means of square wave voltammetry. The microcontroller using for the device utilises an Atmel XMEGA featuring built-in ADC' and DAC's and the operational amplifiers best suited for this application was chosen due to their low input bias current and is the TLC2262CP by Texas Instruments. Using the same sensing resistor the specifications were documented with a current range of 100 nA tp 50 µA, with an applied potential range of -990 mV with a generated wave in the frequency range from 1 to 1000 Hz. The device is controlled by a personal computer with communication via the universal serial bus and weighs a total of 115 g.

Literature reports the device to function as expected after extensive testing was done but the accuracy and resolution of the system is not documented. The device was easily fabricated and a success towards a cheaply built potentiostat but would required some technological expertise for setup and is not very user friendly as a trade-off.

DStat

A potentiostat was developed by Dryden et al. [106] called the DStat with the motivation behind it towards building a user friendly device that doesn't require a high level of expertise and and bridging the gap of the knowledge in potentiostatic operation. The performance of the device was compared to that of the CheapStat with is achieving exceptional applied voltage resolution at the input as a result of a 16 bit DAC for wave generation with a 46 µV resolution. Via simulation and experimentation it was confirmed that the ADC's limitation is due to the signal step size and the system noise is thus negligible. Figure 2.32 shows the calculated standard deviation noise amplitudes of the system during testing while increasing the current to voltage gain, clearly justifying the 16 bit DAC's and ADC's.

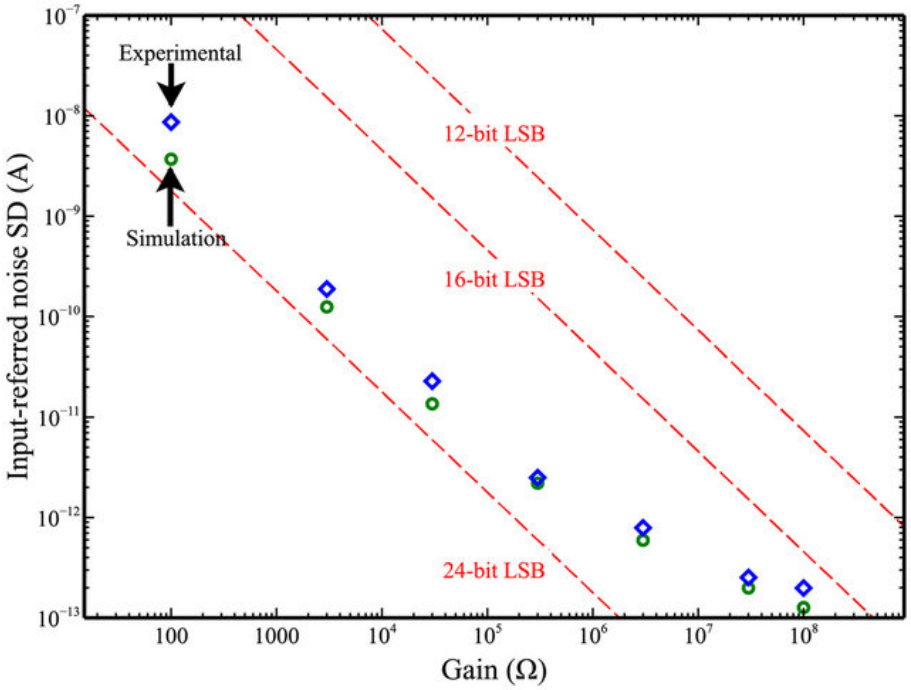

Figure 2.32: Graph showing DStat input noise amplitudes [106]

Towards the development of this device the circuitry was simulated to evaluate applied potential and output current errors and resulted in 1 nV and 50 fA. The control of the system is executed by an ATxmega256A3U microcontroller and is responsible for communication between the computer and the device where the device send measured data to the computer for analysis. The operational amplifiers was chosen by means of a large bandwidth, large open loop gain, low inut bias current and least noise, and the LMP7721 and LMP7702 were chosen where the latter was used for controlling the potential over the reference electrode as well as the feedback buffer, and the prior for the transimpedance amplifier.

UWED

Ainla et al. [108] developed the Universal Wireless Electrochemical Detector (UWED) to enable the usage of electrochemical tests in remote areas making portability a key requirement. Thus the system needed to be handheld, containing a battery and communicating with a smartphone via BLE (Bluetooth Low Energy) and works with an app where data is transmitted to for processing and analysis. The data is uploaded to a cloud server capable of processing the data. The device works by setting up a certain protocol and flashing the device with the supporting software. The drawback is that the supporting software for different protocols must be flashed first before a different protocol can be executed, limiting the device's capabilities if not in an environment where a new protocol could be uploaded. Figure 2.33 shows the setup and basic operation of the UWED.

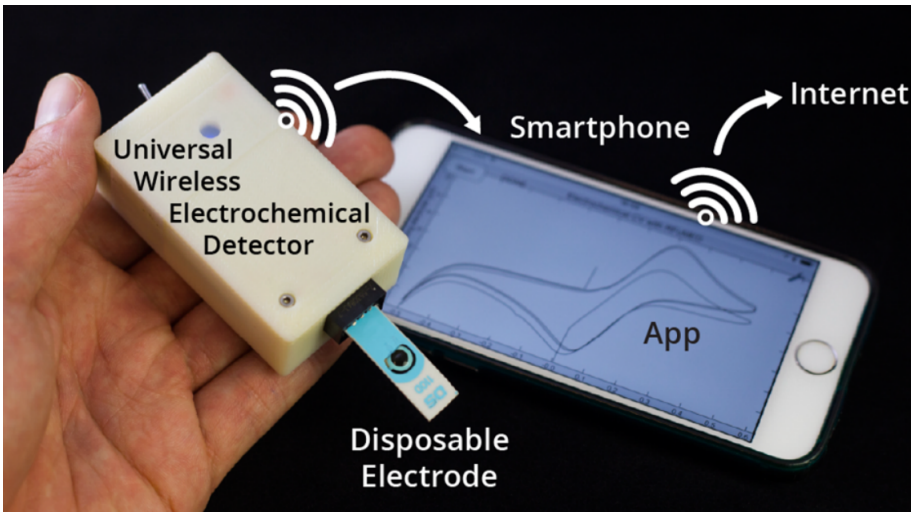

Figure 2.33: Image showing the experimental setup of the UWED [108]

The reported specifications of the device are documented to have a current range of 180 µA and voltage range of -1.5 V, using an Arduino microcontoller with a 10 bit analogue to digital converter. The noise is reported to be in the vicinity of 27 to 47 µV, the waveform generated by the digital to analogue converter was filtered for noise suppression, and all software and hardware design released as open source.

2.4.3.1 Conclusions

Upon review of the literature the highest influential aspect when considering potentiostatic devices as well as the key motivation towards making a conclusion, is the cost of the device. It is expected and clear that the commercial devices outperform the research based devices and is the result of a trade-off between cost versus performance. The research based devices were not well characterised and their specification not as well documented as that of the commercial devices making the comparison of accuracy and resolution much easier when data sheets are provided.

Potentiostats built in-house lack an accurate reliability test, for example when the response of a potentiostat is tested by making used of a dummy cell for cell calibration. The working understanding of potentiostats are explored with literature adding to the knowledge of the requirements and dynamics of these devices, but is required that the current sensing and applied waveform capabilities still be validated before integration.

2.5 Project Aims and Objectives

The main goal of this project is to prove that an electrochemical immunosensor is capable of detecting an autophagy related specific protein, LC3, towards the estimation of autophagy flux. The methods proposed are described below:

Sensor proof of concept

1. Acquire carbon nanofibre screen printed electrodes from Dropsens towards a sensor for proof of concept;

2. The modification of the working electrode for enabling antibody immobilisation by means of electrografting;

3. The activation of support groups created by electrografting through EDC/NHS crosslinking chemistry for the attachment of LC3 antibodies;

4. Electrochemical testing using the Palmsens 4 to execute square wave voltammetry for diagnosis;

5. Development of a data analysis algorithm for accurate signal processing and peak extraction.

Chapter 3

Methodology

This chapter discusses the designing process of a 3-electrode electrochemical biosensor for protein detection towards autophagy flux. A commercially manufactured screen printed electrode was modified for the detection of LC3-II. The methods of modification on the working electrode is explained such as sensor characterisation, electrografting and finally antibody crosslinking. Lastly a software algorithm was developed for accurate analysis of the voltammogram.

3.1 Biosensor Development

The modification process is described in this section for creating a functional biosensor and explains the experimental methods towards the characterisation of the unmodified commercial screen printed electrodes. The sequential steps for the process are as follows: the determination of the electrochemical window of the unmodified electrodes, the characterisation of the electrodes in ferricyanide redox couple with square wave voltammetry, an unmodified electrode reproducibility study, electrochemical reduction of the working electrode with diazonium salt, antibody crosslinking activation through the EDC/NHS protocol, and finally the attachment of LC3-II antibodies unto the working electrode.

The Palmsense 4 potentiostat was used for all electrochemical measurements done on the sensors. All square wave voltammetry measurements was executed in 100 µl of the suitable solution with the potentiostatic parameters as follows: 20 mV pulse size, 5 mV step size, 25 Hz and a 2 second equilibrium time. The potential range was varied for different experiments and are stated in text for each measurement, but all other parameters were set to be similar to that reported in literature[120; 121]. The time the electrochemical cell is held at the initial potential before the scan starts is known as the equilibrium time and is necessary for the migration of ions and the cell reaction to reach equilibrium before the scan starts and after the initial potential is applied. 5 mM $Fe(CN)_6^{3-/4-}$ in PBS(1X, pH 7.4) was used to form the ferricyanide redox couple. Due to the nature of some experiments the pH of the redox couple was changed but is stated in the text of those instances. A summary of the modification process is shown in Figure 3.1.

A diazonium salt mixture was used to electrograft the unmodified sensors through cyclic voltammetry with the purpose of creating functional carboxyl groups on the working electrode surface. The EDC/NHS protocol for crosslinking chemistry is then used for the activation of these functional groups. Subsequent to the activation procedure the LC3-II

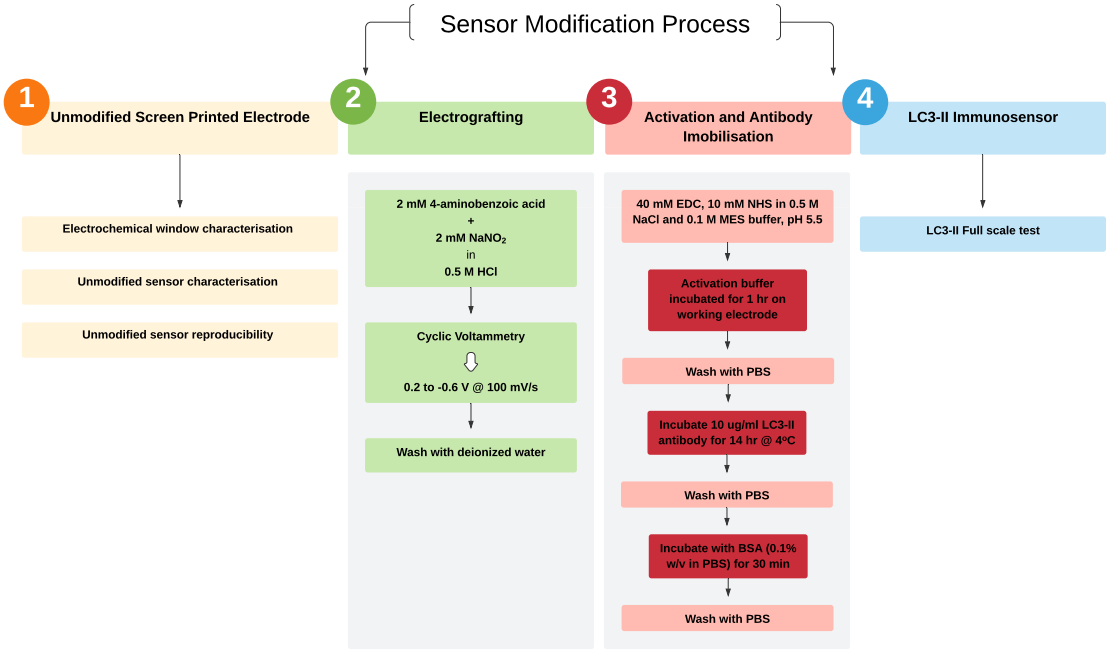

Figure 3.1: Overview of the modification process on a screen printed electrode for LC3-II detection

antibodies are incubated at 4°C overnight in order for the antibodies to attach to the activated functional groups. After BSA is used in the next step as a blocking mechanism where activated carboxyl groups are still available, the LC3-II immunosensor is finished.

3.1.1 Electrochemical Window Characterisation

Different aspects of the electrochemical setup is determined by studying the electrochemical window of the unmodified electrodes. The first is to verify that the redox couple can be accommodated by making sure the electrochemical window of the electrolyte is large enough. Next is to determine and verify that the formal potential of the redox couple is in the range that covers the redox peak generated by the square wave voltammetry experiment, and lastly to make sure that no other redox couple other than ferricyanide is present within the studied potential window. Three sensors were used for this experiment to verify the stability of these tests.

A new batch of ferricyanide redox couple was preconditioned following the method described in appendix A.1. To prevent bubbles from forming on the surface of the electrodes the solution for the specific test was used to wet the surface three times before the actual test was executed. This was done by using a pipette and the solution was removed by slightly tilting the sensor sideways enabling the solution to roll off. This method also removes any impurities that might have formed on the electrode surface, and in any other instance in the text the method of wetting refers to the above.

A cyclic voltammetry sweep from 1 to -0.6 V at a scan rate of 100 mV/s was performed to determine the electrochemical window of PBS. The oxidation and reduction potentials of the ferricyanide redox couple as reported in literature [121; 122; 123] were used to choose the limits to be well positive and negative. A cyclic voltammetry sweep

from 0.7 to -0.5 V at a scan rate of 100 mV/s was performed in the ferricyanide redox couple and again the oxidation and reduction potentials was chosen to be just outside that reported in literature. The potential window of both ferricyanide and PBS was studied and assessed through the voltammogram. The two results were then compared and the oxidation and reduction potential were determined, the method is shown in Figure 3.2.

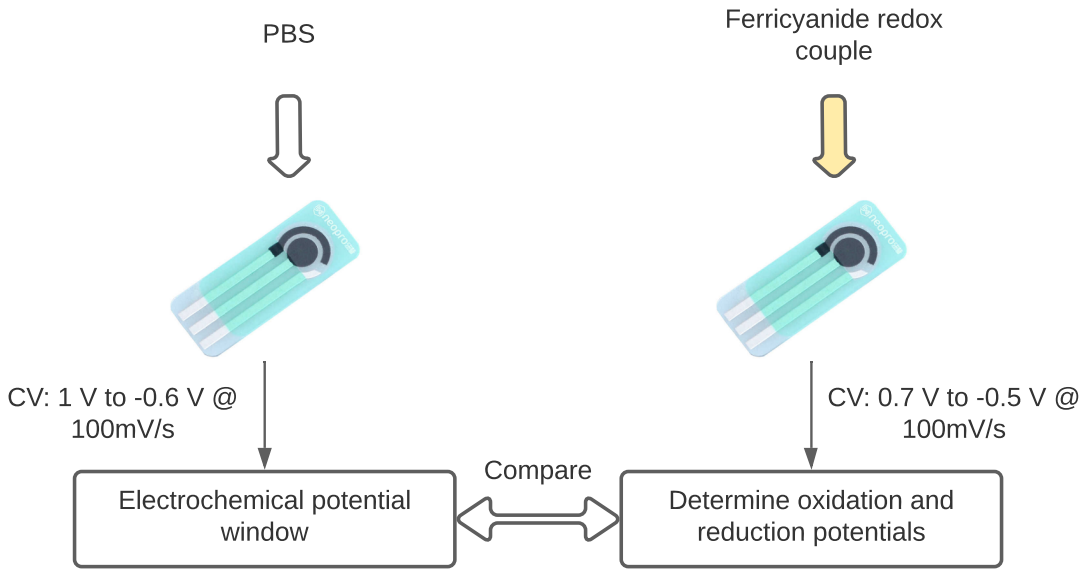

Figure 3.2: Method used for determining the oxidation and reduction potentials of the ferricyanide redox couple and the electrochemical window of PBS

The formal potentials of the setup was then determined by making use of (2.8) and plugging the oxidation and reduction potentials of the ferricyanide redox couple.

3.1.2 Unmodified Sensor Characterisation using Square Wave Voltammetry

New, unused carbon nanofibre sensors were used in order to select an adequate potential range for the ferricyanide redox couple so that the voltammograms can achieve a well define redox peak. The formal potentials of the ferricyanide redox couple as identified in the cyclic voltammetry scans in Section 3.1.1 were used to choose the scanned range to be well positive and negative with the potential range from 1 to -1 V. Three sensors were used to make sure of the stability and reproducibility of these tests.

Deionized water was used to perform the first test. With deionized water being the solvent in PBS this test is necessary to assess possible peaks produced within the scanned range. Next the contribution of PBS to the current response was evaluated by taking another unused, unmodified sensor. This is necessary for data analysis purposes where the scan in PBS with serve as a background scan to be subtracted from the scan performed in ferricyanide redox couple with more in depth discussion in Section 3.3. The final test was done in ferricyanide redox couple by performing a square wave voltammetry scan to

verify that the formal potentials as identified in Section 3.1.1 is close to the redox peak produced by the experiment. The method is shown in 3.3.

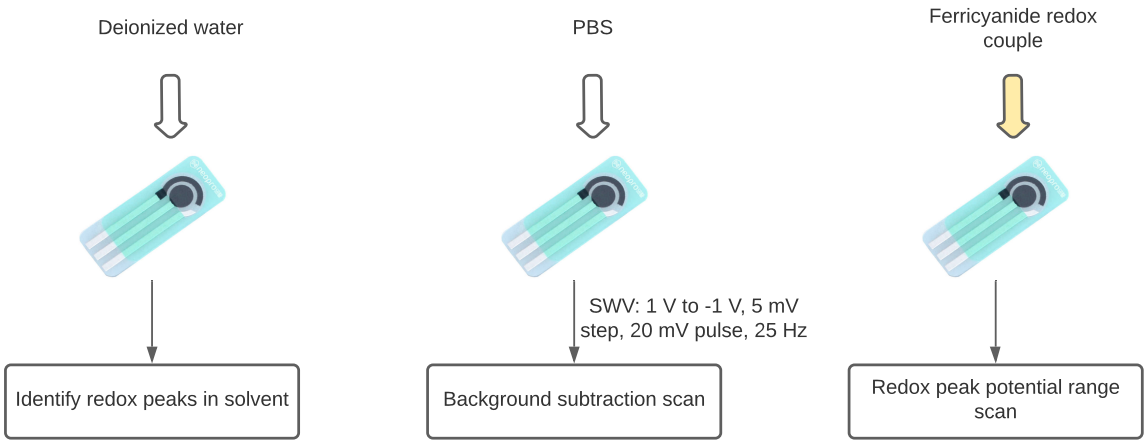

Figure 3.3: Method to identify formal potential range of square wave voltammery scans

The range where the voltammogram produces a well defined redox peak was used in order to determine the appropriate scan range for all future square wave voltammetry tests.

3.1.3 Unmodified Sensor Reproducibility

The reproducibility of the unmodified screen printed electrodes refers to each electrode reacting the same to yield the same test results when performing an experiment. It will verify that the commercial sensors are stable and more importantly, define the best method for comparing each phase throughout the modification steps. If the sensors are exactly reproducible then only one baseline scan result could be used that is taken before te modification process and can be used in all subsequent experiments. This will mean that the step of determining the baseline for each sensor would be removed with the advantage being to avoid possible contamination. The comparison of each experiment would then be with a shared baseline predetermined by a single sensor.

In the case where the sensors are not reproducibly then each sensor will need to be compared to its own baseline that would be determined prior to any experiments. Each sensor will then produce its own unique peak current where furthermore, the relative change from the predetermined baseline to the square wave voltammetry scan after each experiment will be of interest. The disadvantage of this approach is the possibility of the sensor being contaminated through the execution of extra steps, the degradation of the electrode surface due to the added time between experiments and degradation while washing between steps. This method is sub-ideal as it requires extreme care and adds more variables that increases the complexity of the analysis.

The assessment of the unmodified sensor reproducibility was performed by first preparing a fresh batch of ferricyanide redox couple and acquiring three new unused carbon

nanofibre sensors. Each sensor was wetted three times as described in Section 3.1 whereafter 100 µl of the redox couple was pipetted onto the sensors. A total of five tests per sensor was performed where the redox solution was removed through a slight tilting action and the sensor was carefully washed after each square wave voltammetry scan. This method avoids the build up of ions that could possibly contaminate the next reproducibility scan and the square wave voltammetry parameters were set to default as discussed in Section 3.1 with a scan range chosen to be from 0.6 to -0.4 V.

After assessing the results it was decided that a relative change in base current would be more accurate and that each sensor would be compared to its own baseline.

3.1.4 Electrografting of Diazonium Salt unto Unmodified Sensor

Carboxyl functional groups are required that will function as a supporting platform for the LC3-II antibodies so binding to the working electrode could be possible. The method of electrografting is used which creates carboxyl moieties on the working electrode surface by grafting a diazonium salt solution consisting of 4-aminobenzoic acid molecules. The method for the preparation of the diazonium salt solution is explained in appendix A.3. The final solution concentration was chosen to be that reported by literature [121] with 2 mM 4-aminobenzoic acid and 2 mM NaNO2 in 0.5 M HCl as the final diazonium salt solution. A fresh batch of ferricyanide redox couple was prepared for the validation scans.

A free proton is released from the hydroxyl group in the form of an H atom as the carboxyl groups dissociate in the solution and the remaining oxygen atom then owns a negative charge which will repel any negatively charged atom in the area. The ferricyanide molecules are negatively charged and can then be used to evaluate the degree to which these layers are formed. With more layers forming on the electrode surface more negatively charged carboxylic groups will be present causing a higher repulsion of the negatively charged redox probe. In turn this means that for each added layer the current response will have a lower redox peak. Logically more carboxylic groups is desirable due to more surface area for antibodies to bind, but as discussed more layers would reduce sensor sensitivity thus the optimal grafting cycles needs to be determined. To determine the number of optimal cycles three new unused carbon nanofibre sensors were acquired to perform scans of 1, 4 and 8 grafting cycles. A cycles is the grafting process of a cyclic voltammetry scan from 0.2 to -0.6 V and back to 0.2 V. The process of electrografting and baseline comparison is shown in Figure 3.4.

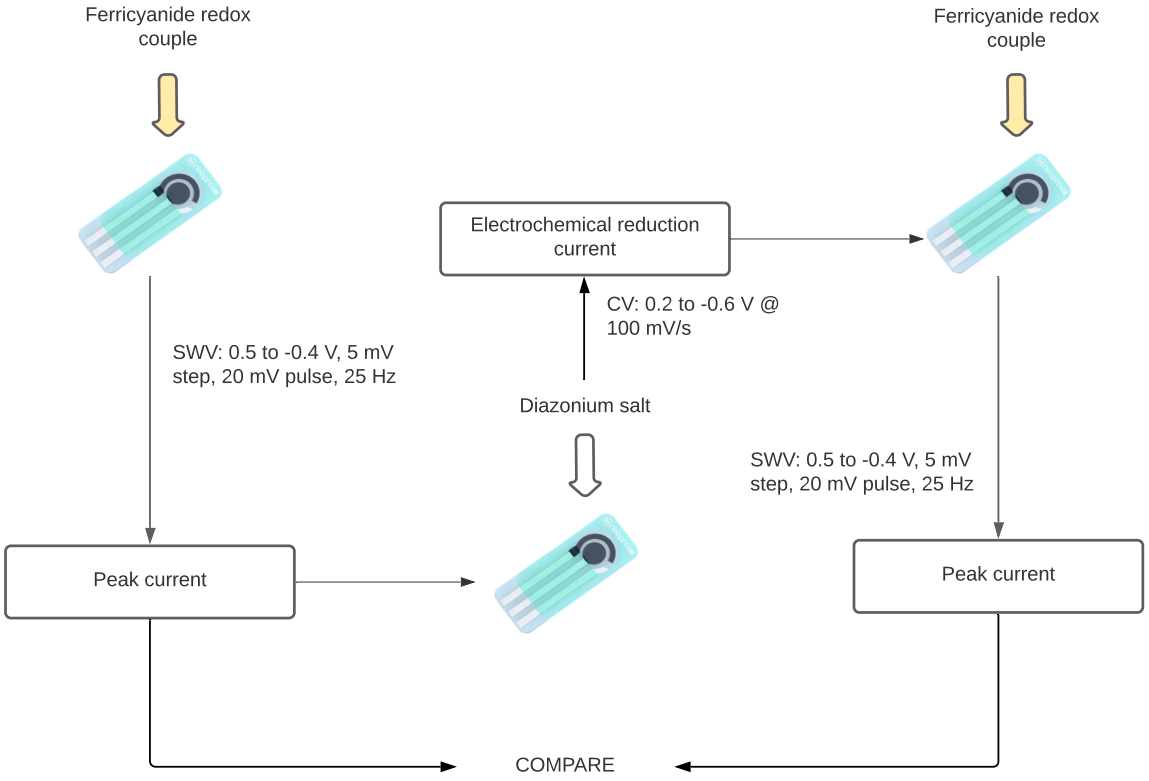

Figure 3.4: Method for electrografting with diazonium salt and verification. 1) Three square wave voltammetry scans were performed to obtain an average peak current. 2) The three sensors were scanned 1, 4 and 8 cycles respectively. 3) Again three SWV scans were performed to obtain an average peak current post modification. 4) Redox peaks generated in ferricyanide were compared.

In order to assess the effects of the grafting process and to determine an optimal number of grafting cycles a square wave voltammetry baseline scan was taken before and after the electrochemical reduction process. Each sensor was thus scanned in ferricyanide redox couple three times before grafting and three times after to retrieve an average peak redox current to assess the reduction in sensor sensitivity. The shape of each cyclic voltammetry scan could also indicate as the electrode surface approaches saturation. After the first baseline scan the sensors was washed in deionized water and left to air dry at room temperature before proceeding to the electrografting process. The sensor was washed by pipetting the sensor with water and holding it tilted allowing the water to freely roll off. After the sensor has dried a 100 µl of diazonium salt solution is pipetted onto the sensor covering the electrode area. A cyclic sweep is performed from 0.2 to -0.6 V and back to 0.2 V at a scan rate of 100 mV/s. After each sensor has completed its respective scans the sensor was again washed by drenching it with water using a pipette and having it air dry at room temperature. A final square wave voltammetry scan was performed in the redox probe to determine the redox peak after grafting and the peak results and cycle shapes were compared. Figure 3.5 shows how the working electrode changes as the modification step is applied.

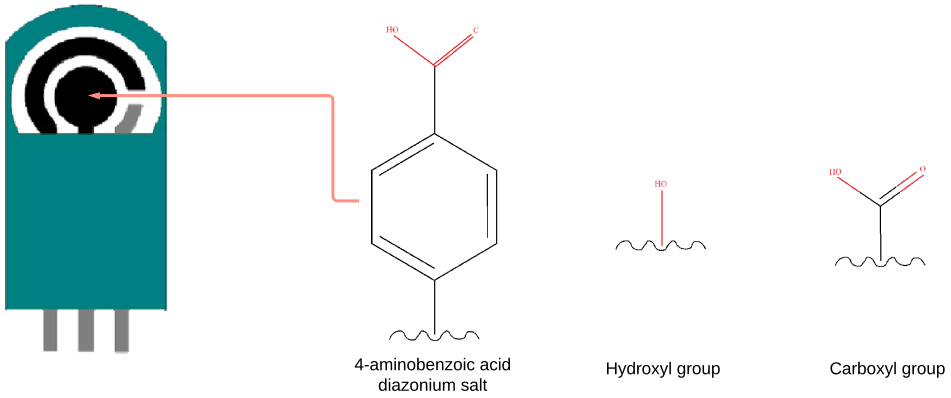

Figure 3.5: Diagram showing functional carboxyl groups on the surface of the working electrode

The diazonium salt molecules are now sticking from the carbon nanofibres and surrounds the carboxyl and hydroxyl groups. The number of cycles chosen based on these results was the number of cycles used for sensor modification in the future and is chosen to be the optimal number of cycle when performing the full scale tests.

3.1.5 Antibody Crosslinking

An immunosensor makes use of antibodies attached to the modified screen printed working electrode to capture a target specific protein. This section describes the procedure of protocols and steps used to covalently bind antibodies to the electrode surface by means of EDC/NHS crosslinking chemistry for the capturing of LC3 protein in a solution.

When considering the attachment of antibodies two key decisions are to be made regarding the incubation that is to say the duration, as well as the concentration of antibody incubation. The values chosen in literature differ depending on the application and method of crosslinking and vary between 100 ng/ml and 100 µl/ml, with ELISA kits mostly using a concentration of 2 µl/ml [43; 84; 124]. The study by Eissa et al. in 2017 where the efficiency of different carbon based sensors for the detection of SMN protein was explored, a concentration of 10 ug/ml was used [43], and is close to that commonly used by an ELISA kit which is a good standard for comparison regarding immunosensors. The incubation time also varies considerably where some incubated for 30 minutes and others overnight reported in literature with similar application [43; 124; 125; 126]. Longer incubation times will not have an external, unaccounted for influence on the efficiency of the sensor but most important that enough time is allowed for antibodies to attach and bind. Thus a concentration of 25 ug/ml of the antibody solution and an incubation time of 4 hours was chosen. The antibodies bind with an exponential decay and is assumed that the bindings taken place after 4 hours to have no noticeable effect, with the concentration ensuring enough antibodies to be present for LC3 capture. The antibodies were prepared by taking 15 ul anti-LC3 at 1 mg/ml in a vial and adding 585 µl of PBS resulting in an antibody solution of 600 µl anti-LC3 at 25 ug/ml. The antibody solution was then stored at -20°C while preparing for immobilisation. Appendix A.4 describes the procedure of preparation for the EDC/NHS crosslinking chemistry solution resulting in 40 mM EDC

and 10 mM sulfo-NHS in 0.1 M MES buffer with 0.5 M NaCl, with the concentrations chosen to be in the vicinity of that reported in literature [34; 43; 53; 127]. The antibody crosslinking solution, the activation buffer, is chosen to have a pH of 5.5 which is optimal according to the protocol by Thermofisher which reports the reaction to be most efficient between a pH of 5 and 6 , with the final solution volume to be 7.5 ml.

One full scale test was executed to test the working of the immunosensor where all solutions for electrografting and crosslinking was prepared in-situ as well as the antibody dilutions. A full scale test consists of the modification process of electrografting, the activation of the carboxyl moieties through EDC/NHS crosslinking chemistry and all the way to the final voltammetry scans after LC3 antibody immobilisation. The final electrochemical testing procedure is further explained in Section 3.2 with the immobilisation strategy explained next.

The full scale test made use of 18 carbon nanofibre screen printed electrode sensors for validation of antibody bindings at different antibody concentrations, and the testing of the immunosensor with different concentrations of LC3 protein. All sensors were modified using the method described in Section 3.1.4 and electrografted for 3 cycles whereafter they were washed with de-ionized water and left to air dry. The validation of electrografting is done in Section 3.1.4 and is assumed that the sensors are all successfully electrografted, thus no square wave voltammetry scans were executed on these sensors to avoid contamination and degradation of the electrodes. Furthermore, for linker activation 30 µl of the activation buffer were pipetted onto the working electrode of each individual sensor and incubated for 1 hour at room temperature in a water saturated environment. The water saturated environment prevents the activation buffer from evaporating allowing the water to evaporate first, and is as simple as placing a container in a layer of water and placing the sensors in the container. Figure 3.6 displays how the linker activation enables the carboxyl moieties to form amine-reactive sulfo- NHS esters on the CNF electrode surface. o-Acylisourea which is an unstable intermediate is formed as the carboxyl group couples with the EDC molecule, whereafter the coupling of the sulfo-NHS to this intermediate occurs to better the reaction efficiency and allow dry-stable amine-reactive esters.

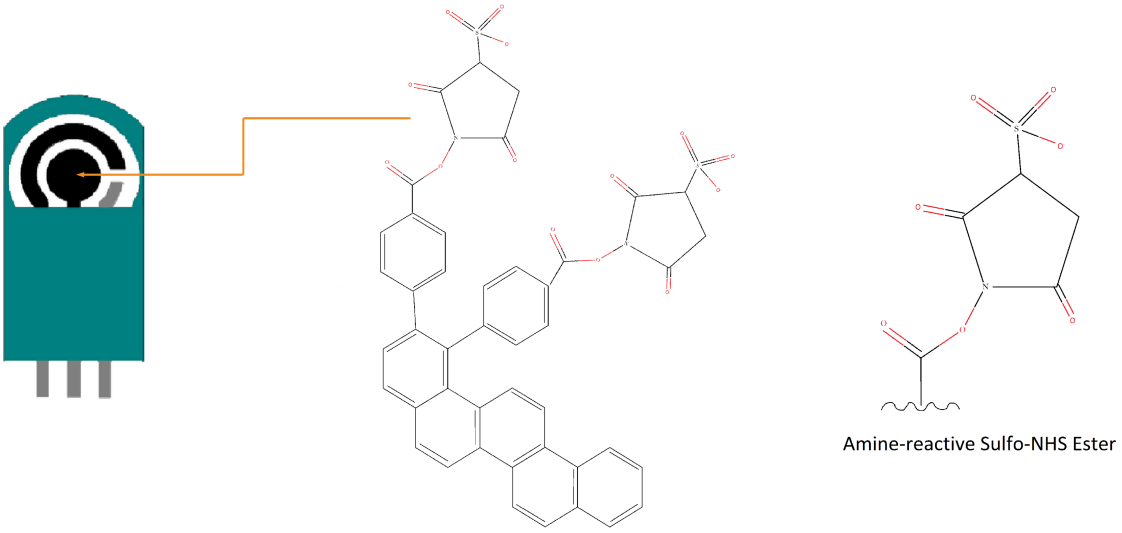

Figure 3.6: Diagram of the amine-reactive sulfo-NHS ester created by the activation buffer

Prior to antibody incubation the working electrode was washed three times with PBS in order to ensure none of the activation buffer is present as well as to raise the pH of the environment to 7.4. The EDC/NHS crosslinking protocol postulates that the amine-reactive sulfo-NHS ester environment have pH between 7.1 and 7.5 for reaction with the antibody. For antibody immobilisation a volume of 30 µl antibodies at 25 ug/ml was placed onto the working electrode and incubated for 4 hours in a water saturated environment. The incubation environment was kept at 4°C, whereafter the remaining unbound antibodies was removed by carefully rinsing the electrodes with PBS. To prevent non-specific proteins from binding to the surface and induce noise a blocking step is performed. The step ensures that there are no more available amine-reactive esters where binding did not occur and increases the specificity of the immunosensor. This step requires a 30 µl droplet of tris(hydroxymethyl) aminomethane placed onto the working electrode and incubated for half an hour at room temperature in a water saturated environment. Furthermore, a washing step with TBST is performed to remove any unbound tris on he sensors and stored at -20°C where they are ready for LC3 detection. Figure 3.7 shows an illustration of the complete CNF working electrode displaying primary amine groups on the lysine residues of the LC3 antibody which have formed covalent bonds with the carboxyl groups, as well as the bound tris filling the remaining active amine esters.

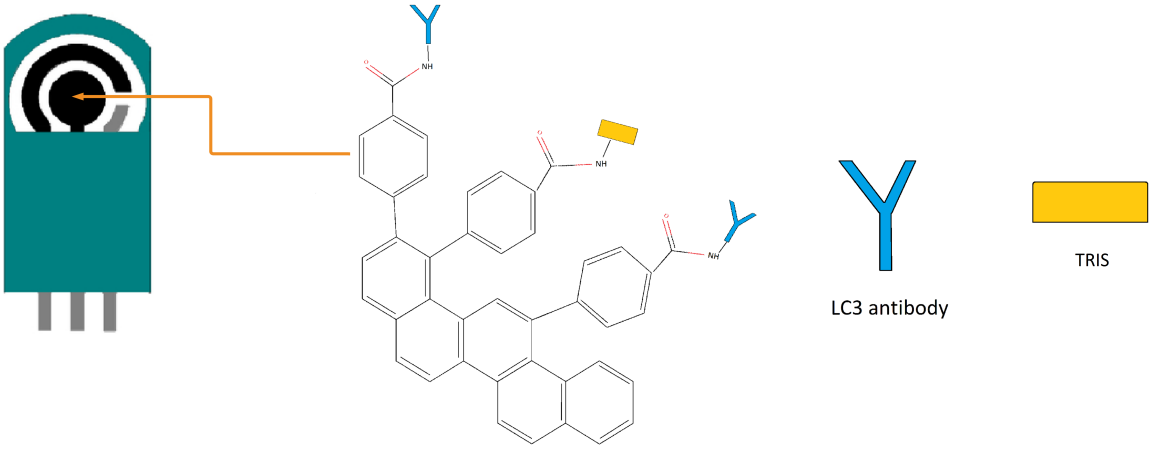

Figure 3.7: Diagram of the final immunosensor showing bound LC3 antibodies and BSA

The pH of the PBS in which the antibodies was prepared was kept at 7.4, ensuring the antibodies to be more positively charged in the solution resulting in them to have an increased attraction to the negatively charged sulfo-NHS ester groups. The isoelectric point is the pH at which the antibody will have no net charge and is reported to be more or less 7.5 for the antibody [128], meaning that a pH lower than 7.5 will result in it being more positively charged. The crosslinking protocol by Thermofisher requires a pH between 7 and 8 for optimal bindings, thus the pH was not moved below those limits. A 100 µl droplet of PBS was added to the sensors when stored to keep them in a physiological environment for preservation.

3.1.6 Fluorescent Validation Study

Before the full scale testing procedure was executed for testing the working of the immunosensor, a fluorescent study was undergone to confirm the successful binding of anti-LC3 onto the carbon nanofibre electrodes. The study would also exploit the effects of square wave voltammetry scans on the antibody bindings, ensure that the antibodies are not washed off and if these effects are of influence. A secondary antibody able to bind to a primary rabbit monoclonal antibody (where LC3 falls in this category) is required. A secondary fluorescent anti-rabbit IgG Alexa Fluor®488 antibody was chosen to be sufficient for binding to the immunosensor surface.

A total of 4 carbon nanofibre sensors were used in the fluorescent study. The first three was used to analyse the binding of three different anti-LC3 concentrations with concentrations of 10, 25 and 50 µg/ml respectively, and the last sensor used as control without any modification to determine any autofluorescence. The modified sensors were electrografted for three cycles each using the method described in Section 3.1.4 whereafter they were treated for linker activation via EDC/NHS crosslinking chemistry following the same antibody attachment procedure described in Section 3.1.5. After the tris blocking step the sensors were preserved in PBS and kept on ice where they were each retrieved and scanned with 3 successive square wave voltammetry cycles with parameters 5 mV step size, 20 mV pulse size and a scan range of 0.5 to -0.4 V at 25 Hz. After carefully

rinsing off the remainder of ferricyanide with TBST the secondary antibody was attached and incubated with a 100 µl droplet for 1 hour allowing binding to the primary antibody to occur. Subsequent to the fluorescent marker incubation the sensors were washed with TBST and placed onto a microscope slide. Only one unmodified sensor was used as a control test. The purpose of this test was to analyse the autofluorescence of the carbon nanofibre material and see if there is any possible fluorescence that the confocal microscope might pick up that could influence the data retrieved when assessing the sensors with the attached primary and secondary antibodies.

Live cell imaging was performed using a Carl Zeiss (Oberkochen, Germany) confocal microscope equipped with a humidified chamber at 37°C supplemented with 5% CO_2. The raw image stacks/series was acquired using a high NA objective (Olympus Plan APO N 60x/1.42 Oil/0.17/FN26.5) using an Argon multiline laser 25 mW at 488 nm and Diode 405 nm CW/PS and 633 nm laser as a light source with a GaAsP detector. Laser power and master gain were chosen for 405 nm (LysoB), 488 nm (GFP), 514 nm (LysoR) and 633 nm (SiR Tubulin) to ensure an optimal signal/noise ratio with minimal pixel saturation. Track filters were set as follows; LysoB: 410-471 nm, GFP: 490-597 nm, LysoR: 566-690 nm and SiR Tubulin: 638-759 nm.The study was limited to only 1 sensor for each concentration due to a shortage on sensors and was assumed that all other sensors would react in a similar fashion.

3.2 Electrochemical Immunosensor Measurements with Palmsense 4

This section describes the process of LC3 protein immobilisation and the procedures for running the full scale tests on the immunosensor. Figure 3.8 shows the a diagram of the method used in executing the full scale test.

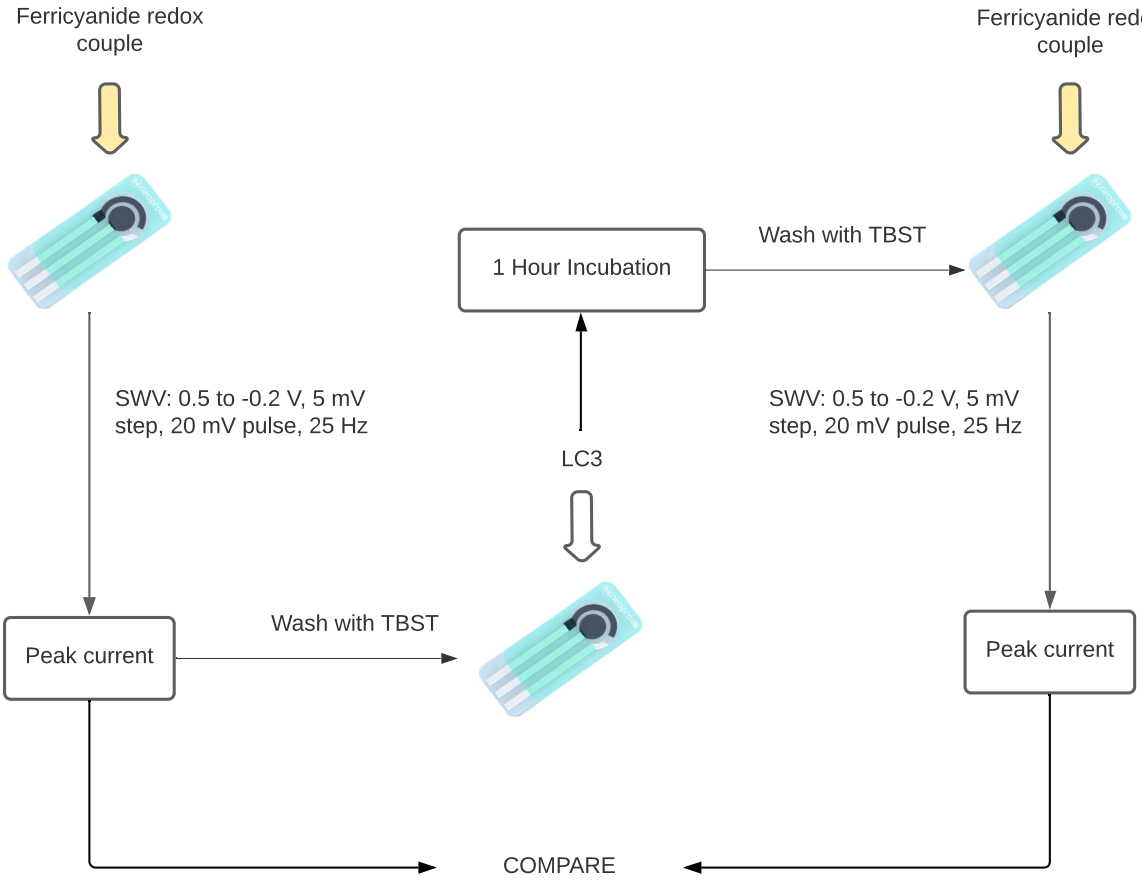

Figure 3.8: Method for performing the the electrochemical test for immunosensor functionality validation

Prior to protein immobilisation the sensors were prepared by first washing them with PBS and scanned in ferricyanide redox probe to obtain a baseline peak current. 3 Square wave voltammetry scans were executed to ensure the sensors have a stable response whereafter they were washed with TBST and incubated with LC3 protein for 1 hour. After incubation the sensors were washed with TBST to remove any unbound proteins and again scanned in ferricyanide to obtain the resulting peak current after LC3 immobilisation. The lab setup is shown in Figure 3.9 with the measurements executed using the Palmsens 4 and screen printed electrodes from Dropsens held by a DRP-CAC cable connected to the potentiostat.

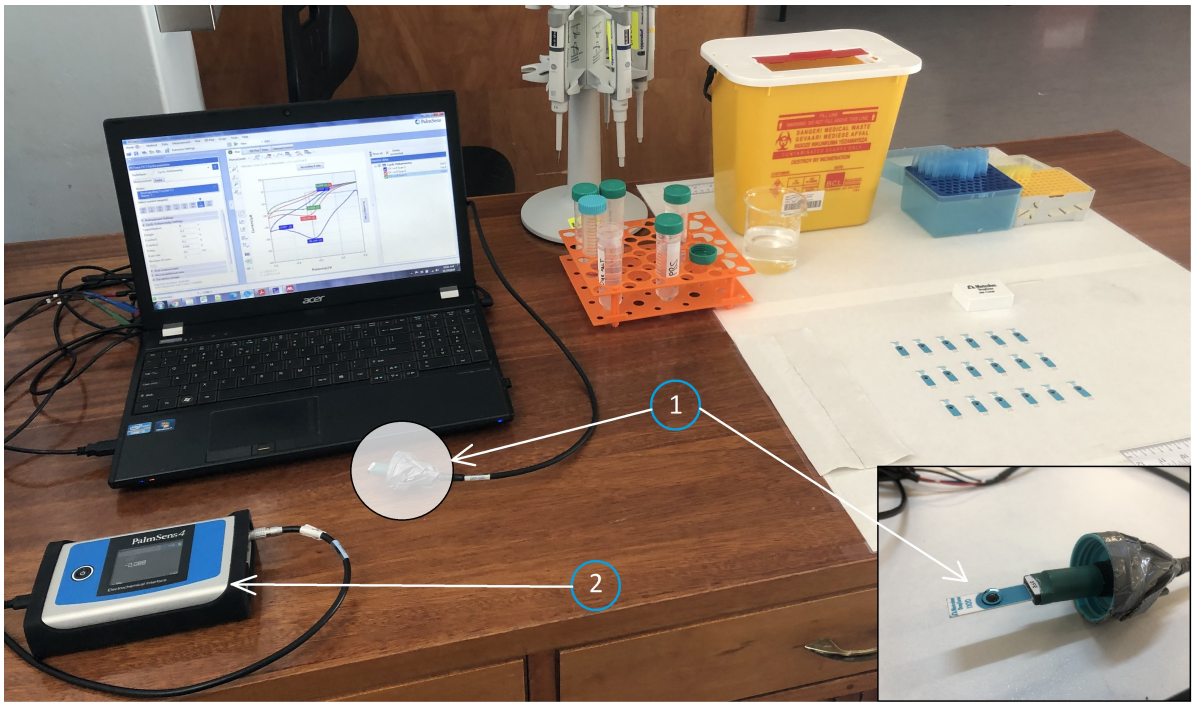

Figure 3.9: Image showing the electrochemical setup. 1) shows a CNF Dropsens sensor connected to the DRP-CAC cable and 2) shows the Palmsens 4 used for running experiments

3.2.1 Measurements using Square Wave Voltammetry

To test the response of the immunosensor a wide range with different concentrations of LC3 proteins are incubated, expecting a linear range of peak current response to use as calibration. A longer incubation time allows for more protein to be captured by the antibodies but will reach a point where more time results in little effect, thus an optimal period of protein incubation is to be chosen. A wide range of incubation periods are reported by literature with times varying from 15 minutes [84; 125], to 30 minutes [47; 124; 129] to 1 hour [130] for similar immunosensor applications. Eissa et al. [43] executed an experiment to determine the optimal amount of time required for effective protein immobilisation experimenting with a range of incubation times from 10 to 50 minutes, resulting in an optimal time of 45 minutes. Due to limited time and electrodes the experiment could not be reproduced and was decided to use an incubation time of 1 hour allowing enough time for most proteins to bind.

A total of 18 carbon nanofibre immunosensors were used to test a range of 6 different concentrations and using 3 sensors per concentration for the full scale test. Multiple sensors were used per concentration to obtain an average sensor response as well as a statistical variation for each sensor grouping. The protein dilutions was prepared by first taking 2 µg of LC3 protein in 20 µl solution buffer resulting in a stock concentration of 100 µg/ml. The solution was further diluted by adding 180 µl of PBS in the vial resulting in 200 µl of LC3 at 10 µg/ml which was the highest concentration used for the full scale test. The solution was further diluted with PBS and placed in a new vial for each concentration and stored at 4°C with the dilution procedure described in appendix A.7 whereafter they were labelled to be ready for immobilisation. The experimental setup for each concentration used is expressed in Table 3.1 for all CNF sensors. Ferricyanide was

prepared in situ prior to protein immobilisation with SWV parameters 20 mV pulse size, 5 mV step size, 0.5 to -0.2 V, 25 Hz and 2 seconds equilibrium time for electrochemical experiments with the Palmsens 4.

Grouping	Sensors	LC3 Concentration
1	1-3	10 ng/ml
2	4-6	100 ng/ml
3	7-9	500 ng/ml
4	10-12	1 µg/ml
5	13-15	5 µg/ml
6	16-18	10 µg/ml

Table 3.1: Experimental setup for LC3 immunosensor full scale test.

First a baseline peak current is established for all sensors before LC3 protein immobilisation by executing four consecutive square wave voltammetry scans without interfering with the redox couple. Following the baseline scans the sensors are carefully washed with TBST to ensure non of the redox couple is left behind. After the washing step a 30 µl droplet of LC3 is pipetted onto the sensor for each specific concentration and incubated for 1 hour in water saturated environment. Another TBST washing step is performed to remove any unbound LC3 and the sensors stored at $4°C$ awaiting its SWV scan. A diagram to show the binding of LC3 is shown in Figure 3.10 as a result of protein incubation.

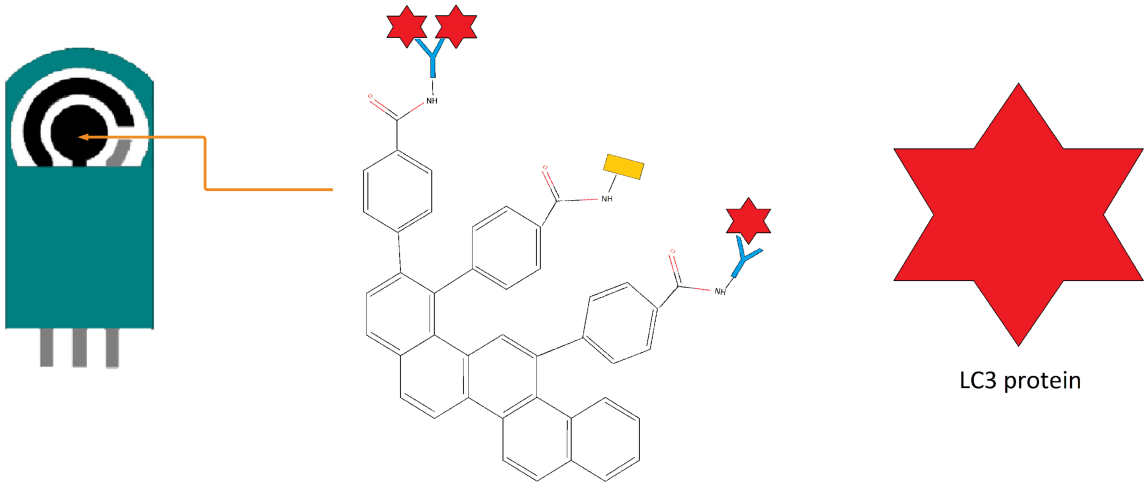

Figure 3.10: Diagram of the final immunosensor showing captured LC3 proteins

After protein immobilisation a final square wave voltammetry test is required to determine the change in peak current by performing another four consecutive scans in the same untouched redox couple. The tests were performed in groupings of the same LC3

concentration with three sensors per concentration stored in the same water saturated environment, starting the tests at the lowest (10 ng/ml) and moving up to the highest (10 µg/ml). The first scan before and after LC3 immobilisation was not as reproducible as the ones that followed thus a further three scans were performed. The average of the last three scans were used as a comparable measure by taking the difference of the two averages. The mean of three different sensors' percentage change of the averages before and after immobilisation was plotted on a logarithmic scale versus LC3 protein concentration. The resulting data was used to evaluate the response of the immunosensor with the standard deviation between of three sensors per concentration also plotted using error bars.

Prior to the full scale test a validation step was included to evaluate the binding of antibodies on the working electrode. This was done by incubating 3 different concentrations (10, 25 and 50 µg/ml anti-LC3) and binding a secondary to them for fluorescent assessment. This was to ensure the SWV scan prior to protein immobilisation does not wash off any antibodies and to make sure the antibody immobilisation process worked as expected. The procedure followed for fluorescent assessment is described in Section 3.1.6.

3.3 Data Analysis

Square wave voltammetry in a redox probe produces a peak current which is used as a comparison to different experiments and is the main determination factor. The raw data of a voltammogram produced by square wave voltammetry is rendered useless of not filtered and processed due to certain elements embedded in the signal. System noise that enters through digital data sampling is the most common of these elements but can be countered by implementing a simple low pass filter assuming the signal to noise ratio is not too high. Other elements that also play a major role in the peak analysis of the electrochemical reaction is the start up current as well as the general trend, resulting in a method of analysis which will look at relative change instead of absolute values.

Certain algorithms are developed towards the purpose of optimising specific parameters and extracting necessary features hidden from the naked eye. Practical examples of electrochemistry in recent years have produced research in transformation algorithms with the application and operation of these algorithms to extract information without losing any important data. The algorithms include specifically digital low pass filters for curve smoothing and baseline correction. A knowledge of signal processing is necessary before its application but Section 3.3 explains certain methods used to remove undesirable distortion and background data and how the key elements of the curve is extracted through implementing powerful signal processing techniques.

Data Framing

The start up current can clearly be observed as shown in Figure 3.11. These data points causes the baseline correction algorithms to draw a faulty baseline due to the change in minimum or maximum points but has zero effect on the redox peak generated. The current increases as a potential is applied at the start up of the experiment and reaches an equilibrium reacting similar to a charging capacitor.

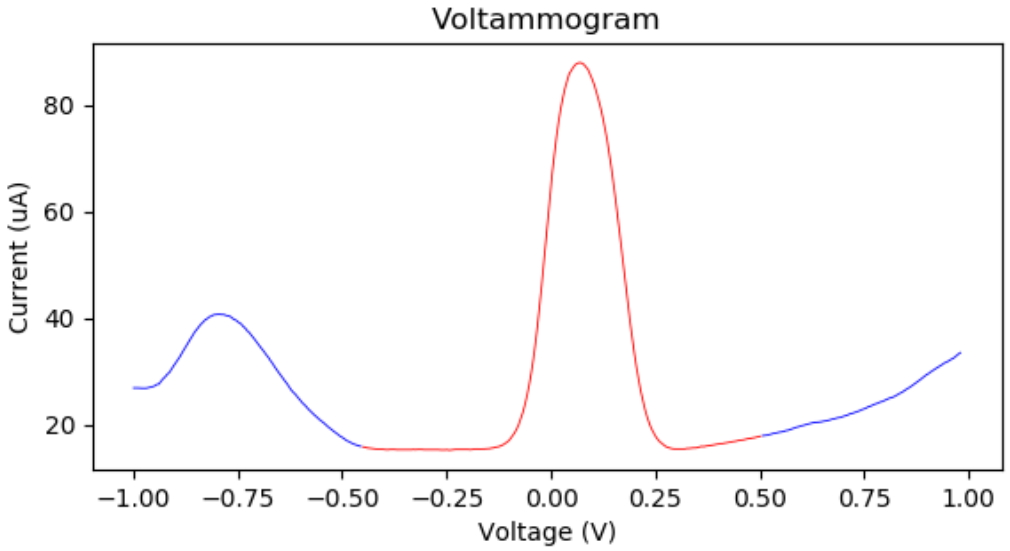

Figure 3.11: Figure indicating the framed section of the data, the blue data points to be discarded and the red data points to form the remaining data set

Without having any effect on the desired data the start up current was removed and framed out as shown in Figure 3.11 in order to determine the signal baseline.

Smoothing Filter

A low pass filter is applied to the data to get rid of any noise that entered the system and to smooth out the signal. A Savitzky-Golay filter is a widely used filter for signal smoothing and is the standard for similar experiments due to the focus on preserving the signal's original form by employing convolution. This method uses a polynomial function to approximate the fundamental signal and opposes the approach of a moving average technique. The smoothing filter exploits the method of a least squares fit by fitting the curve with a polynomial of a certain degree and focuses on a small frame of specific data points. After a fit is complete it moves on to a next frame with the same amount of data points and by this iterates through he curve, each time including the next data point. By increasing the polynomial order the curve will look more like the original, and likewise with a polynomial decrease the curved will be more smoothed out.

Professional software created by groups that specialises in electrochemical study such as Gamry EchemAnalyst, uses a 16 data point frame with a 4^{th} polynomial order and is the parameters used in the majority of experiments. It was chosen to use the same parameters for signal smoothing by utilising the *scipy* package in Python and employing the filter. Figure 3.12 shows the effect of the applied filter.

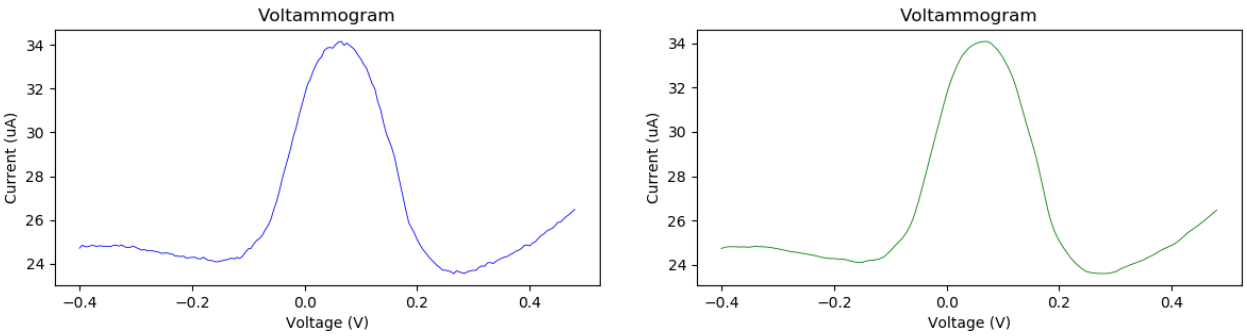

Figure 3.12: Figure showing data before (blue) and after (green) subjection to the Savitzky-Golay filter

Background Subtraction

Background subtraction is sometimes necessary to get rid of unwanted redox peaks that can contaminate the data and bares no value, and depending on the solution used can infiltrate the voltammogram. The solvent used for ferricyanide is PBS, thus 100 µl of PBS is added onto the sesnor and a square wave voltammetry background scan is done showing no contribution of the buffer. Performing this experiment with carbon nanofibre sensors shows the subtraction of the buffer solution current (blue) from the ferricyanide couple current (green) has zero effect on the measured redox peak and can be seen in Figure 3.13.

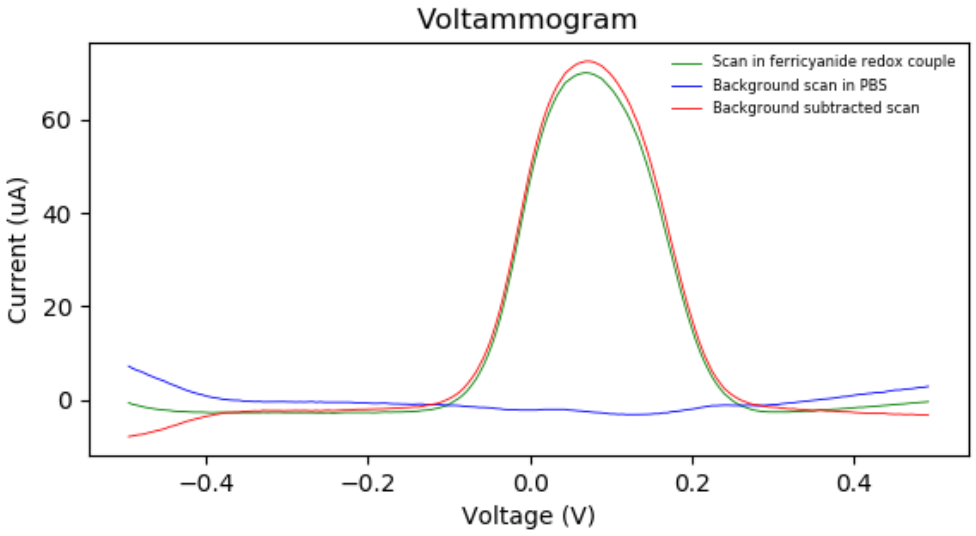

Figure 3.13: Resulting background subtraction scan with PBS vs $Fe(CN)_6^{3-/4-}$

All sensors were tested in the same redox couple solution and was assumed that they would have no unwanted redox peaks. The result of the solution buffer scan is dependent

on the supporting electrolytic couple, but since the background subtraction shows no clear effect and the supporting electrolyte remains constant it was assumed safe to remove this step from future testing.

3.3.1 Baseline Analysis Methods

The relative change of the current generated measured from the signal baseline to the redox peak is the value that needs to be assessed for analysing the voltammogram. An amplitude shift is usually present throughout the entire signal and is due to additional reactions and the sensor's overall capacitance. In order for the data to be useful these induced amplitude shifts needs to be compensated for by determining the signal's baseline and calculating the relative change of the redox peak. This section describes methods for extracting the baseline of an electrochemical experiment signal.

3.3.1.1 Inflection Point Baseline Identification

A straightforward method for determining the baseline of a signal is the inflection point baseline analysis. After applying a smoothing filter as discussed in Section 3.3 the next step would be to find and identify the inflection points on both sides of the redox peak. First the peak is located which was assumed to always be in the vicinity of 0.0 to 0.2 V, whereafter the algorithm travels from this point to the left and afterwards also to the right and calculates the gradient between these points. As the algorithm moves to the right the inflection point is identified as soon as the selected point has a positive gradient and likewise, as it moves to the left the inflection point will be at the instance where to gradient becomes negative. The identified peak and inflection points are shown as dots in Figure 3.14. The baseline is then drawn as the two inflection points are connected through a straight line.

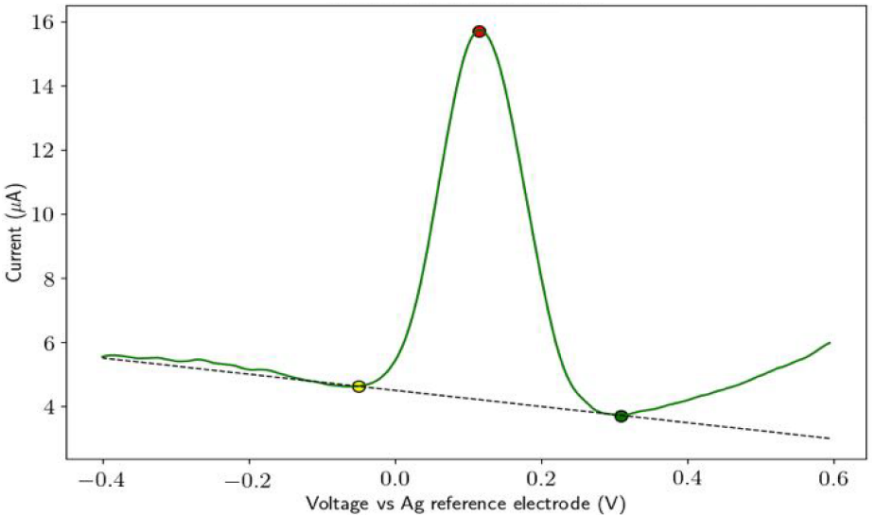

Figure 3.14: Computing of Inflection Point Locations [110]

After the baseline is created the baseline data points is subtracted from the filtered data points which places the inflection point the the y-axis origin. The absolute measured peak value is now the relative change of current from the baseline to the redox peak. However, this method is very limited as it can only handle a minimum and maximum of

2 inflection points and will not work for if the data set has more unwanted peaks or if the frame taken of the set does not contain at least 2 inflection points. A more automated algorithm is required for this type of signal processing.

3.3.1.2 Asymmetric Least Squares Baseline Correction

The asymmetric least squares (AsLS) method is a method proposed by Eilers in 2005 which is based on Whittaker smoothing and is not dependent on the number of inflection points, hence it can generate all square wave voltammetry baselines. A supposed vector $y = y_1, y_2, ..., y_i$ is defined as i, which is the frequency domain spectral intensities [131]. The smoothing sequence $z = z_1, z_2, ..., z_i$ follows y. The least squares function is then simplified:

$$F = \sum_i (y_i - z_i)^2 + \lambda \sum_i (\Delta^2 z_i)^2 \tag{3.1}$$

with $\Delta^2 z_i = (z_i - z_{i-1}) - (z_{i-1} - z_{i-2}) = z_i - 2z_{i-1} + z_{i-2}, i \in [1, 2, 3, ..., m]$, Δ is a second-order differential operator[131]. The factor λ is established to adjust the counterweight between the smoothness and fitness. Lastly, the vector w is characterised as the weights of fitness and the minimized function is established accordingly:

$$F = \sum_i w_i (y_i - z_i)^2 + \lambda \sum_i (\Delta^2 z_i)^2 \tag{3.2}$$

with (3.2) simplifying to

$$(W + \lambda D^2 D)z = Wy \tag{3.3}$$

with $W = diag(w)$, W is the diagonal matrix for vector w, T identifies as the transpose of a matrix, and D is the second order differential matrix: $Dz = \Delta^2 z$.

Generally, a lighter smoothing is capable of removing the noise, otherwise, stronger smoothing can eliminate the true signal. Too much weight on smoothing could be destructive to the original signal but is necessary to remove background noise. In order to identify the true background a more complex and accurate function is required that focuses on the deviations in the positive path. However, the positive and negative residual weights $y - z$ are the same for the Whittaker smoother. Therefore, a key parameter of asymmetric least squares for baseline correction, $p(0 < p < 1)$, is established and calculated: $w_i = p$ if $y_i > z_i$, otherwise $w_i = 1 - p$ [131; 132].

The following function was built in Python and produces the baseline of any given curve using Asymmetric Least Squares fitting as discussed,

```
def baseline_als(y, lam, p, niter=10):
    L = len(y)
    D = sparse.diags([1, -2, 1], [0, -1, -2], shape=(L, L - 2))
    w = np.ones(L)
    for i in range(niter):
        W = sparse.spdiags(w, 0, L, L)
        Z = W + lam * D.dot(D.transpose())
        z = spsolve(Z, w * y)
        w = p * (y > z) + (1 - p) * (y < z)
    return z
```

and is the preferred method for baseline correction. It combines a smoother with the asymmetric weighting of deviations from the smooth trend to form an effective baseline estimation method with it being powerful and non-destructive.

3.4 Final Statements

The purpose of this chapter is to take the choices made upon the study of reviewed literature and discuss in detail how the design and modification methods was used to develop an LC3 selective biosensor. Choices were made regarding the type of biosensor, transducer material, as well as measuring technique. For the purpose of this project an electrochemical biosensor was chosen to be most applicable, using carbon nanofibres as the electrode material and applying square wave voltammetry for final measurements.

Before any modification took place some parameters of the electrochemical setup was required and determined by experimentation leading to a study of the electrochemical window. The methods used for determining the parameters and redox potentials are explained in detail as well as how the sensors were characterised before modification. The modification process involved electrografting of diazonium salt molecules onto carbon nanofibre electrodes to form carboxyl support groups on the working electrode, followed by EDC/NHS crosslinking chemistry discussing how these methods are used for LC3 antibody immobilisation. The process of fluorescent validation is discussed followed by the exact operation of how the final full scale test was executed. Lastly the chapter shows how the produced data was handled by software algorithms to extract relevant information and proves that the algorithm does not alter important aspects of the measurement.

This chapter is a step by step ‘walk-through’ of exactly why and how each method was executed for the development of an electrochemical immunosensor using square wave voltammetry. The findings produced by these methods are discussed in chapters 4 and 5.

Chapter 4

Results

This chapter discusses the findings produced during the development process of the LC3 electrochemical immunosensor. The data generated while characterising the sensor is expressed and explained, followed by the results produced for the electrografting process. Further the validation of successful antibody crosslinking is discussed and finally the immunosensor LC3 calibration curve response.

4.1 Metrohm Dropsens 110D Sensor Results

The characterisation of the sensor produced by Metrohm Dropsens was executed using square wave and cyclic voltammetry waveforms produced by the Palmsens 4. The characterising of the electrochemical window, the determination of the voltage required for square wave voltammetry as well as the results of the sensor reproducibility tests is displayed. The effects of different electrografting cycles was explored and also validates the modification method which is followed by the results of the immunosensor response.

4.1.1 Electrochemical Window Characterisation

The voltammogram generated shown in Figure 4.1 is the result of executing a cyclic voltammetry scan in PBS and the supporting electrolyte, ferricyanide, to determine the electrochemical window of the immunosensor setup. The curve generated in PBS (blue) demonstrates that the buffer has marginal contribution to the current in the voltammetry range with rapid oxidation and reduction only occurring at -0.5 and 1 V, meaning the window for the supporting electrolyte is about 1.5 V. A cyclic scan with the supporting electrolyte (red) in the potential range of 0.7 to -0.5 V shows reduction with is peak in the vicinity of -0.1 V and oxidation occurring at about 0.3 V, resulting in a formal potential at 0.1 V. The study of shows that the PBS solution buffer is adequate as it does not effect the oxidation and reduction peak currents of the redox couple. Identical peak currents is expected with slightly different results that could be due to human measurement error, with identical peaks suggesting the the experiment is reversible.

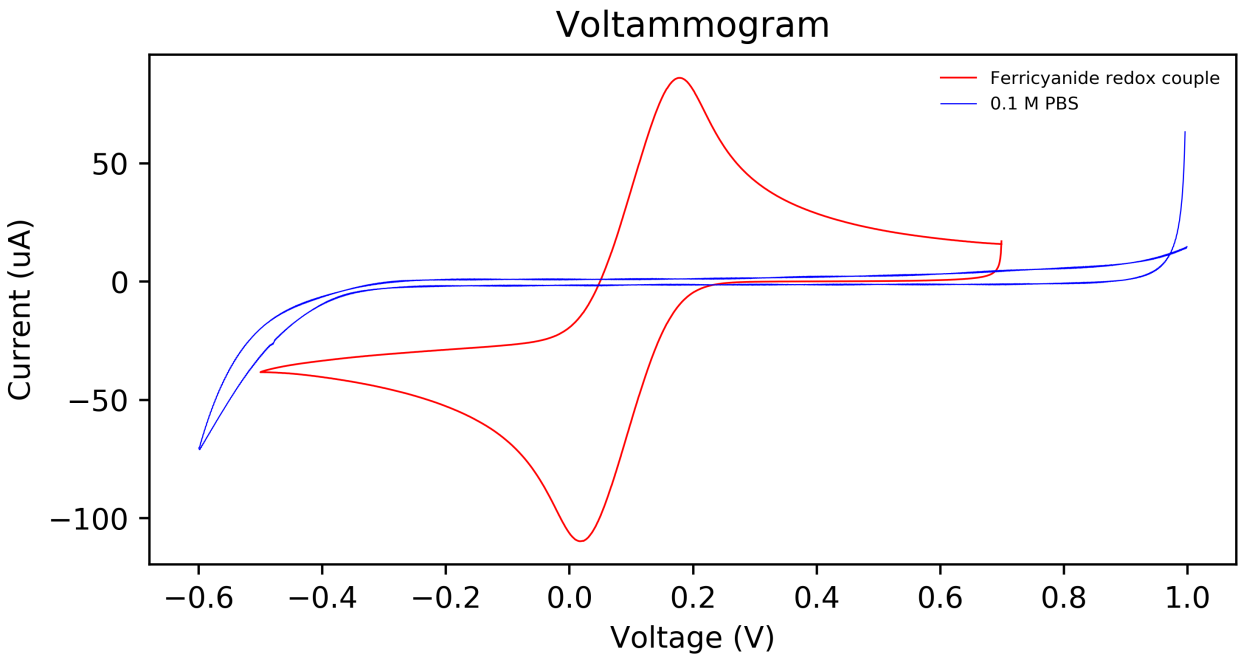

Figure 4.1: Cyclic voltammetry scans using carbon nanofibre electrodes. The blue scan in 0.1 M PBS shows the contribution of the buffer solution and the red scan in 5 mM ferricyanide redox couple solution ranging from 0.7 to -0.5 V

4.1.2 Unmodified Sensor Characterisation using Square Wave Voltammetry

Sensor characterisation using square wave voltammetry was executed by performing tests in de-ionised water (blue), PBS (green) and the ferricyanide redox couple (red). Figure 4.2 shows the resulting voltammogram of the experiment with water showing no contribution to the produce current in the potential range. The scan in PBS is to verify that the buffer solution has no contribution to the current generated in the redox couple and although the background scan is non-negligible, it is safe to continue using PBS with no background subtraction as it has no produced peaks in the defined peak for SWV with the supporting electrolyte. Next a sweep on the carbon nanofibre sensors with square wave voltammetry was done in the range of 0.6 to -0.4 V producing a voltammogram (red) that confirms no superimposition in the PBS (green) scan and validates the decision for no background subtraction during data processing. The SWV scan in the ferricyanide redox couple produce a peak just positive of 0 V which is expected for a formal potential of 0.1 V. All subsequent SWV scan were executed in a smaller range to focus on the produced peak with parameters: 20 mV pulse size, 5 mV step size, 25 Hz, starting potential of 0.5 V, final potential of -0.2 V with an equilibrium time of 2 s.

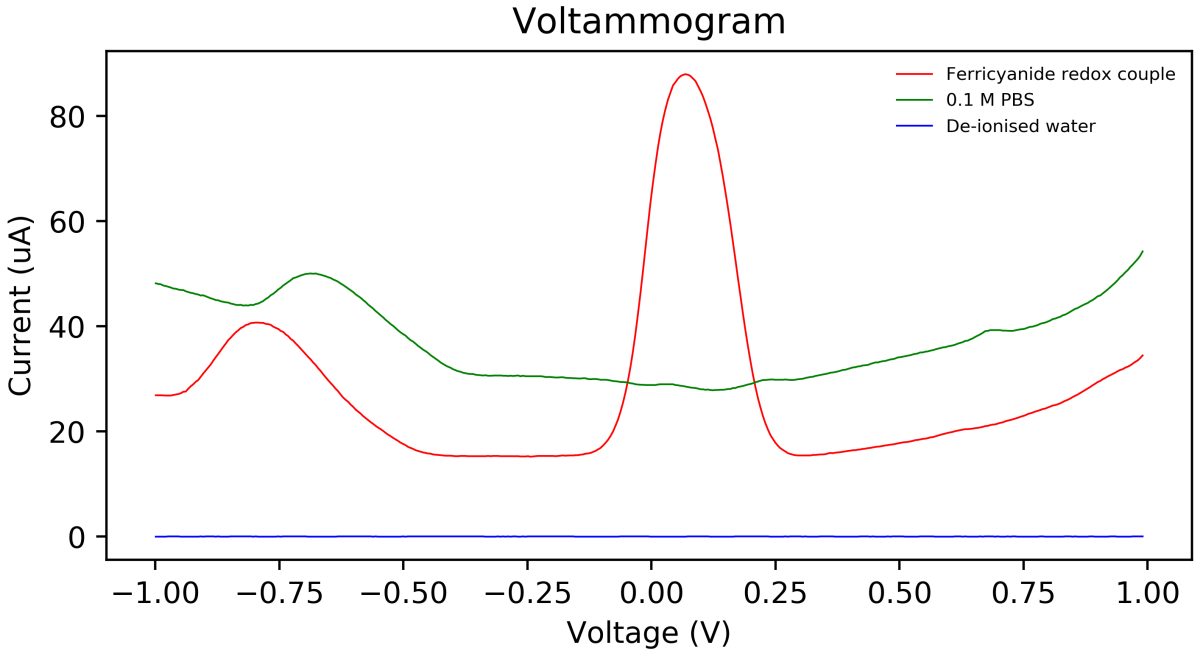

Figure 4.2: Graph showing characterisation of carbon nanofibre electrodes using square wave voltammetry. Three scans were executed, the first in de-ionised water (blue), second in the redox solution buffer PBS (green) and the last in ferricyanide redox couple (red).

4.1.3 Unmodified Sensor Reproducibility

The reproducibility of the carbon nanofibre electrodes manufactured by Dropsens were tested through square wave voltammetry in a supporting electrolyte with the produced voltammogram shown in Figure 4.3. Three different sensors were scanned three times and taking the last scan to ensure the sensors are stable, with the mean of the different sensors 90.23 µA and a standard deviation of 0.96 µA. The resulting graph shows the waveforms to be identical in shape and magnitude for the same experimental setup.

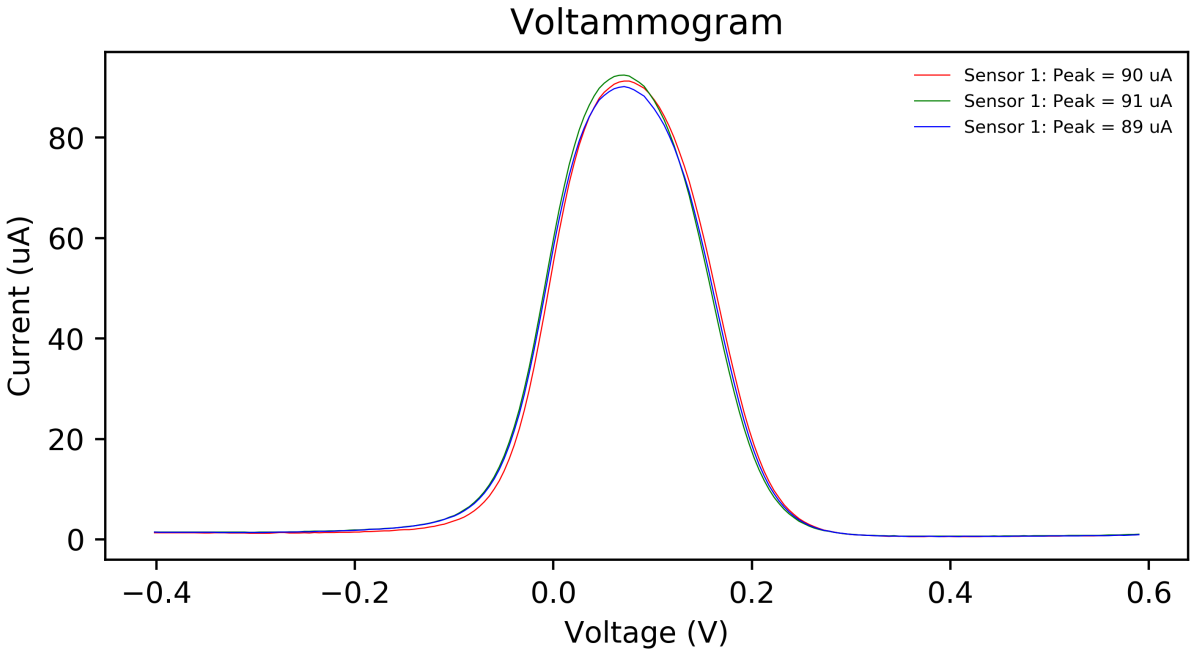

Figure 4.3: Graph showing peaks produced by SWV in ferricyanide on three different sensors for reproducibility test.

The carbon nanofibre sensor's square wave voltammogram shown in Figure 4.3 proves the sensors to be reproducible. A CNF sensor were also used in an experiment to explore its stability by executing 20 successive SWV scans and evaluating the resulting current response to investigate the similarities. The results proves the sensors to be stable in the supporting electrolyte with the twenty scans having a mean of 88.03 µA and a standard deviation of 0.77 µA.

4.1.4 Electrografting of Diazonium Salt unto Unmodified Sensor

By executing cyclic voltammetry scans in a 4-carboxyphenyl diazonium salt mixture carboxyl groups are coated onto the working electrode with the step known as electrografting. An aryl radical is formed which attached to the electrode surface while the salt solution molecule gets reduced, with each successive scan to coat the surface with another layer of support groups. The cyclic voltammogram is shown in Figure 4.4 for 8 consecutive cycles of electrografting with the potential scanned from 0.2 to -0.6 V and back at 100 mV/s. The first grafting cycle is shown by the blue curve having a reduction peak at more or less -0.28 V with the peak decreasing for each consecutive cycle. The decrease in peak reduction current is due to a decrease in electron transfer efficiency as more layers of carboxyl groups diminishes available electrografting space. An exponential decrease in peak current confirms that the highest portion of groups are grafted in the first cycle.

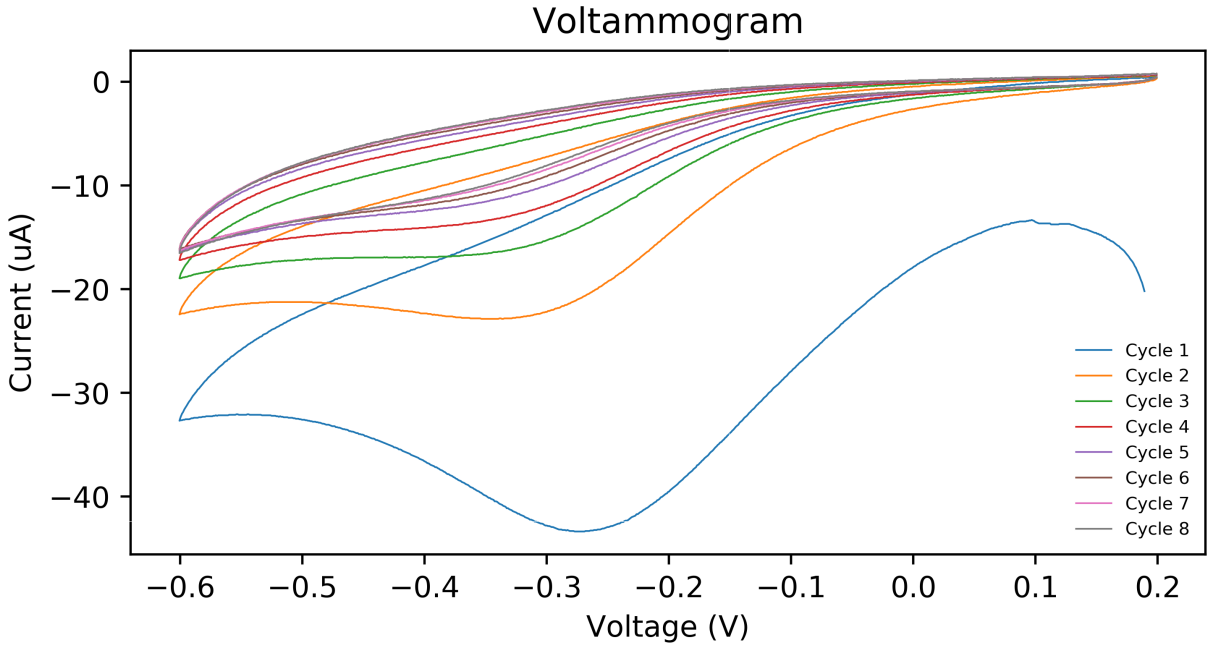

Figure 4.4: Graph showing 8 cyclic voltammetry cycles while electrografting unto the carbon nanofibre electrodes.

Carbon nanofibre electrodes are known for their large surface area and thus requires more than one cycle of grafting to properly cover the electrode surface with carboxyl groups. The effect of this is seen with the peak of the first scan not completely decreasing but decreases with each cycle as the surface is covered with more support groups.

The carboxyl support groups created on the electrode surface is known to repel the electroactive molecule and would produce a resulting voltammogram with a decrease peak current. This effect caused by electrografting can be verified doing square wave voltammetry with the redox couple before and after electrografting. The voltammogram shown in Figure 4.5 shown the SWV current response of the same sensor before and after eight cycles of grafting with diazonium salt. Three successive scan after grafting is expressed by the greatly diminished peak curves reduced from 76.60 to 21.31 µA. The decrease in peak current verifies the crosslinking method of electrografting and proves the electrode surface to be fully covered with support groups.

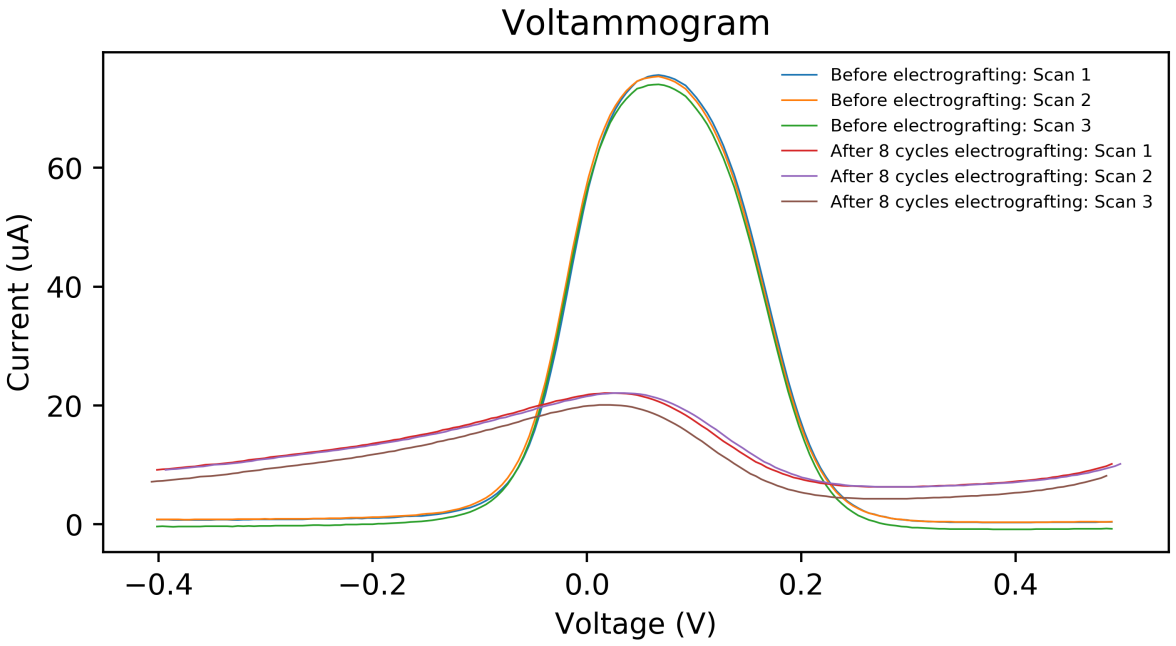

Figure 4.5: Graph showing SWV scans on carbon nanofibre sensors before and after 8 cycles of electrografting for validation by reduction in peak current.

The voltammogram in Figure 4.5 aids as a visual confirmation of the electrografting process shown by the clear reduction in peak current. Furthermore, a detailed experiment showing the effects of the grafting process of different voltammetry cycle numbers is expressed by the histogram in Figure 4.6. Three different sensors were used to explore the effect of three different cycle numbers with a SWV scan performed before grafting on the unmodified sensors shown by the blue bars and produced similar peak around 74 µA. Similar peak currents again proves the stability and reproducibility of the CNF sensors. The experiments for grating of different cycles were performed and shown by the red bars for cycles of 1, 4 and 8 respectively.

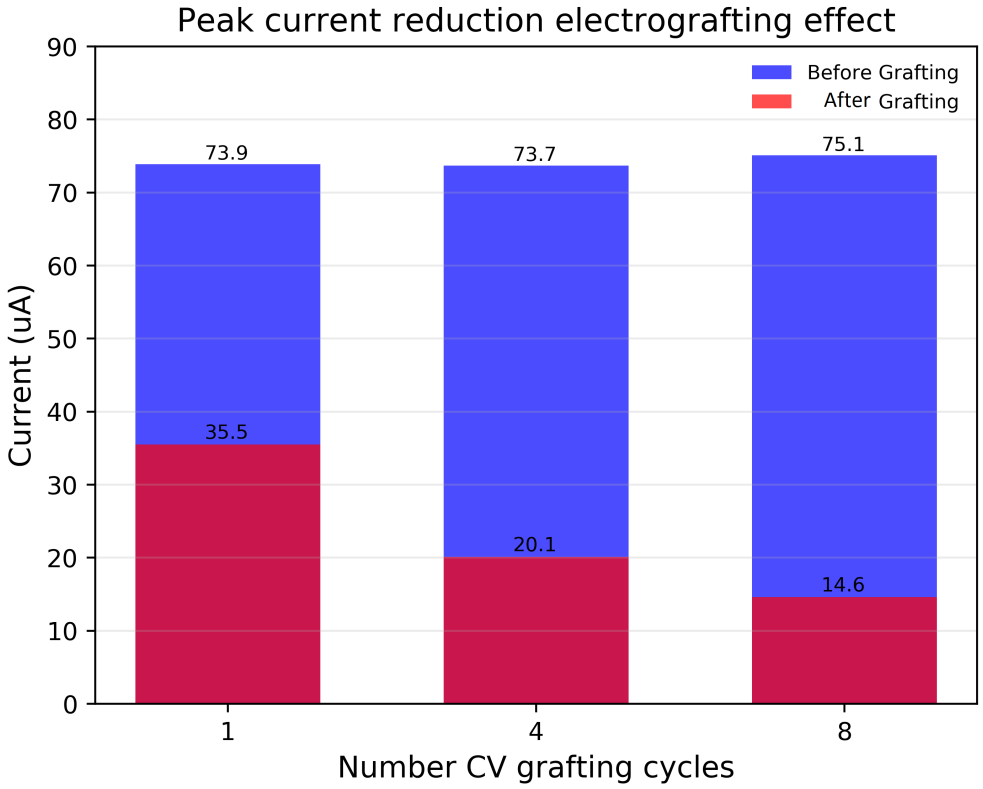

Figure 4.6: Graph showing the effect of different number of CV cycles coating layers of carboxyl groups on the working electrode, with the histogram expressing caused reduction in peak current.

It was expected that more cycles of electrografting would lead to a reduction in peak current due to the repulsion molecule grafted onto the electrode surface and is precisely what the trend of the red bars peak current showed. The reduction in peak current has a non-linear trend and shows that the electrode surface is moving towards saturation with the first peak having a reduction of 52%, the second a reduction of 73% and 81% for 8 cycles of grafting.

4.1.5 Antibody Crosslinking and Fluorescent Validation Study

To confirm that anti-LC3 antibodies was successfully immobilised onto the carbon nanofibre working electrode a fluorescent validation study was executed. This study will also ensure that the procedure of determining the baseline peak with square wave voltammetry in a redox couple before LC3 protein immobilisation does not wash off the antibodies. The imaging in Figure 4.7 shows the fluorescence of the secondary antibody bound to the primary antibody with its presence also confirming the success of the carboxylic support groups created by electrografting. Figure 4.7A is the fluorescent imaging of an unmodified sensor acting as a control test, checking for any autofluorescence. Figure 4.7B-D is the fluorescence of three different concentrations to check if an increase in antibody concentration produces a great change in bindings confirmed by an increase of fluorescence.

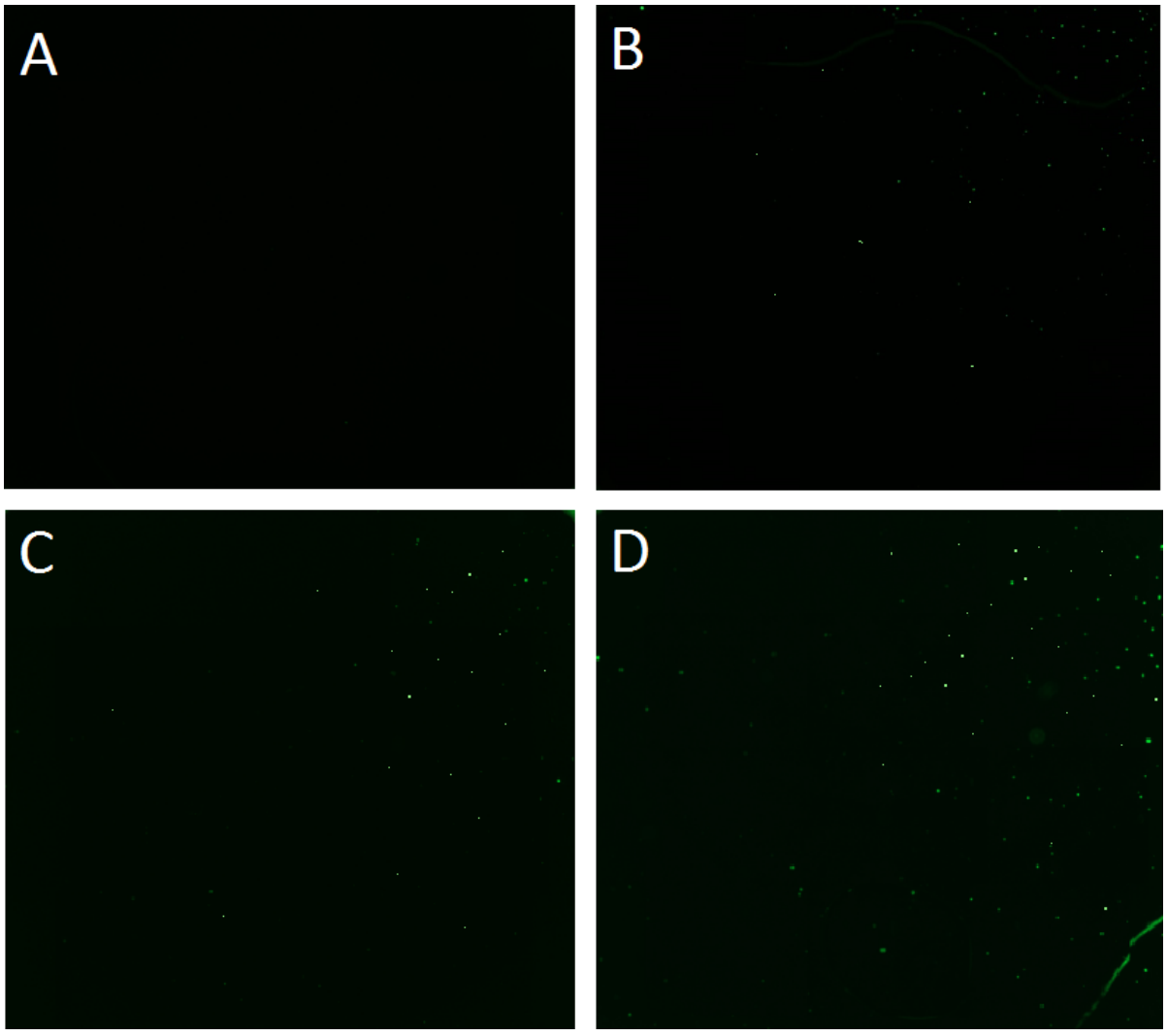

Figure 4.7: Imaging of the fluorescent study undergone to validate antibody binding. Three different concentrations of anti-LC3 was immobilised with 10 µg/ml (B), 25 µg/ml (C) and 50 µg/ml (D) and studied as well one unmodified sensor as control (A).

Figure 4.7B-D is photos of fluorescent imaging done on the sensors with increase concentration of anti-LC3. The sensors all went for three square wave voltammetry scans each in the ferricyanide redox couple before sent for imaging to validate the antibodies as they would be right before protein immobilisation. Looking closely it is observed that there is indeed an increase in fluorescence compared to the control test as well as an increase as a higher concentration anti-LC3 is immobilised which suggest that the method of antibody crosslinking was successful and the baseline scans before protein immobilisation does not wash off the antibodies. From the presented imaging the intricate detail is unclear but with software used for performing the imaging, higher levels of fluorescent is observed and despite its non-linearity it still proves that a higher concentration is more effective for immobilisation.

4.2 LC3-II Immunosensor Response measured with Palmsense 4

A full scale test was conducted on the carbon nanofibre sensors to test the response of the immunosensor using the Palmsens 4 in the ferrocyanide redox couple, with this section presenting the findings of the full scale test.

The final full scale test executed produce the results seen in Figure 4.8 and would be the calibration curve generated for the carbon nanofibre sensors. The peaks generated by SWV were extracted using the methods described in Section 3.3 and were plotted according to their concentration LC3 versus the percentage change relative to a predetermined baseline peak. The calibration curve presents the plotted results with each point containing the mean of three sensors as well as an error bar to visually express the standard deviation of each concentration with multiple sensors. Over the range of LC3 concentrations an overall difference can be seen with an increase of concentration versus percentage change, meaning that the sensor was capable of detecting the presence of LC3 with no overlapping error bars. The curve is non-linear meaning the sensor is inaccurate and not sensitive enough for picking up small levels of LC3 but confirms the immunosensor's proof of concept.

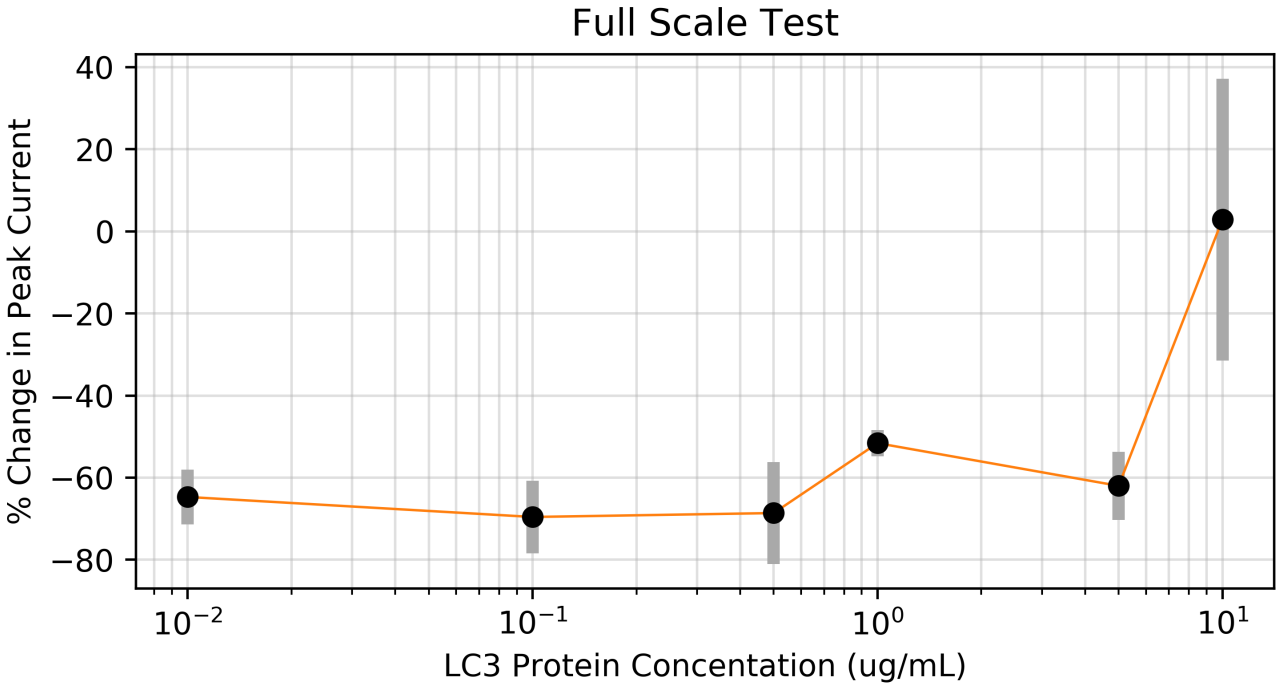

Figure 4.8: Graph showing the percentage change of each protein concentration after immobilisation as the full scale test, serving as a calibration curve.

Chapter 5

Discussions

This chapter serves as a link between the literature and the results discussed in chapter 4 and reviews the findings as well the the efficiency of the developed immunosensor. Certain choices made regarding the design of the sensor lead by literature is discussed as well as the data analysis algorithm and noise elimination methods used to extract the data produced by the Palmsens 4. The findings observed during sensor modification is discussed in detail followed by the final review of the developed LC3 immunosensor to explain how well the sensor works by reviewing the full scale test calibration curve.

5.1 Noise Elimination & Data Analysis Algorithm

All electrochemical experiments require a level of signal processing and data analysis in order to compare the waveforms produced and is possible through standard hardware and in depth software implementation. The aim of this process is to implement methods to reduce the noise generated as much as possible and finally extract a peak value relative to the curve's baseline without changing critical information hidden inside the signal.

External noise is usually induced into a system due to factors in the surrounding environment, and is caused by frequencies in electrical fields to which open cables are exposed to. Noise of this nature is usually in the range of 10^{-9} to 10^{-12}A and could be reduced by implementing a Faraday cage to shield the experimental equipment [133]. The currents observed that are produced in the electrochemical experiments are in the range of 10^{-6} A and discovered to be negligible when analysing the peak currents and therefore not implemented which greatly simplifies the experimental setup. Commercial potentiostats such as the Palmsens 4 and Gamry 1000E are designed with high quality low noise components ensuring the devices to have high quality noise specifications with current to be in the 10^{-9} A range, thus using such devices enables the experiments to take these currents to have no noticeable effect.

Due to the nature of electrochemical experiments the signal generating the a redox couple could be superimposed on the signal generated by its solution buffer in which case a background scan is required [134]. After performing a scan in the solution buffer the produced signal is observed to not produce any unwanted peaks in the range of the redox produced peak and has no effect on the extracted data. Therefore no background subtraction was necessary and only a Savitsky-Golay filter was implemented to reduce signal noise.

With the commercial screen printed electrode not being perfectly reproducible the measured peak relative to the origin will produce invaluable data and thus requires to be measured relative to the curve's own baseline. To measure a baseline peak current algorithms were developed to extract a curve's baseline by method of leading edge identification, inflection point identification and least square baseline correction.The latter was the method of choice with the first two method being highly subjected to human error. Certain parameters are to be chosen before analysis that requires consideration of the signal before processing. These methods are observed to be quite reluctant, time consuming and inaccurate therefore chosen to not be the main method of baseline extraction. The method of least squares baseline correction is an algorithm that requires only two parameters dependant on the scale of the produced signal and with the scale of the electrochemical experiment being relatively similar the parameters does not require any alteration once established. Figure 5.1 and 5.2 is a visual representation of a smoothed signal being subjected to the baseline correction algorithm while changing its parameters p and λ with the values recommended to be in the range of $0.0001 \leq p \leq 0.1$ and $10^2 \leq \lambda \leq 10^9$. The graphs in Figure 5.1 and 5.2 is the result of keeping one parameter constant while changing the other to show the different effects of the correction algorithm with the blue curve the original smoothed signal and the red the corrected baseline. Experimentation with these parameters are shown in grey with the optimal values determined through trial and error resulting in the final value of $p = 0.0001$ and $\lambda = 100000$.

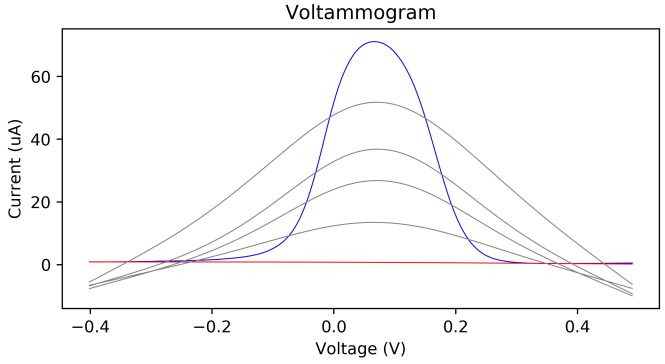

Figure 5.1: Graph showing the effect of of changing the parameter p of baseline correction algorithm when executed onto the produced voltammogram

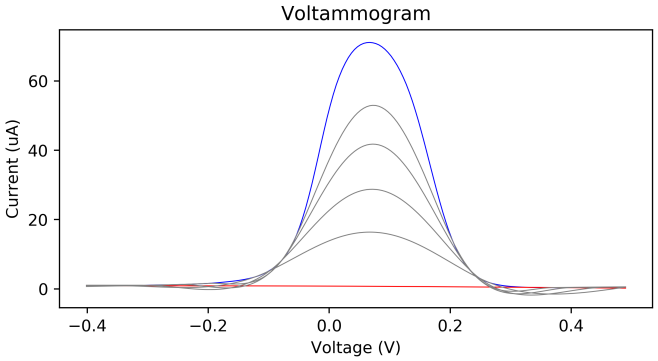

Figure 5.2: Graph showing the effect of of changing the parameter λ of baseline correction algorithm when executed onto the produced voltammogram

The methods used for data analysis was successful, it is capable of eliminating noise as well as extract the necessary peak information required for sensors evaluation and curve comparison. The method used for baseline extraction does not require any expertise and consideration once established and will be successful for experiments of the same scale. Experiments that produce larger currents over greater potential ranges will only require a small adjustment which could be easily implemented. The peaks are then calculated by using a high-level function to located the absolute peak and subtraction the baseline from this value to determine the relative baseline peak.

5.2 Biosensor Development

This section covers the modification process towards an LC3 specific immunosensor and discusses the findings produce by choices made relating to the setup by which measurements were taken as well as crosslinking through electrografting, activation and antibody immobilisation.

5.2.1 Measurements in the Electrochemical Setup

It is required that all modification steps towards antibody immobilisation be exactly the same as well as the handling of each electrode to ensure that changes of the peak current are not due to inconsistent experimental setups. Following the first electrochemical SWV scans it was observed that the first scan (yellow) differs quite significantly from the second (blue) and third (green) scan as witnessed in Figure 5.3. Analysing the process of pipetting ferricyanide onto a fresh unused electrode bubbles are observed on the surface. Thus two steps was implemented namely wetting and washing which is to be consistent throughout all experiments to remove any bubbles and impurities on the electrode surface. To make sure the sensor has a stable response multiple scans were executed with the latter scan the final curved saved for observation. The washing step was performed using PBS for all steps prior to antibody immobilisation and TBST was used for all subsequent washing steps as TBST is known to effect unbound molecules to be less "sticky" and will ensure that any unbound protein and tris is washed off. After the wetting and washing steps were added the sensors proved have an increase in reproducibility making the results more trustworthy and was implemented for all sensor modification steps.

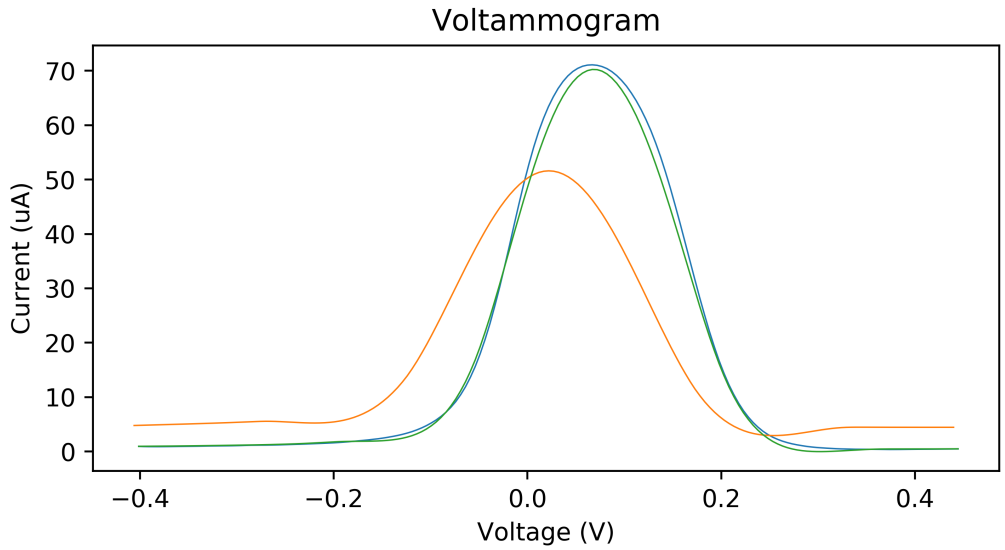

Figure 5.3: Voltammogram of an unmodified carbon nanofibre sensor produced by executing three SWV scans in ferricyanide using no wetting procedures.

Due to different solutions used by each modification step the wetting and washing steps were important to make sure that the solution required for a specific process is the only liquid present in the step. Furthermore, to ensure the sensors are unchanged between steps, especially after antibody immobilisation, all sensors were pipetted with a

100 µl droplet of PBS and stored on ice to place it in an unchanging physiological environment awaiting voltammetry and LC3 immobilisation. A water saturated environment was created by soaking a paper towel in de-ionised water and placing it in an enclosed plastic container. All incubation and modification steps were performed inside this environment to prevent the liquids on the electrode surface from evaporating and to maintain a constant environment.

5.2.2 Electrochemical Window

The behaviour of the supporting electrolyte in an electrochemical setup is widely studied with the principle of operation for this project based upon an article by Eissa et al. [43] towards building a biosensor for detection of SMN protein. Although Eissa et al. explored the potential window, electron transfer rate and redox potential parameters, it is still necessary to confirms these parameter to ensure an optimal electrochemical setup. Limited resources kept this project from validating the electron transfer rate, but is not of interest for this thesis and would not contribute to the electrochemical setup. The electrochemical potential window was validated and used to determine the formal potential of the supporting electrolyte.

The main reason for exploring these parameters was to make sure that the materials used for the sensor transducer in combination with the redox couple of choice is compatible and that the setup is electroactive. The electrochemical window for different transducer materials found in literature varies for example graphene oxide screen printed electrodes in PBS to have a window around 2.5 V and GPHOX SPE's larger than 1.5 V, with no reference on the potential window of carbon nanofibre transducers in PBS. This project explored the potential window and determined it to be around 1.5 V with ferricyanide redox couple capable of accommodating the potential window.

An important consideration for taking into account was the concentration ratios used of the redox couples versus the redox molecules. The concentrations were chosen as such that the ions of the supporting electrolyte would have a much higher chance of moving compared to the ions of the redox probe. This ensures that the supporting electrolyte would be used for balancing the charge instead of the redox molecules by choosing PBS to have a concentration of 0.1 M and ferricyanide to have a concentration of 5 mM.

The requirements necessary for an electrochemical cell as discussed in Section 2.3 is satisfied and the choice of transducer material, supporting electrolyte and redox potentials is justified.

5.2.3 Sensor Reproducibility

The importance of checking the reproducibility of a sensor is based on trying to avoid false and inaccurate data readings. The reproducibility of the commercially manufactured SPE's by Dropsens is studied to ensure that they are trustworthy and will give an indication to what data processing is required to compare results of different sensors. The reproducibility study of the carbon nanofibre screen printed electrodes shows similar peaks and waveform shapes that no extra signal processing other than baseline extraction is necessary, and that the sensors would suffice for an immunosensor proof of concept.

5.2.4 Crosslinking by Electrografting

To immobilise antibodies to the surface of a transducer it requires support groups for them to covalently bind to the material. Support groups called carboxyl groups can be easily created by method of electrografting which proves to be time and cost effective. The total preparation time for making the diazonium salt solution is 15 minutes, uses low cost materials and requires a device to perform cyclic voltammetry on an electrochemical cell. Eissa et al. explored different materials as traducers including carbon nanofibres and serves as a good measure of comparison for this project. Figure 5.4 shows the grafting of diazonium salt onto CNF sensors reported by Eissa et al. against Figure 5.5 which is the grafting results of 3 successive cycles used in this project. It is explained in Section 4.1.4 that there is a trade-off of carboxyl groups versus sensor sensitivity and after consideration of Figure 4.4 the optimal grafting cycles are chosen to be 3. The reduction peaks for this project is similar to that reported by Eissa et al. but differs for the peaks produced with reduction occurring in the vicinity of -0.25 V and the peaks produced in this project twofold than reported in literature at 45 compared to 20 µA.

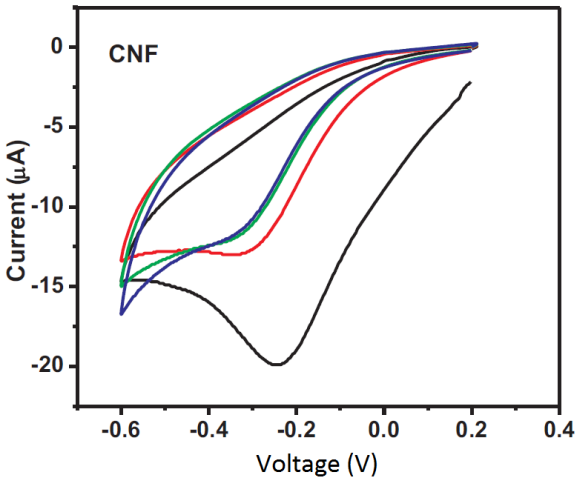

Figure 5.4: Electrografting voltammogram of 4 cycles by Eissa et al. [43].

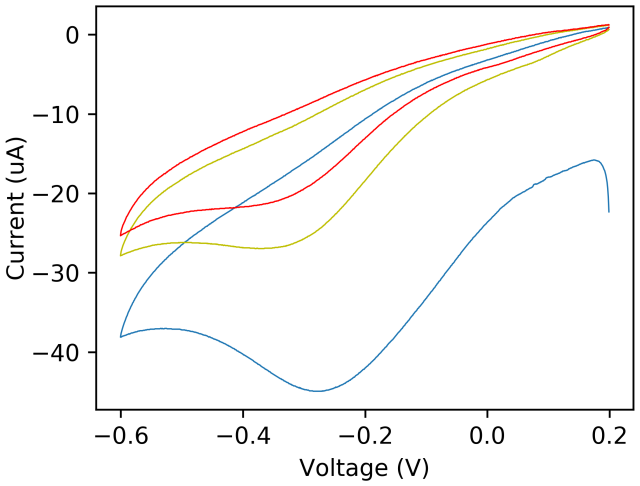

Figure 5.5: Electrografting voltammogram of 3 cycles for this project.

The current response produced through square wave voltammetry in Figure 5.4 is part of a larger group of sensors of various materials that were up for experimentation to evaluate their efficiency. Intricate details baring important information like the cycle number of a specific curve as well as the exact experimental setup was left out but leaves the reader with a conclusion that an increase in grafting cycles will result in decreased SWV current peaks. The carbon nanofibre sensors received from Dropsens proved to be stable and could compare to the results reported by Eissa et al. where the voltammogram in Figure 5.7 is the resulting current response. Three different sensors were used to evaluate the peak reduction underdone for each electrografting cycle. Using different sensors ensures no contamination by the redox couple occurring while doing SWV scans to determine current peaks and was assumed that the same procedure was followed by Eissa et al.. Peak reduction occurs as expected which validates the crosslinking process and after comparing the peaks with that of literature it is found that the initial peak

be much lower found in this project with the peak being 70.5 compared to 120 µA. The larger current response could be an indication that the sensors used by Eissa et al. were of better quality and more sensitive hence producing better results towards detection of the target protein.

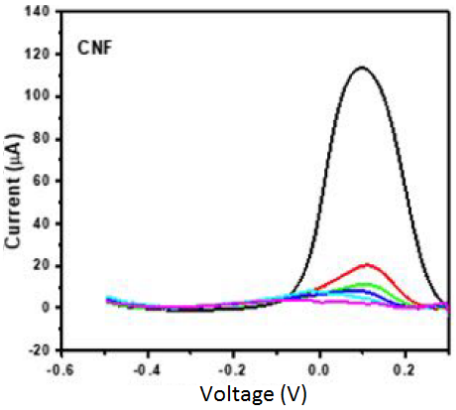

Figure 5.6: Peak reduction for electrografting cycles by Eissa et al. [43].

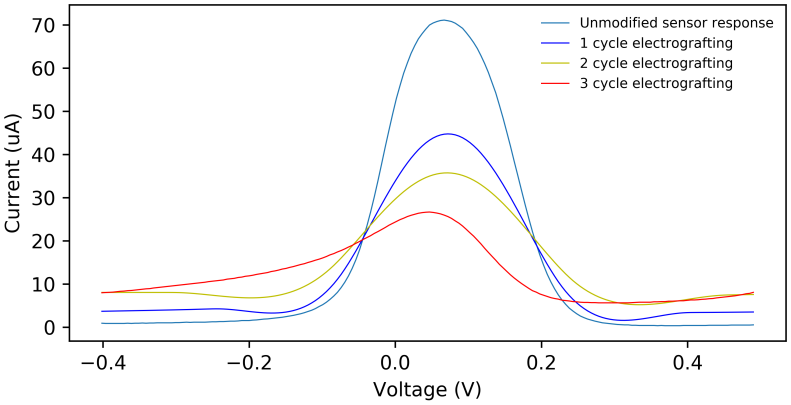

Figure 5.7: Peak reduction for electrografting cycles for this project.

There are various methods to optimise the process of electrografting with some of these methods being Raman spectroscopy and X-ray photoelectron spectroscopy (XPS) that can be used to optimise the surface coverage of the working electrode. The use of these methods was not possible for this thesis due to a lack of resources as these methods require expensive materials en a large amount of expertise. These methods would also require accurate account of some variables such as the exact concentration of diazonium salt and antibody solutions, the pH of some solutions as well as the surface area of the CNF working electrode. The use of these advanced methods would not largely improve the sensor's response and another educated choice wade made based upon the current response of the cyclic voltammogram during electrografting for 8 cycles. The current response shows saturation of the surface with carboxyl groups as the shape of each subsequent cycle becomes more unchanging so the cycle number was chosen at 3 where the cycles are as little as possible to preserve sensitivity but also enough that with an exponential decay another cycle will not be of great impact. The large surface area of the carbon nanofibre working electrode allowed for more cycles but it was decided to have one less cycle than that used by Eissa et al. due to the sensors of this project already being less responsive and relatively insensitive.

The presence of carboxyl support groups were confirmed in literature by using Raman and X-ray photoelectron spectroscopy, but due to these resources not available the reduction in peak currents were sufficient for confirming the presence of functional groups coated onto the working electrode. The findings were similar to that of Eissa et al. and was assumed to be close to optimal.

5.2.5 Crosslinking Activation and Antibody Immobilisation

The immobilisation procedure of LC3 is continued by the method of EDC/NHS crosslinking chemistry which is the activation of the linker in order for the antibodies to bind to

the carboxyl groups which were created through electrografting. Antibody immobilisation is greatly dependant on the execution variables and parameters of this method as the efficiency of the process is directly proportionate to the total bound antibodies. The application of this procedure is unique for every application and a process of trial and error is required to optimise the concentration to ensure optimal surface coverage with these variable to be EDC/NHS concentrations, solution pH, antibody concentration, number of available carboxyl groups, solution volumes and incubation times. A perfect combination of these parameters would results in optimal crosslinking activation but for this project a combination of parameters retrieved from literature and professional guidance from the physiology department of Stellenbosch university was used to determine the method parameters.

The concentrations of the EDC/NHS incubation process were increased from that reported by Eissa et al. to ensure that the functional support groups are properly activated and the incubation time of LC3 was also extended making sure that enough time is allowed for binding to take place. Optimisation of the crosslinking procedure was outside the scope of this thesis but fluorescent imaging confirms the success thereof which validates all steps prior to LC3 protein immobilisation.

5.3 LC3-II Biosensor for Detecting Autophagy Flux

A measure of how well a biosensor performs is based on its performance in five categories namely reproducibility, sensitivity, selectivity, stability and lastly accuracy which relates to the linearity of the sensor response. All categories are of equal importance and a lack in any of these fields will result in falsely produced information on the process its measuring. Firstly the sensor needs to be reproducible, for the generated response is based on relative data and needs to be compared in analysis and is the ability of the sensor to have similar behaviour in the same experimental conditions. The sensor's sensitivity would determine its ability to detect very small concentrations of the target protein and also contributes to the accuracy of the measurement and could either be increased by increasing the surface area of the working electrode or suing more specific detection techniques such as electrochemical impedance spectroscopy (EIS). The selectivity of the biosensor is its ability to not be affected by any noisy proteins in the sample as it would ultimately be a plasma sample extracted from blood and the binding of non-specific proteins would generate inaccurate readings. The stability of the sensor is a measure of robustness and is the ability to not be effected by its environment for example external noise injected into the system via the electronic measurement circuitry and the temperatures at which the experiments take place. The sensor's accuracy is based on its ability to linearly detect an increase in protein concentration with the success thereof ultimately proving the success of the developed immunosensor. All these parameters contribute to the working of the developed biosensor and is discussed next with its response generated during a full scale test. The findings showed in chapter 4 are explored taking these parameters into account and is used to conclude on the success of the immunosensor.

5.3.1 Measurements executed with the Palmsens 4

The reproducibility of the unmodified carbon nanofibre electrodes from Dropsens showed to be excellent and produced current responses of the exact same shape with baseline peaks

to be of little difference. The absolute peaks drifted thus baseline correction was necessary. The change in absolute peaks could be due to variables in the manufacturing process that causes each sensor to have an unequal amount of carboxyl groups and ultimately different electron transfer behaviour. Figure 5.9 shows the baseline peaks extracted from the sensor's current response during the full scale test and shows the relative peaks before and after LC3 immobilisation. It is clear that from the peaks before immobilisation that the reproducibility of the modified sensors are low and thus justifies the measure of comparison to look at the percentage change in peak currents. The peak current produced by sensor 12 is clearly an outlier and causes the average of the sensor grouping to rise and explains the data point in Figure 3.8 being outside the trend for increasing concentration. This is due to manufacturing inconsistencies with the cause of this phenomenon explained by Figure 5.8 where a deterioration of the reference electrode is witnessed.

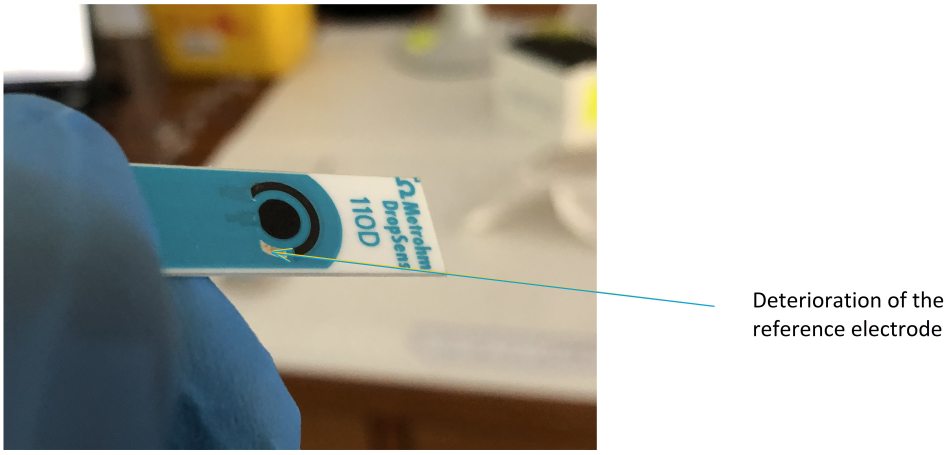

Figure 5.8: Image showing evidence of poor manufacturing resulting in deterioration of the reference electrode.

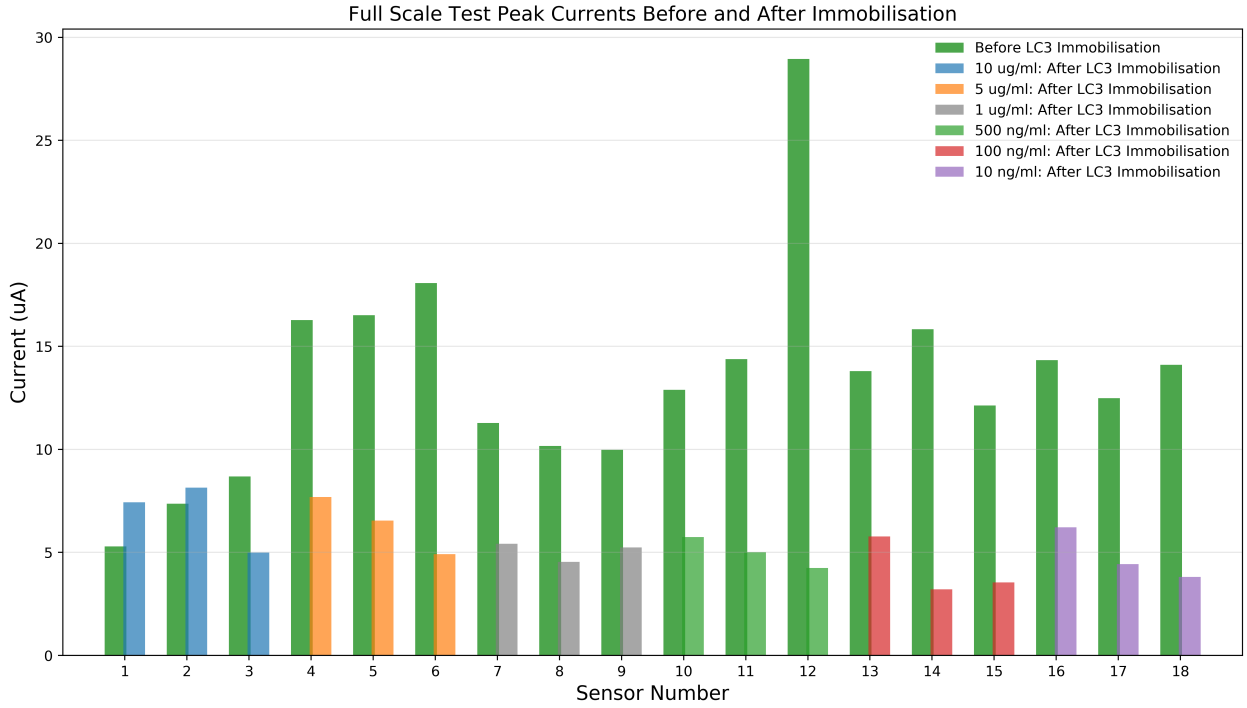

Figure 5.9: Peak currents of full scale test before and after LC3 protein immobilisation.

Figure 5.9 serves as a breakdown of the main test result of figure 4.8, The CNF sensors had peak currents in the vicinity of 10-15 µA after antibody immobilisation and the tris blocking step with peaks reducing to an average of 5 µA for the full scale test. The stability of the sensors were not explored in this project as well as not the selectivity due to limited time and resources. The resulting data showing the percentage change versus increase in concentration in Figure 4.8 shows no linearity and states the sensor to be inaccurate. The outlier produced by sensor 12 causes the result for 1 µg/ml LC3 to be false but the general trend for an increase in LC3 protein is witnessed. Over the range of the full scale test a trend is seen that verifies the basic operation and proof of concept of the immunosensor as the trend states that an increase in concentration results in an increase of LC3 bindings onto the working electrode. The sensor shows low sensitivity and not able to detect any increase in the lower concentration ranges but works for higher concentrations showing the immunosensor to be successful in a certain range. Propositions for making the sensor more sensitive and accurate are discussed in the final chapter as well as how a working LC3-II immunosensor would be used to estimate autophagy flux.

Chapter 6

Conclusions

This chapter summarises and integrates all facets explore in the project and concludes on the work done. Limiting factors, recommendations and future development proposals are discussed followed by an overall final conclusion.

6.1 Thesis Summary

The propose of this project was to develop a biosensor with the main goal to have a sensor capable of detecting LC3 protein in a physiological environment and using developed software for peak extraction. Data analysis algorithms will generate a calibration curve in which LC3 concentration can be found, using this in conjunction with blocking steps for the estimation of LC3-II towards an autophagy flux measurement.

An in depth literature study considers various sensing techniques, highlighting features optimal for this project as well as methods to integrate them. Various biochemical techniques were explored with the information found aiding in the development of an electrochemical biosensor.

As a result of the literature study, carbon nanofibre screen printed electrodes commercially manufactured by Dropsens were attained to explore the possibility of electrochemical detection of LC3 as a proof of concept. In order to attach LC3 antibodies to the transducer surface the sensor surface needed bio- and electrochemical modification. The surface was modified by electrografting of diazonium salt through cyclic voltammetry for the creation of carboxylic support groups, followed by cross-linker activation for antibody attachment by EDC/NHS. Lastly a blocking step followed by square wave voltammetry scans before and after LC3 protein immobilisation.

The proof of concept involves using a commercial industry standard potentiostat, the Palmsens 4, for all electrochemical modification i.e. cyclic voltammetry for electroactive reduction and measurement scans. The device was used to perform the full scale test and required the execution of square wave voltammetry scans in the same electroactive species before and after LC3 protein immobilisation with the voltammetry parameters consistent over the testing spectrum.

For this project a successful proof of concept was established towards the detection of LC3 in a physiological solution. Full sensor optimization was not possible due to the

lack of resources relating to time resulting in inaccurate sensor readings and a lack of sensitivity with the overall concept proven. The proof of concept is deemed successful after observing an obvious increase in peak current which identifies the LC3 protein in figure 4.8, which serves as the major final result of this project. The results indicate that the sensor is capable of quantifying LC3 with further development to increase sensor sensitivity and conducting more test over a wider range of protein concentrations to validate this. If time allowed the cross reactivity of the sensor would have been tested but is not present in this thesis thus, in further development it is highly important to first explore this before proceeding. Binding of the LC3 protein reduces the relative baseline peaks measured confirming the electron repulsion due to protein charge and shows successful detection of LC3 in the overall spectrum of concentrations. The immunosensor utilised carbon nanofibre electrodes in a ferricyanide redox couple and monitors electron transfer between them with a decreased peaks in the vicinity of 50% reduction. Further experimentation is necessary to ensure the reduction is due to selective LC3 protein bindings. A software algorithm was developed in parallel for automated peak extraction and is one step closer to having a complete autophagy measurement device.

6.2 Thesis Objectives

The main goals of this project were:

i To develop an electrochemical biosensor for detection of LC3-II as proof of concept towards an autophagy flux estimation.

ii To develop optimized software algorithms for extraction of valuable information for interpretation of the protein signature into autophagic activity.

The first objective of the project, to have a biosensor as proof of concept, was partially fulfilled as an increase of protein concentration in a physiological environment is observed. However an increase is observed over the entire spectrum of LC3 concentrations and looking closer, the sensor is unable to accurately determine LC3 concentrations due to no linearity in the results. The lower concentrations seem to have no effect on the biosensor showing that it also lacks sensitivity but serves as a proof of concept and is successful in that regard. The principle of the biosensor was confirmed showing that a charged protein binding to the working electrode repels the redox molecule and deems the proof of concept ready for further development.

This project made use of commercially manufactured carbon nanofibre screen printed electrodes by Dropsens, with these electrodes showing evidence of manufacturing defects that could be the product of error in big scale manufacturing, defects forming from shipping as well as the amount of time passed from manufacturing. These defects cause some sensors to behave differently and allows for deterioration of the working electrode resulting in a decrease in sensitivity. Manufacturing the electrodes in house enables control of parameters like the total area of the working electrode that is directly proportional to the sensor sensitivity gives control on electrode preservation. The next step would be to manufacture the sensors in house, reproduce the results and comparing them for further analysis.

The second objective of developing software to successfully extract valuable information was successful and can be used in all following experiments. The method does not need any adjustments and knowledge on its working principle but can simply be executed and will generate relevant information. Further development of a potentiostat to specifically executed square wave voltammetry towards estimation of autophagy flux can incorporate this algorithm.

6.3 Limitations

Resources and expertise towards a fully optimised biosensor was limited for crosslinking surface coverage using the methods of Raman and X-ray photoelectron spectroscopy (XPS). The validation of peak reduction was sufficient but optimization could play a big role in the final biosensor.

Due to Covid-19 the year of 2020 involved periods of country-wide lock-down causing access to lab equipment and resources to be abstracted. Restricted access reduced the period of development and testing resulting in less validation experiments and further sensor development. Development for that period is discussed in the next section and is the process following the success of the immunosensor proof of concept. The sensor response in a complex solution such as whole blood was outside the scope for this project.

6.4 Future Recommendations

With each environment being unique there are minor differences for duplication of experiments that can cause major errors. Thus it is recommended that electrochemical parameters are not assumed from previous research but that all parameters be determined before further modification to ensure legitimacy of the electrochemical setup, simplifying the debugging process in future experiments. This requires the determination of the electrochemical potential window and key redox potentials to make sure the transducer material is compatible with the electroactive species.

For optimal efficiency in the development of an electrochemical biosensor it is recommended that the effect of each modification step be verified before succeeding to the next step. Confirmation of each step removes the guesswork during debugging further down the modification process and adds towards optimisation of each step. Various confirmation techniques are available for recommendation and is dependent on the modification technique where for this project voltammetry techniques and fluorescent microscopy was use for validation. Other techniques for composition studies would be beneficial and is recommended for future development, especially in-house built CNF electrodes for evaluating the surface topology such as scanning electron and confocal microscopy as well as Fourier transform infrared spectroscopy. Square wave voltammetry was used to validate the formation of carboxyl support groups on the surface of the working electrode but is not sufficient for complete optimisation, and the binding of a secondary fluorescent marker to the antibody produced imaging by fluorescent microscopy that is used to validate the binding of anti-LC3. The presence of fluorescence found by microscopy to validate the

binding of anti-LC3 is also a validation of other modification steps such as the linker activation by EDC/NHS crosslinking chemistry, and is also a second degree of validation of the electrografting process. However, if unsuccessful the factor of multiple variables causes uncertainty in the error and is exactly why it is recommended to validate each step individually.

A secondary fluorescent tag was aquired to confirm the bindings of LC3 antibodies but only basic validation was performed. A control test was done with no modification on the electrodes performed as well as a test to evaluate the effect of three different protein concentrations. It is recommended that the study be taken further by executing a control test on an unmodified sensor to check if any bindings take place that adds noise to the image, as well as a test where a modified sensor is incubated in a solution containing non-specific protein.

The semi positive results retrieved from the full scale test could further be validated by repeating the full scale tests and executing the experiments by testing the various concentrations at random to ensure that time does not play a role in the current response. The inaccurate data produced by sensor 12 can also be removed from the data set and reproduced to find a more stable response. The sensors showed to be insensitive for lower proteins thus it is recommended that the sensors be built in-house. Doing this will allow the control of influencing variable that is directly proportional to the sensor sensitivity and the quality will be assured. Manufacturing the sensors in-house will allow the working electrode to have a bigger radius and thus a larger surface area to produce a higher current response. A higher current response will lead directly to a more sensitive sensor and the bigger surface area minimises the error margin for non-specific bindings.

6.4.1 Proposed methodology for determining autophagy flux

The process of autophagy is accompanied by various autophagy related proteins where these proteins are formed during different phases of degradation. Each phase is identified by a specific protein and the accumulation of a protein will be an estimate towards the rate of the autophagic process. The phagophore membrane grows where completion of the spherical vesicle is called the autophagosome, with the formation of an autophagosome relating to the LC3-II protein. An increase in LC3-II is directly proportional to the total autophagosomes formed as discussed in Section 2.1.1.2, thus to determine autophagy flux the levels of LC3-II are to be measured.

The problem with an immunosensor is that anti-LC3 captures the whole LC3 protein and cannot distinguish LC3-II from LC3-I. The solution to this problem is taking a sample and chemically blocking the autophagic process before taking a measurement to determine the total accumulated LC3-I in a sample whereafter a second measurement is taken when autophagy is induced to determine the total level of LC3. The difference between the levels of LC3 before the blocking step and after produces the total accumulated LC3-II. The levels of LC3-II can be monitored by adding certain protease inhibitors to ensure the interpretation of the measurement is towards the accumulation of autophagosomes. An inhibitor to induce autophagy is used known as E64 with it being a calpain inhibitor proposed for this purpose specifically [135]. If treatment with bafilomycin A1 causes an increased level of LC3-II with a specific chemical, the treatment in only bafilomycin A1 suggests an increase in the rate of LC3-II accumulation [135], tracing back to the forma-

tion of autophagosomes, hence autophagy flux.

Thus, after an optimised LC3 immunosensor is developed the determination of autophagy will require a few simple steps in conjunction with a user friendly device to produce an autophagy flux reading.

6.5 Final Conclusions

The main goal towards a proof of concept immunosensor for the detection of LC3 protein was successful. The research provide all the means and recommendations for further exploitation and through optimisation and development of a complete device the measurement of autophagy flux will be possible. The sensor does not make use of a tag or signal amplifier contributing to the simplicity of the sensor. The data analysis algorithm developed is successful in a manner to which the process can be automated. The algorithm can be utilised by the final system with minor parameter changes as required.

The complete autophagy measurement system will consist of disposable electrodes that plugs into an electronic system designed specifically to executed a voltammetric measurement and produce an autophagic flux reading.

Appendices

Appendix A

Chemical Solutions & Dilutions

A.1 Ferricyanide Redox Couple

All electrochemical experiments were performed in potassium ferricyanide ($K_3Fe(CN)_6$) electroactive species. For all experiments involving ferricyanide redox couple, a 50 ml batch was prepared in situ at 5 mM. PBS (1X, pH 7.4) was used as the supporting electrolyte buffer and prepared using the following protocol:

1. Add 50 ml of PBS(1X, pH 7.4) to a falcon tube;
2. Add 82.31 mg of $K_3Fe(CN)_6$ to the same tube for a 5 mM solution;
3. Stir solution with a vortex mixer until all solids are properly dissolved.

A.2 Hydrochloric Acid Dilution

The electrografting procedure uses a diazonium salt mixture which requires a hydrochloric acid solution for its preparation. The method requires 0.5 M HCl and was prepared by executing the following steps:

1. 32 % wt/wt HCl was acquired at the physiology molecular lab;
2. 4.957 ml of the stock solution was pipetted into a 100 ml beaker filled with 50 ml de-ionized water;
3. The solution was added to a 100 ml volumetric flask and filled to obtain 100 ml HCl at 0.5 M concentration.

This hydrochloric acid solution was prepared in situ for all electrografting experiments.

A.3 Diazonium Salt Solution

For all electrografting experiments the 0.5 M HCl solution as prepared in section A.2 is used to create the 2 mM diazonium salt mixture. Equal ratios of 4-aminobenzioc acid and sodium nitrite ($NaNO_2$) forms 2 mM diazonium salt and was prepared by succeeding the following protocol:

1. 25 ml of the HCl solution prepared in section A.2 was added to a falcon tube;
2. 34.5 mg of NaNO2 was added to the same tube to obtain a concentration of 20 mM;
3. 68.57 mg of 4-aminobenzoic acid was added to the tube to obtain a concentration of 20 mM;
4. The solution was stirred for a few minutes with a vortex mixer at room temperature until the solids were completely dissolved;
5. 40.5 ml of the HCl solution was added to a clean falcon tube;
6. 4.5 ml of the 20 mM concentrate solution was added to the 40.5 ml HCl solution in the new falcon tube to get a total of 45 ml;
7. This resulted in a diluted mixture of 2 mM diazonium salt solution with 4-aminobenzoic acid and NaNO2 in similar ratios;
8. The final solution was stirred with a vortex mixture before used.

To simplify measurements a diazonium salt concentrate was first prepared then diluted to form the 2 mM solution that was used for electrografting.

A.4 EDC/NHS Crosslinking Protocol

The EDC/NHS solution required for crosslinking activation was prepared in situ using the following protocol:

1. A stock solution of 0.1 M MES Buffer was prepared by taking 1.464 g MES and adding it to 75 ml de-ionized water;
2. Adjust pH to 5.5 using NaOH and stored stock solution at room temperature;
3. Add 7.5 ml of the stock solution to a falcon tube;
4. 57.51 mg EDC was added to the tube producing a concentration of 40 mM;
5. 16.285 mg sulfo-NHS was added to the tube producing a concentration of 10 mM.

The final solution for EDC/NHS crosslinking chemistry was 40 mM EDC and 10 mM sulfo-NHS in 0.1 M MES buffer.

A.5 Anti-LC3 Fluorescent Study Dilution

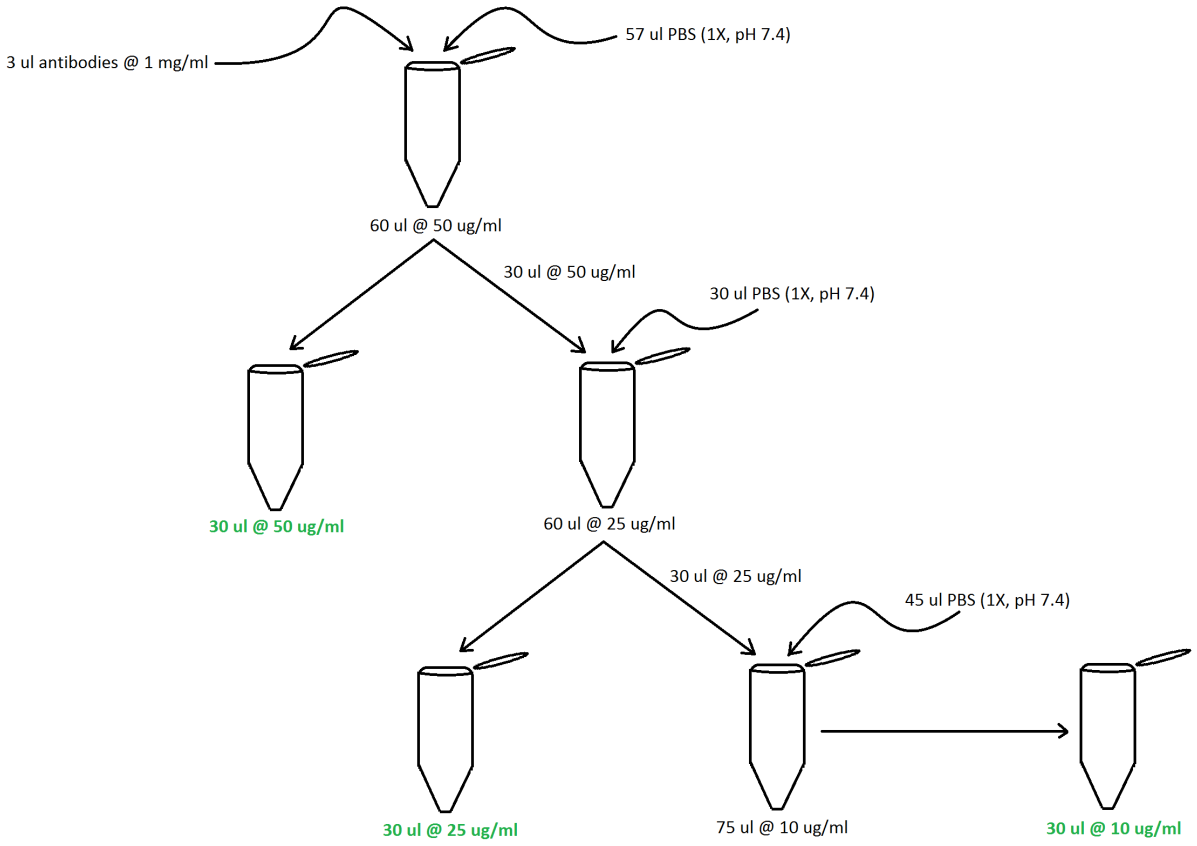

Figure A.1: Figure showing how the antibody concentration was diluted for anti-LC3 immobilisation for the fluorescent validation study.

A.6 Anti-LC3 Full Scale Test Dilution

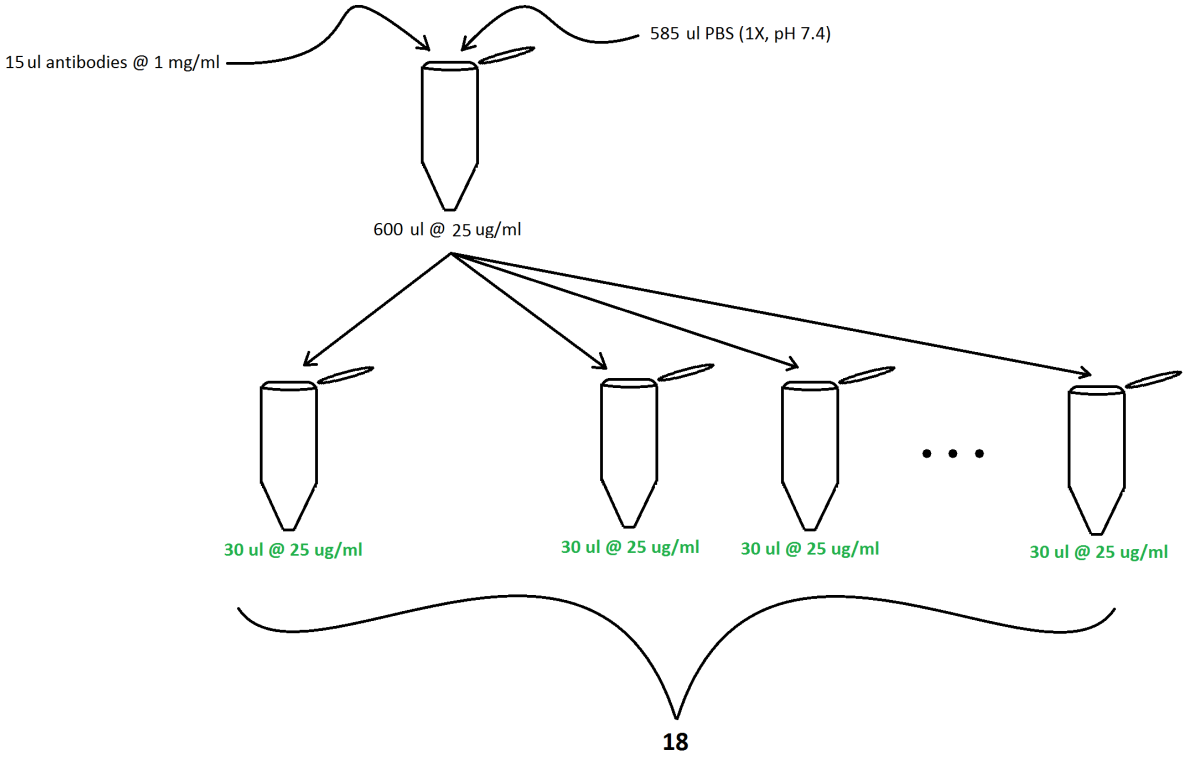

Figure A.2: Figure showing how the antibody concentration was diluted for anti-LC3 immobilisation for the fluorescent validation study.

A.7 LC3 Protein Full Scale Test Dilution

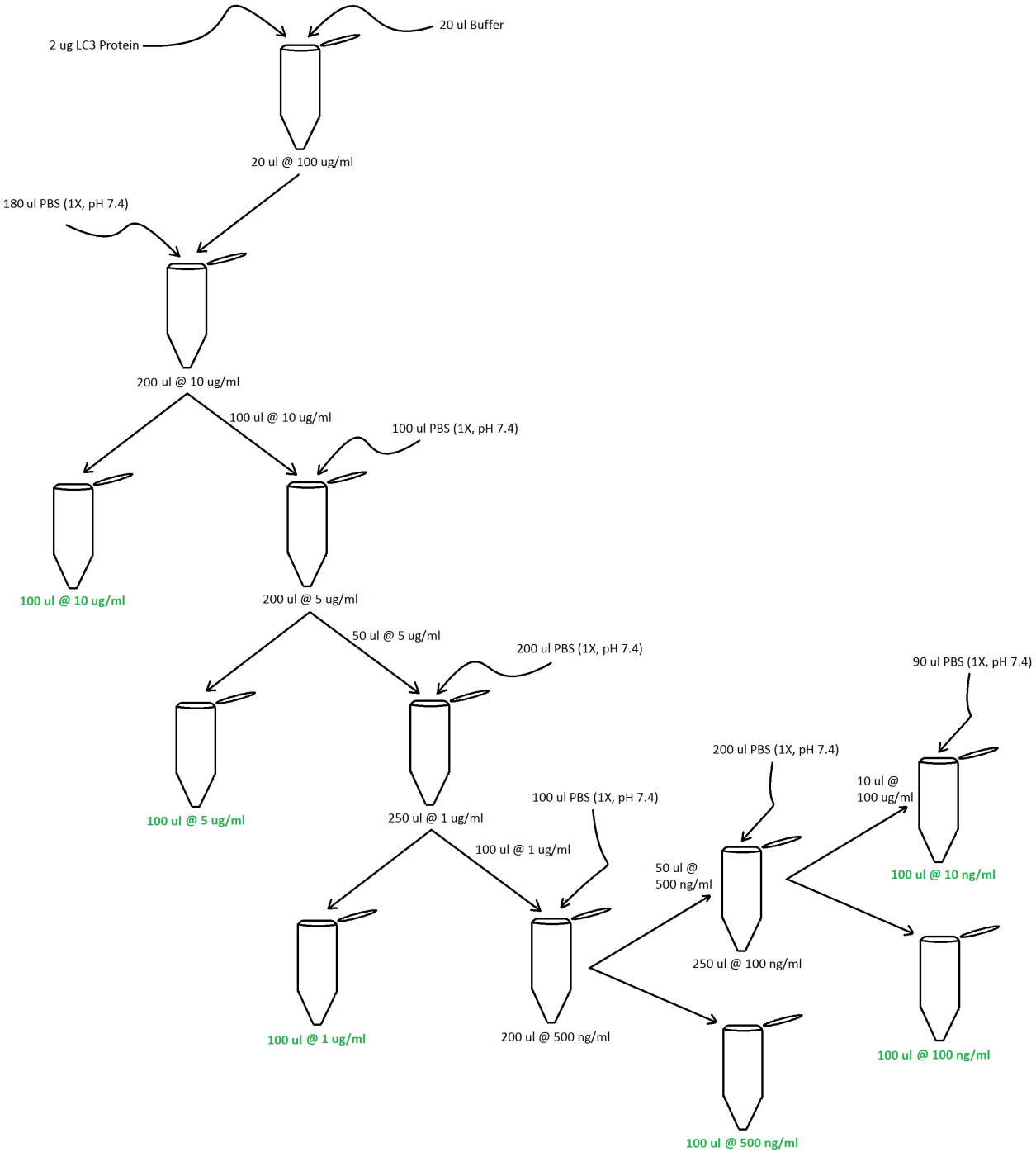

Figure A.3: Figure showing how LC3 protein concentration was diluted for LC3 immobilisation during the final full scale test.

Appendix B

Code

B.1 Asymmetric Least Squares Baseline Correction Algorithm

```
def baseline_als(y, lam, p, niter=10):
    L = len(y)
    D = sparse.diags([1, -2, 1], [0, -1, -2], shape=(L, L - 2))
    w = np.ones(L)
    for i in range(niter):
        W = sparse.spdiags(w, 0, L, L)
        Z = W + lam * D.dot(D.transpose())
        z = spsolve(Z, w * y)
        w = p * (y > z) + (1 - p) * (y < z)
    return z

```

B.2 Basic Plotting Code

```
    X = np.array([10/1, 5/1, 1/1, 500/1000, 100/1000, 10/1000])
    Yavg = np.array([avg10ug, avg5ug, avg1ug, avg500ng, avg100ng, avg10ng])
    Ystd = np.array([std10ug, std5ug, std1ug, std500ng, std100ng, std10ng])

    fig = plt.figure()

    ax = fig.add_axes([0.12, 0.25, 0.8, 0.5])
    ax.set_xlabel('LC3 Protein Concentation (ug/mL)')
    ax.set_ylabel('% Change in Peak Current')
    ax.set_title('Full Scale Test')

    ax.plot(X, Yavg, lw=0.8, color='C1')

    plt.grid(True, which="both", alpha=0.4)
    plt.xscale("log")
    plt.errorbar(X, Yavg, yerr=Ystd, fmt='o', color='black',
                 ecolor='darkgray', elinewidth=4, capsize=0)
    plt.show()
```

Appendix C

Data sheets

C.1 Palmsens 4

PalmSens4 Measurement Specifications

PalmSens4 Measurement Specifications

The following table shows limits for technique-specific parameters.

	Parameter	Min	Max
All techniques (unless otherwise specified)	Conditioning time	0	1600 s
	Deposition time	0	1600 s
	Equilibration time	0	1600 s
	Step potential	0.076 mV	250 mV
	Pulse potential	0.076 mV	250 mV
	N data points	3	1,000,000
• **Normal Pulse Voltammetry (NPV)** • **Differential Pulse Voltammetry (DPV)**	Scan rate	0.1 mV/s (76.3 µV step)	100 mV/s (5 mV step)
	Pulse time	10 ms	100 mV/s (5 mV step)
• **Square Wave Voltammetry (SWV)**	Frequency	1 Hz	1250 Hz [1]
• **AC Voltammetry (ACV)**	Frequency	1 Hz	2000 Hz [1]
• **Linear Sweep Voltammetry (LSV)**	Scan rate	0.01 mV/s (76.3 µV step)	500 V/s (10 mV step)
• **Cyclic Voltammetry (CV)**	Scan rate	0.01 mV/s (76.3 µV step)	500 V/s (200 mV step)
• **Fast Cyclic Voltammetry (CV)**	Scan rate	0.4 V/s (76.3 µV step)	500 V/s (10 mV step)
	N averaged scans	2	255
	N equilibration scans	1	255
• **Pulsed Amperometric Detection (PAD)**	Interval time	50 ms	300 s
	Pulse time	1 ms	1 s
	N data points		1,000,000 (> 100 days at 10 s interval)
• **Multiple-Pulse Amperometric Detection (MPAD)**	Pulse time	100 ms	2 s
	Run time	1.2 s	100,000 s
	N potential levels	3	
• **Chronoamperometry (CA)** • **Chronopotentiometry (CP)** • **Open Circuit Potentiometry (OCP)**	Interval time	0.4 ms	300 s
	Level switching overhead time	+/-80 ms	
	N levels	1	255
	N cycles	1	20,000
	Run time	1 ms	> year
• **Fast Amperometry (FAM)**	Interval time	0.02 ms	1 s
	Run time	1 ms	30 s
	N data points	3	4000 for interval time < 0.2 ms

[1] *PSTrace provides the option to measure forward and reverse currents separately.*

PalmSens4 System Specifications

General			
▪ dc-potential range	model	PS4.F#.05 ±5 V	PS4.F#.10 ±10 V
▪ compliance voltage	±10 V		
▪ maximum current	±30 mA (typical)		
▪ max. acquisition rate	150,000 points/s		

Potentiostat (controlled potential mode)	
▪ applied dc-potential resolution	76.3 µV
▪ applied potential accuracy	≤ 0.1% ±1 mV offset
▪ current ranges	100 pA to 10 mA (9 ranges)
▪ measured current accuracy	≤ 0.1% at Full Scale Range
▪ measured current resolution	0.005% of current range (5 fA on 100 pA range) 0.0025% of 10 mA range

Galvanostat (controlled current mode)	
▪ current ranges	1 nA to 10 mA (8 ranges)
▪ applied dc-current range	±6 x applied current range
▪ applied dc-current resolution	0.0076% of applied current range (<10 mA) 0.0038% of 10 mA range
▪ measured dc-potential resolution	78 µV at ±10 V (gain 1) 7.8 µV at ±1 V (gain 10) 0.78 µV at ±0.1 V (gain 100)
▪ measured dc-potential accuracy	≤ 0.05% or ±1 mV (for |E| < ±9 V) ≤ 0.2% (for |E| ≥ ±9 V)

FRA / EIS (impedance measurements)			
▪ frequency range	model	PS4.F1.## 10 µHz to 100 kHz	PS4.F2.## 10 µHz to 1 MHz
▪ ac-amplitude range	1 mV to 0.25 V rms, or 0.7 V p-p		

GEIS (galvanostatic impedance measurements)			
▪ frequency range	model	PS4.F1.## 10 µHz to 100 kHz	PS4.F2.## 10 µHz to 100 kHz
▪ ac-amplitude range	0.001 x CR to 0.4 x CR (<10 mA) 0.001 x CR to 0.2 x CR (10 mA) (CR=current range)		

Electrometer	
▪ electrometer amplifier input	> 1 TΩ // 10 pF
▪ bandwidth	1 MHz

PalmSens4 System Specifications

Other	
▪ electrode connections	2 mm banana pins for RE, WE, CE and GND
▪ housing	aluminium body with rubber sleeve: 15.7 x 9.7 x 3.5 cm^3
▪ weight	+/- 500 g
▪ temperature range	0 °C to +50 °C
▪ power supply	USB or internal LiPo battery
▪ communication	USB and Bluetooth
▪ battery time	> 16 hours idle time > 5 hours idle time with BiPot module installed > 4 hours with cell on at max. current Extendible by means of power bank
▪ internal storage space	8 GB or +/- 800000 measurements incl. method parameters (assuming 200 data points per measurement)

Auxiliary port (D-Sub 15)	
▪ analog input	±10 V, 18-bit
▪ analog output	0-10 V, 12-bit (1 kOhm output impedance)
▪ 4 digital outputs	5 V
▪ 1 digital input	5 V
▪ i-out and E-out	raw output of current and potential E-out ±10 V (1 kOhm output impedance) i-out ±6 V (1 kOhm output impedance)
▪ power	5 V-output (max. 150 mA)

PalmSens4 EIS Contour Accuracy Plot

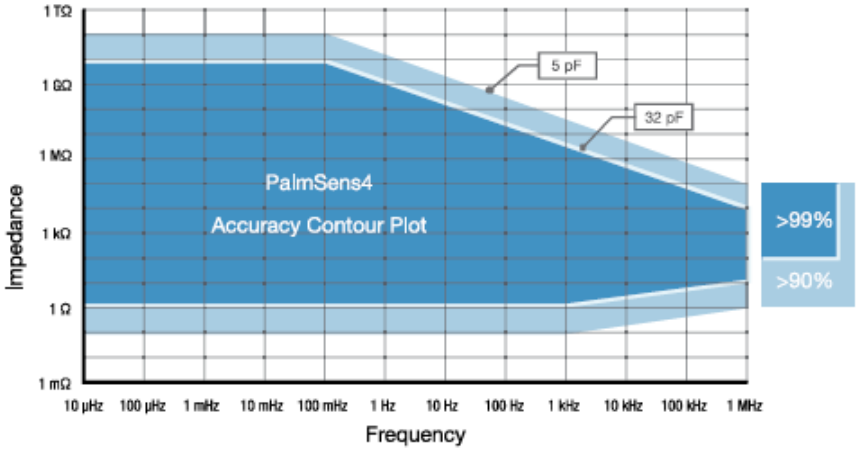

Note
The accuracy contour plot was determined under lab conditions and should be used for reference purposes. Please note that the true limits of an impedance measurement are influenced by all components in the system, e.g. cables, the environment, and the cell.

C.2 Dropsens 110D

DROPSENS

CSQ MED ISO 13485 CSQ ISO 9001:2008

Carbon Nanofibres modified Screen-Printed Carbon Electrodes

Refs. 110CNF X1110CNF

Carbon Nanofibres modified Screen-Printed Carbon Electrode
Ref. 110CNF

Carbon Nanofibres modified Dual Screen-Printed Carbon Electrode
Ref. X1110CNF

These disposable **Screen-Printed Carbon Electrodes** (SPCEs) modified with **Graphitized Carbon Nanofibres (CNFs)** are designed for the development of (bio) sensors with an enhanced electrochemical active area.

Ceramic substrate: L33 x W10 x H0.5 mm
Electric contacts: Silver

The electrochemical cell consists on:
Working electrode(s): CNF / Carbon
Auxiliary electrode: Carbon
Reference electrode: Silver

CNFs SPCEs are commercialised in 50 units packs. Store at room temperature, protected from light in a dry place.

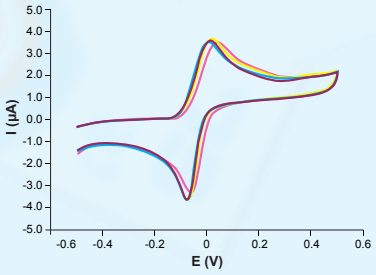

*Cyclic voltammograms of $1{\cdot}10^{-4}$ M **hydroquinone** in 0.1 M acetate buffer solution pH 5.0 at 50 mV/s. n = 5 (different CNFs SPCEs ref. DRP-110CNF) **RSD% = 4%***

Also, specific **connectors** that act as an interface between the screen-printed electrode and any potentiostat (ref. **DSC, CAC**) and other accessories are available at ***DropSens***.

Related products


110CNT


110GPH


DSC


CAC


FLWCL


STAT400

Full Catalogue

DS

Contact Form

Parque Tecnológico de Asturias - Edif. CEEI. 33428 LLanera (Asturias). Spain
(+34) 985 27 76 85 - info@dropsens.com - www.dropsens.com

Bibliography

[1] The 2016 nobel prize in physiology or medicine - press release.
Available at: https://www.nobelprize.org/prizes/medicine/2016/press-release/

[2] Uddin, M.S., Stachowiak, A., Al Mamun, A., Tzvetkov, N.T., Takeda, S., Atanasov, A.G., Bergantin, L.B., Abdel-Daim, M.M. and Stankiewicz, A.M.: Autophagy and Alzheimer's disease: From molecular mechanisms to therapeutic implications. Jan 2018.
Available at: /pmc/articles/PMC5797541/ pmc/articles/PMC5797541/ https://www.ncbi.nlm.nih.gov/pmc/articles/PMC5797541/

[3] Martinez-Lopez, N., Athonvarangkul, D. and Singh, R.: Autophagy and aging. *Advances in Experimental Medicine and Biology*, vol. 847, pp. 73–87, 2015. ISSN 22148019.
Available at: /pmc/articles/PMC4644734/ https://www.ncbi.nlm.nih.gov/pmc/articles/PMC4644

[4] Chen, H.Y. and White, E.: Role of autophagy in cancer prevention. vol. 4, no. 7, pp. 973–983, Jul 2011. ISSN 19406207.
Available at: www.aacrjournals.org

[5] Autophagy: Definition, diet, fasting, cancer, benefits, and more.
Available at: https://www.healthline.com/health/autophagy

[6] du Toit, A., Hofmeyr, J.-H.S., Gniadek, T.J. and Loos, B.: Measuring autophagosome flux. *https://doi.org/10.1080/15548627.2018.1469590*, 2018.
Available at: https://www.tandfonline.com/doi/abs/10.1080/15548627.2018.1469590

[7] Lilienbaum, A.: Relationship between the proteasomal system and autophagy. 2013.
Available at: www.ijbmb.org

[8] Levy, J.M., Towers, C.G. and Thorburn, A.: Targeting autophagy in cancer. Sep 2017.
Available at: https://www.nature.com/articles/nrc.2017.53

[9] Three Main Types of Autophagy.
Available at: https://app.biorender.com/biorender-templates/t-5ef23de52d1d8e00ae7b5e15-th

[10] Viviers, C., du Toit, A., Perold, W., Loos, B. and Hofmeyr, J.: A resistive biosensor for the detection of lc3 protein in autophagy. *IEEE Sensors Journal*, vol. PP, pp. 1–1, Feb 2020.

[11] Noda, N.N. and Fujioka, Y.: Atg1 family kinases in autophagy initiation. Aug 2015.
Available at: https://link.springer.com/article/10.1007/s00018-015-1917-z

[12] Johansen, T. and Lamark, T.: Selective autophagy mediated by autophagic adapter proteins. 2011.
Available at: /pmc/articles/PMC3060413/ /pmc/articles/PMC3060413/report=abstract https://www.ncbi.nlm.nih.gov/pmc/articles/PMC3060413/

[13] Xie, Z. and Klionsky, D.J.: Autophagosome formation: Core machinery and adaptations. vol. 9, no. 10, pp. 1102–1109, Oct 2007. ISSN 14657392.
Available at: `https://www.nature.com/articles/ncb1007-1102`

[14] Xie, Z. and Klionsky, D.J.: Autophagosome formation: Core machinery and adaptations. Oct 2007.
Available at: `https://www.nature.com/articles/ncb1007-1102`

[15] Loos, B., Du Toit, A. and Hofmeyr, J.H.S.: Defining and measuring autophagosome flux - concept and reality. vol. 10, no. 11, pp. 2087–2096, Nov 2014. ISSN 15548635.
Available at: `/pmc/articles/PMC4502790/report=abstract https://www.ncbi.nlm.nih.gov/pmc/articles/PMC4502790/`

[16] Streeter, A., Menzies, F.M. and Rubinsztein, D.C.: LC3-II tagging and western blotting for monitoring autophagic activity in mammalian cells. *Methods in Molecular Biology*, vol. 1303, pp. 161–170, 2016. ISSN 10643745.
Available at: `https://pubmed.ncbi.nlm.nih.gov/26235065/`

[17] Mauthe, M., Orhon, I., Rocchi, C., Zhou, X., Luhr, M., Hijlkema, K.J., Coppes, R.P., Engedal, N., Mari, M. and Reggiori, F.: Chloroquine inhibits autophagic flux by decreasing autophagosome-lysosome fusion. *Autophagy*, vol. 14, no. 8, pp. 1435–1455, Aug 2018. ISSN 15548635.
Available at: `/pmc/articles/PMC6103682/ /pmc/articles/PMC6103682/report=abstract https://www.ncbi.nlm.nih.gov/pmc/articles/PMC6103682/`

[18] Labbadia, J. and Morimoto, R.I.: Huntington's disease: Underlying molecular mechanisms and emerging concepts. Aug 2013.
Available at: `/pmc/articles/PMC3955166/ /pmc/articles/PMC3955166/report=abstract https://www.ncbi.nlm.nih.gov/pmc/articles/PMC3955166/`

[19] Sanderson, M.J., Smith, I., Parker, I. and Bootman, M.D.: Fluorescence microscopy. *Cold Spring Harbor Protocols*, vol. 2014, no. 10, pp. 1042–1065, Oct 2014. ISSN 15596095.
Available at: `/pmc/articles/PMC4711767/ /pmc/articles/PMC4711767/report=abstract https://www.ncbi.nlm.nih.gov/pmc/articles/PMC4711767/`

[20] Guan, W., Wang, S., Lu, C. and Tang, B.Z.: Fluorescence microscopy as an alternative to electron microscopy for microscale dispersion evaluation of organic-inorganic composites. *Nature Communications*, vol. 7, no. 1, pp. 1–7, Jun 2016. ISSN 20411723.
Available at: `www.nature.com/naturecommunications`

[21] Kumar, S. and Jana, A.: Enzyme nanoparticles (enps) based biosensors. Dec 2010.

[22] Marco, M.-P. and Barceló, D.: Chapter 22 fundamentals and applications of biosensors for environmental analysis. vol. 21, pp. 1075 – 1105, 2000. ISSN 0167-9244.
Available at: `http://www.sciencedirect.com/science/article/pii/S0167924400800281`

[23] Patel, S., Nanda, R., Sahoo, S. and Mohapatra, E.: Biosensors in health care: The milestones achieved in their development towards lab-on-chip-analysis. *Biochemistry Research International*, vol. 2016, pp. 1–12, Mar 2016.

[24] Grieshaber, D., MacKenzie, R., Vörös, J. and Reimhult, E.: Electrochemical Biosensors - Sensor Principles and Architectures. *Sensors*, vol. 8, no. 3, pp. 1400–1458, Mar 2008. ISSN 1424-8220.
Available at: `http://www.mdpi.com/1424-8220/8/3/1400`

[25] Thévenot, D., Toth, K., Durst, R. and Wilson, G.: Electrochemical biosensors: Recommended definitions and classification. *Biosensors and Bioelectronics*, vol. 16, pp. 121–131, Jan 2001.

[26] Irfan, J. and Raza, A.: Biosensors: Their fundamentals, designs, types and most recent impactful applications: A review. Jan 2017.

[27] Shukla, A.P.: Biosensors.

[28] Varzakas, T.: *Portable Biosensing of Food Toxicants and Environmental Pollutants, 2013, CRC PRESS*. Oct 2013. ISBN ISBN 9781466576322.

[29] Bhardwaj, T.: Review of biosensor technologies. *International Journal of Advanced Research in Engineering and Technology*, vol. 6, pp. 36–62, Mar 2015.

[30] Lin, P., Yan, F., Yu, J., Chan, H. and Yang, m.: The application of organic electrochemical transistors in cell-based biosensors. *Advanced materials (Deerfield Beach, Fla.)*, vol. 22, pp. 3655–60, Sep 2010.

[31] Zhang, M., Lin, P., Yang, m. and Yan, F.: Fabrication of organic electrochemical transistor arrays for biosensing. *Biochimica et biophysica acta*, vol. 1830, Sep 2012.

[32] Radhakrishnan, R., Suni, I., Bever, C. and Hammock, B.: Impedance biosensors: Applications to sustainability and remaining technical challenges. *ACS Sustainable Chemistry and Engineering*, vol. 2, pp. 1649–1655, Jun 2014.

[33] Pruna, R., Palacio, F., Baraket, A., Bausells, J., Errachid, A. and López, M.: Low-cost impedance measurements for lab-on-a-chip architectures: Towards potentiostat miniaturization. *Proceedings*, vol. 1, p. 604, Aug 2017.

[34] Pruna, R., Palacio, F., Baraket, A., Zine, N., Streklas, A., Bausells, J., Errachid, A. and López, M.: A low-cost and miniaturized potentiostat for sensing of biomolecular species such as tnf-α by electrochemical impedance spectroscopy. *Biosensors and Bioelectronics*, vol. 100, pp. 533 – 540, 2018. ISSN 0956-5663.
Available at: `http://www.sciencedirect.com/science/article/pii/S0956566317306577`

[35] Prabhakar, N. and Thakur, H.: *Electrochemical biosensors: Fabrication and applications in biodiagnostics*. Jan 2016. ISBN 978-1-84919-950-6.

[36] Wang, J.: Electrochemical biosensors: Towards point-of-care cancer diagnostics. vol. 21, pp. 1887–92, May 2006.

[37] Luppa, P., Sokoll, L. and Chan, D.: Immunosensors - principles and applications to clinical chemistry. *Clinica Chimica Acta*, vol. 314, pp. 1–26, Jan 2002.

[38] Hammond, J.L., Formisano, N., Estrela, P., Carrara, S. and Tkac, J.: Electrochemical biosensors and nanobiosensors. *Essays in Biochemistry*, vol. 60, no. 1, pp. 69–80, Jun 2016. ISSN 00711365.
Available at: `/pmc/articles/PMC4986461/report=abstract https://www.ncbi.nlm.nih.gov/pmc/articles/PMC4986461/`

[39] Lawrence, C., Tan, S. and Floresca, C.: A "green" cellulose paper based glucose amperometric biosensor. *Sensors and Actuators B Chemical*, vol. 193, pp. 536–541, Mar 2014.

[40] Yoo, E.-H. and Lee, S.-Y.: Glucose biosensors: An overview of use in clinical practice. *Sensors (Basel, Switzerland)*, vol. 10, pp. 4558–76, May 2010.

[41] Voltammetric methods - chemistry libretexts.
Available at: https://chem.libretexts.org/Under_Construction/Purgatory/Book%3A_Analytical_Chemistry_2.0_(Harvey)/11_ Electrochemical_Methods/11.4%3A_Voltamm

[42] Li, J., Chia, L., Goh, N., Tan, S. and Ge, H.: Mediated amperometric glucose sensor modified by the sol-gel method. *Sensors and Actuators B-chemical - SENSOR ACTUATOR B-CHEM*, vol. 40, pp. 135–141, May 1997.

[43] Eissa, S., Alshehri, N., Abdel Rahman, A., Dasouki, M., Abu-Salah, K. and Zourob, M.: Electrochemical immunosensors for the detection of survival motor neuron (smn) protein using different carbon nanomaterials-modified electrodes. *Biosensors and Bioelectronics*, vol. 101, Oct 2017.

[44] Chen, A. and Shah, B.: Electrochemical sensing and biosensing based on square wave voltammetry. *Anal. Methods*, vol. 5, pp. 2158–2173, Apr 2013.

[45] Li, Z. and Zhu, M.: Detection of pollutants in water bodies: electrochemical detection or photo-electrochemical detection. *Chemical Communications*, vol. 56, no. 93, pp. 14541–14552, Dec 2020. ISSN 1364548X.
Available at: https://pubs.rsc.org/en/content/articlehtml/2020/cc/d0cc05709f https://pubs.rsc.org/en/content/articlelanding/2020/cc/d0cc05709f

[46] Snir, E., Amit, E., Friedler, A. and Yitzchaik, S.: A highly sensitive square wave voltammetry based biosensor for kinase activity measurements. *Biopolymers*, vol. 104, no. 5, pp. 515–520, Sep 2015. ISSN 10970282.
Available at: https://pubmed.ncbi.nlm.nih.gov/25851749/

[47] Li, L., Zhao, H., Chen, Z., Mu, X. and Guo, L.: Aptamer biosensor for label-free square-wave voltammetry detection of angiogenin. *Biosensors and bioelectronics*, vol. 30, pp. 261–6, Dec 2011.

[48] Bollella, P. and Gorton, L.: Enzyme based amperometric biosensors. *Current Opinion in Electrochemistry*, vol. 10, pp. 157 – 173, 2018. ISSN 2451-9103.
Available at: http://www.sciencedirect.com/science/article/pii/S2451910318301005

[49] Guan, J.-G., Miao, Y.-Q. and Zhang, Q.-J.: Impedimetric biosensors. *Journal of Bioscience and Bioengineering*, vol. 97, no. 4, pp. 219–226, Jan 2004. ISSN 13891723.

[50] Electrochemical tests | electrochemical impedance spectroscopy.
Available at: https://www.gscsg.com/Electrochemical-Impedance-Spectroscopy.html

[51] Strimbu, K. and Tavel, J.A.: What are biomarkers. Nov 2010.
Available at: https://pubmed.ncbi.nlm.nih.gov/20978388/

[52] Duan, N., Wu, S., Dai, S., Gu, H., Hao, L., Ye, H. and Wang, Z.: Advances in aptasensors for the detection of food contaminants. *The Analyst*, vol. 141, May 2016.

[53] Feng, L., Chen, Y., Ren, J. and Qu, X.: A graphene functionalized electrochemical aptasensor for selective label-free detection of cancer cells. *Biomaterials*, vol. 32, pp. 2930–7, Apr 2011.

[54] Shan, W., Pan, Y., Fang, H., Guo, M., Nie, Z., Huang, Y. and Yao, S.: An aptamer-based quartz crystal microbalance biosensor for sensitive and selective detection of leukemia cells using silver-enhanced gold nanoparticle label. *Talanta*, vol. 126, pp. 130–135, Aug 2014. ISSN 00399140.

[55] Xie, Q., Tan, Y., Guo, Q., Wang, K., Yuan, B., Wan, J. and Zhao, X.: A fluorescent aptasensor for sensitive detection of human hepatocellular carcinoma smmc-7721 cells based on graphene oxide. *Anal. Methods*, vol. 6, Jul 2014.

[56] Zhang, J.J., Zheng, T.T., Cheng, F.F., Zhang, J.R. and Zhu, J.J.: Toward the early evaluation of therapeutic effects: An electrochemical platform for ultrasensitive detection of apoptotic cells. *Analytical Chemistry*, vol. 83, no. 20, pp. 7902–7909, Oct 2011. ISSN 00032700.
Available at: `https://pubmed.ncbi.nlm.nih.gov/21888423/`

[57] Saglam, Ö., KIzIlkaya, B., Uysal, H. and Dilgin, Y.: Biosensing of glucose in flow injection analysis system based on glucose oxidase-quantum dot modified pencil graphite electrode. *Talanta*, vol. 147, pp. 315–321, Jan 2016. ISSN 00399140.

[58] Devasenathipathy, R., Mani, V., Chen, S.M., Huang, S.T., Huang, T.T., Lin, C.M., Hwa, K.Y., Chen, T.Y. and Chen, B.J.: Glucose biosensor based on glucose oxidase immobilized at gold nanoparticles decorated graphene-carbon nanotubes. *Enzyme and Microbial Technology*, vol. 78, pp. 40–45, Oct 2015. ISSN 18790909.

[59] Giménez-Gómez, P., Gutiérrez-Capitán, M., Capdevila, F., Puig-Pujol, A., Fernández-Sánchez, C. and Jiménez-Jorquera, C.: Monitoring of malolactic fermentation in wine using an electrochemical bienzymatic biosensor for l-lactate with long term stability. *Analytica Chimica Acta*, vol. 905, pp. 126–133, Jan 2016. ISSN 18734324.

[60] Umar, A., Rahman, M., Mohammad (Ph.D.), V. and Hahn, Y.-B.: Ultra-sensitive cholesterol biosensor based on low-temperature grown zno nanoparticles. *Electrochemistry Communications*, vol. 11, pp. 118–121, Jan 2009.

[61] Lata, K., Dhull, V. and Hooda, V.: Fabrication and optimization of che/cho/hrp-aunps/c-mwcnts based silver electrode for determining total cholesterol in serum. *Biochemistry Research International*, vol. 2016, pp. 1–11, Jan 2016.

[62] Xie, C., Lin, P., Yan, F., Huang, P. and Hsing, I.-M.: Organic electrochemical transistor array for recording transepithelial ion transport of human airway epithelial cells. *Advanced materials (Deerfield Beach, Fla.)*, vol. 25, Dec 2013.

[63] Introducing the antibody.
Available at: `https://rockland-inc.com/antibodies.aspx`

[64] Fowler, J.M., Wong, D.K., Brian Halsall, H. and Heineman, W.R.: Recent developments in electrochemical immunoassays and immunosensors. In: *Electrochemical Sensors, Biosensors and their Biomedical Applications*, pp. 115–143. Elsevier Inc., 2008. ISBN 9780123737380.
Available at: `https://researchers.mq.edu.au/en/publications/recent-developments-in-electr`

[65] Sharma, S., Byrne, H. and O'Kennedy, R.J.: Antibodies and antibody-derived analytical biosensors. *Essays in Biochemistry*, vol. 60, no. 1, pp. 9–18, Jun 2016. ISSN 00711365.
Available at: `https://pubmed.ncbi.nlm.nih.gov/27365031/`

[66] Chemistry of Crosslinking | Thermo Fisher Scientific - ZA.
Available at: `https://www.thermofisher.com/za/en/home/life-science/protein-biology/protei`

[67] Bélanger, D. and Pinson, J.: Electrografting: A powerful method for surface modification. *Chemical Society Reviews*, vol. 40, no. 7, pp. 3995–4048, Jun 2011. ISSN 14604744.
Available at: `https://pubs.rsc.org/en/content/articlehtml/2011/cs/c0cs00149j`
`https://pubs.rsc.org/en/content/articlelanding/2011/cs/c0cs00149j`

[68] McCreery, R.L.: Advanced carbon electrode materials for molecular electrochemistry. Jul 2008.
Available at: `https://pubs.acs.org/doi/full/10.1021/cr068076m`

[69] Pinson, J. and Podvorica, F.: Attachment of organic layers to conductive or semiconductive surfaces by reduction of diazonium salts. *Chemical Society Reviews*, vol. 34, no. 5, pp. 429–439, Apr 2005. ISSN 14604744.
Available at: `https://pubmed.ncbi.nlm.nih.gov/15852155/`

[70] Chehimi, M.M., Lamouri, A., Picot, M. and Pinson, J.: Surface modification of polymers by reduction of diazonium salts: Polymethylmethacrylate as an example. *Journal of Materials Chemistry C*, vol. 2, no. 2, pp. 356–363, Jan 2014. ISSN 20507526.
Available at: `https://pubs.rsc.org/en/content/articlehtml/2014/tc/c3tc31492h` `https://pubs.rsc.org/en/content/articlelanding/2014/tc/c3tc31492h`

[71] Corgier, B.P., Marquette, C.A. and Blum, L.J.: Diazonium Protein Adducts for Graphite Electrode Microarrays Modification: Direct and Addressed Electrochemical Immobilization. *Journal of the American Chemical Society*, vol. 127, no. 51, pp. 18328–18332, Dec 2005. ISSN 0002-7863.
Available at: `https://pubs.acs.org/doi/10.1021/ja056946w`

[72] Brett, C.M.A. and Brett, A.M.O.: *Electrochemistry: principles, methods, and applications*. Oxford University Press, 1993.

[73] Salam, F., Uludag, Y. and Tothill, I.E.: Real-time and sensitive detection of Salmonella Typhimurium using an automated quartz crystal microbalance (QCM) instrument with nanoparticles amplification. *Talanta*, vol. 115, pp. 761–767, 2013. ISSN 00399140.
Available at: `https://pubmed.ncbi.nlm.nih.gov/24054660/`

[74] Sinn, S., Müller, L., Drechsel, H., Wandel, M., Northoff, H., Ziemer, G., Wendel, H.P. and Gehring, F.K.: Platelet aggregation monitoring with a newly developed quartz crystal microbalance system as an alternative to optical platelet aggregometry. *Analyst*, vol. 135, no. 11, pp. 2930–2938, 2010. ISSN 13645528.

[75] Jiang, X., Wang, R., Wang, Y., Su, X., Ying, Y., Wang, J. and Li, Y.: Evaluation of different micro/nanobeads used as amplifiers in QCM immunosensor for more sensitive detection of E. coli O157:H7. *Biosensors and Bioelectronics*, vol. 29, no. 1, pp. 23–28, Nov 2011. ISSN 09565663.
Available at: `https://pubmed.ncbi.nlm.nih.gov/21862307/`

[76] Kergoat, L., Piro, B., Berggren, M., Horowitz, G. and Pham, M.C.: Advances in organic transistor-based biosensors: From organic electrochemical transistors to electrolyte-gated organic field-effect transistors. Feb 2012.
Available at: `https://pubmed.ncbi.nlm.nih.gov/21910013/`

[77] Liao, C. and Yan, F.: Organic semiconductors in organic thin-film transistor-based chemical and biological sensors. *Polymer Reviews*, vol. 53, no. 3, pp. 352–406, Jul 2013. ISSN 15583724.

[78] Torun, Ö., Hakki Boyaci, I., Temür, E. and Tamer: Comparison of sensing strategies in SPR biosensor for rapid and sensitive enumeration of bacteria. *Biosensors and Bioelectronics*, vol. 37, no. 1, pp. 53–60, Aug 2012. ISSN 09565663.

[79] Chinowsky, T.M., Quinn, J.G., Bartholomew, D.U., Kaiser, R. and Elkind, J.L.: Performance of the Spreeta 2000 integrated surface plasmon resonance affinity sensor. *Sensors and Actuators, B: Chemical*, vol. 91, no. 1-3, pp. 266–274, Jun 2003. ISSN 09254005.

[80] Baccar, H., Mejri, M.B., Hafaiedh, I., Ktari, T., Aouni, M. and Abdelghani, A.: Surface plasmon resonance immunosensor for bacteria detection. *Talanta*, vol. 82, no. 2, pp. 810–814, Jul 2010. ISSN 00399140.
Available at: https://pubmed.ncbi.nlm.nih.gov/20602974/

[81] Damborský, P., Švitel, J. and Katrlík, J.: Optical biosensors. *Essays in Biochemistry*, vol. 60, no. 1, pp. 91–100, Jun 2016. ISSN 00711365.
Available at: /pmc/articles/PMC4986466/report=abstract https://www.ncbi.nlm.nih.gov/pmc/articles/PMC4986466/

[82] Wang, Y., Ping, J., Ye, Z., Wu, J. and Ying, Y.: Impedimetric immunosensor based on gold nanoparticles modified graphene paper for label-free detection of Escherichia coli O157: H7. *Biosensors and Bioelectronics*, vol. 49, pp. 492–498, Nov 2013. ISSN 09565663.

[83] Chiu, N.F., Fan, S.Y., Yang, C.D. and Huang, T.Y.: Carboxyl-functionalized graphene oxide composites as SPR biosensors with enhanced sensitivity for immunoaffinity detection. *Biosensors and Bioelectronics*, vol. 89, no. Pt 1, pp. 370–376, Mar 2017. ISSN 18734235.
Available at: https://pubmed.ncbi.nlm.nih.gov/27396822/

[84] Roy, S., Soin, N., Bajpai, R., Misra, D.S., McLaughlin, J.A. and Roy, S.S.: Graphene oxide for electrochemical sensing applications. *Journal of Materials Chemistry*, vol. 21, no. 38, pp. 14725–14731, Oct 2011. ISSN 13645501.
Available at: https://pubs.rsc.org/en/content/articlehtml/2011/jm/c1jm12028j https://pubs.rsc.org/en/content/articlelanding/2011/jm/c1jm12028j

[85] Evaluating the Effectiveness and Efficiency of a Graphene-Oxide Water Filtration System Young Scientists Journal.
Available at: https://ysjournal.com/evaluating-the-effectiveness-and-efficiency-of-a-grap

[86] Azadbakht, A., Abbasi, A.R., Derikvand, Z. and Karimi, Z.: Preparation of the carboxylic acid-functionalized graphene oxide/gold nanoparticles/5-amino-2-hydroxybenzoic acid as a novel electrochemical sensing platform. *Monatshefte fur Chemie*, vol. 147, no. 4, pp. 705–717, Apr 2016. ISSN 00269247.
Available at: https://link.springer.com/article/10.1007/s00706-015-1527-3

[87] Sun, W., Zhang, Y., Ju, X., Li, G., Gao, H. and Sun, Z.: Electrochemical deoxyribonucleic acid biosensor based on carboxyl functionalized graphene oxide and poly-l-lysine modified electrode for the detection of tlh gene sequence related to vibrio parahaemolyticus. *Analytica Chimica Acta*, vol. 752, pp. 39–44, Nov 2012. ISSN 00032670.

[88] Guadagno, L., Raimondo, M., Vittoria, V., Vertuccio, L., Lafdi, K., De Vivo, B., Lamberti, P., Spinelli, G. and Tucci, V.: The role of carbon nanofiber defects on the electrical and mechanical properties of CNF-based resins. *Nanotechnology*, vol. 24, no. 30, Aug 2013. ISSN 09574484.
Available at: https://pubmed.ncbi.nlm.nih.gov/23843601/

[89] Metrohm dropsens : Screen-printed electrodes.
Available at: http://www.dropsens.com/en/screen_printed_electrodes_pag.html

[90] Biosensors for monitoring autophagy | intechopen.
Available at: https://www.intechopen.com/books/biosensors-emerging-materials-and-applicat

[91] Devenish, R., Mijaljica, D., Carlos and Prescott: Biosensors for Monitoring Autophagy. In: *Biosensors - Emerging Materials and Applications*. InTech, Jul 2011.
Available at: www.intechopen.com

[92] Katayama, H., Yamamoto, A., Mizushima, N., Yoshimori, T. and Miyawaki, A.: GFP-like proteins stably accumulate in lysosomes. *Cell Structure and Function*, vol. 33, no. 1, pp. 1–12, 2008. ISSN 03867196.
Available at: `https://pubmed.ncbi.nlm.nih.gov/18256512/`

[93] Shvets, E., Fass, E. and Elazar, Z.: Utilizing flow cytometry to monitor autophagy in living mammalian cells. *Autophagy*, vol. 4, no. 5, pp. 621–628, Jul 2008. ISSN 15548635.
Available at: `https://pubmed.ncbi.nlm.nih.gov/18376137/`

[94] Kimura, S., Noda, T. and Yoshimori, T.: Dissection of the autophagosome maturation process by a novel reporter protein, tandem fluorescent-tagged LC3. *Autophagy*, vol. 3, no. 5, pp. 452–460, 2007. ISSN 15548635.
Available at: `https://pubmed.ncbi.nlm.nih.gov/17534139/`

[95] Farré, J.C., Krick, R., Subramani, S. and Thumm, M.: Turnover of organelles by autophagy in yeast. Aug 2009.
Available at: `https://pubmed.ncbi.nlm.nih.gov/19515549/`

[96] Van Der Vaart, A., Mari, M. and Reggiori, F.: A picky eater: Exploring the mechanisms of selective autophagy in Human Pathologies. Mar 2008.
Available at: `https://pubmed.ncbi.nlm.nih.gov/17988219/`

[97] Rosado, C.J., Mijaljica, D., Hatzinisiriou, I., Prescott, M. and Devenish, R.J.: Rosella: A fluorescent pH-biosensor for reporting vacuolar turnover of cytosol and organelles in yeast. *Autophagy*, vol. 4, no. 2, pp. 205–213, Feb 2008. ISSN 15548635.
Available at: `https://pubmed.ncbi.nlm.nih.gov/18094608/`

[98] Mijaljica, D., Prescott, M. and Devenish, R.J.: The intricacy of nuclear membrane dynamics during nucleophagy. *Nucleus*, vol. 1, no. 3, pp. 213–223, May 2010. ISSN 1949-1034.
Available at: `/pmc/articles/PMC3027025/report=abstract https://www.ncbi.nlm.nih.gov/pmc/articles/PMC3027025/`

[99] Nowikovsky, K., Reipert, S., Devenish, R.J. and Schweyen, R.J.: Mdm38 protein depletion causes loss of mitochondrial K+/ H+ exchange activity, osmotic swelling and mitophagy. *Cell Death and Differentiation*, vol. 14, no. 9, pp. 1647–1656, Sep 2007. ISSN 13509047.
Available at: `https://pubmed.ncbi.nlm.nih.gov/17541427/`

[100] Anoop, A.E., Mohan, N.M. and Guruvayurappan, K.: Simulation of a multi-strip blood glucometer. In: *IEEE Region 10 Annual International Conference, Proceedings/TENCON*, vol. 2015-January. Institute of Electrical and Electronics Engineers Inc., Jan 2015. ISBN 9781479940752. ISSN 21593450.

[101] Elgrishi, N., Rountree, K.J., McCarthy, B.D., Rountree, E.S., Eisenhart, T.T. and Dempsey, J.L.: A Practical Beginner's Guide to Cyclic Voltammetry. *Journal of Chemical Education*, vol. 95, no. 2, pp. 197–206, Feb 2018. ISSN 19381328.
Available at: `https://pubs.acs.org/sharingguidelines`

[102] Cyclic Voltammetry - Chemistry LibreTexts. .
Available at: `https://chem.libretexts.org/Bookshelves/Analytical_Chemistry/Supplemental_M`

[103] Allen J. Bard, L.R.F.: *Electrochemical methods : fundamentals and applications*. Wiley, 2001.

[104] Cyclic Voltammetry - Chemistry LibreTexts. .
Available at: `https://chem.libretexts.org/Bookshelves/Analytical_Chemistry/Supplemental_M`

[105] Lattach, Y.: Development and characterization of sensing layers based on molecularly imprinted conducting polymers for the electrochemical and gravimetrical detection of small organic molecules. Tech. Rep., Oct 2011.
Available at: `https://tel.archives-ouvertes.fr/tel-00699628`

[106] Dryden, M.D.M. and Wheeler, A.R.: DStat: A Versatile, Open-Source Potentiostat for Electroanalysis and Integration. *PLOS ONE*, vol. 10, no. 10, p. e0140349, Oct 2015. ISSN 1932-6203.
Available at: `https://dx.plos.org/10.1371/journal.pone.0140349`

[107] Huang, C.-Y.: Design of a Portable Potentiostat with Dual-microprocessors for Electrochemical Biosensors. *Universal Journal of Electrical and Electronic Engineering*, vol. 3, no. 6, pp. 159–164, Nov 2015. ISSN 2332-3280.

[108] Ainla, A., Mousavi, M.P., Tsaloglou, M.N., Redston, J., Bell, J.G., Fernández-Abedul, M.T. and Whitesides, G.M.: Open-Source Potentiostat for Wireless Electrochemical Detection with Smartphones. *Analytical Chemistry*, vol. 90, no. 10, pp. 6240–6246, May 2018. ISSN 15206882.
Available at: `https://pubs.acs.org/sharingguidelines`

[109] Basic overview of the working principle of a potentiostat/galvanostat (PGSTAT) electrochemical cell setup.
Available at: `https://www.metrohm.com/en/applications/AN-EC-008`

[110] Laubscher, W.A. and Perold, W.J.: Design of a soluble P-selectin biosensor for detecting platelet activation. Tech. Rep., 2019.
Available at: `https://scholar.sun.ac.za`

[111] PalmSens4 - PalmSens.
Available at: `https://www.palmsens.com/product/palmsens4/`

[112] Gamry Interface 1010 Teaching Edition Potentiostat. .
Available at: `https://www.gamry.com/potentiostats/interface-1010t-teaching-potentisotat/`

[113] PGSTAT101.
Available at: `https://www.metrohm-autolab.com/Products/Echem/CompactNonModular/PGSTAT101.`

[114] Metrohm dropsens : Potentiostats.
Available at: `http://www.dropsens.com/en/potentiostats_pag.html#stat200`

[115] DropStat Portable Electrochemical Reader.
Available at: `https://www.metrohm.com/en-za/products-overview/electrochemistry/portable-p`

[116] The Best Potentiostat First Understand Potentiostat Specifications. .
Available at: `https://www.gamry.com/application-notes/instrumentation/understanding-specs`

[117] Bezuidenhout, P., Kumar, S., Wiederoder, M., Schoeman, J., Land, K. and Joubert, T.-H.: The characterisation and design improvement of a paper-based E.coli impedimetric sensor. In: *Fourth Conference on Sensors, MEMS, and Electro-Optic Systems*, vol. 10036, p. 100360L. SPIE, Feb 2017. ISBN 9781510605138. ISSN 1996756X.

[118] LMP91000 data sheet, product information and support | TI.com.
Available at: `https://www.ti.com/product/LMP91000`

[119] Rowe, A.A., Bonham, A.J., White, R.J., Zimmer, M.P., Yadgar, R.J., Hobza, T.M., Honea, J.W., Ben-Yaacov, I. and Plaxco, K.W.: Cheapstat: An open-source, "do-it-yourself" potentiostat for analytical and educational applications. *PLoS ONE*, vol. 6, no. 9, Sep 2011. ISSN 19326203.
Available at: `https://pubmed.ncbi.nlm.nih.gov/21931613/`

[120] Eissa, S., Alshehri, N., Abdel Rahman, A., Dasouki, M., Abu-Salah, K. and Zourob, M.: Electrochemical immunosensors for the detection of survival motor neuron (smn) protein using different carbon nanomaterials-modified electrodes. *Biosensors and Bioelectronics*, vol. 101, Oct 2017.

[121] Li, L., Zhao, H., Chen, Z., Mu, X. and Guo, L.: Aptamer biosensor for label-free square-wave voltammetry detection of angiogenin. *Biosensors and bioelectronics*, vol. 30, pp. 261–6, Dec 2011.

[122] Huang, C.-Y.: Design of a portable potentiostat with dual-microprocessors for electrochemical biosensors. *Universal Journal of Electrical and Electronic Engineering*, vol. 3, pp. 159–164, Nov 2015.

[123] Diouani, M.F., Ouerghi, O., Refai, A., Belgacem, K., Tlili, C., Laouini, D. and Essafi, M.: Detection of esat-6 by a label free miniature immuno-electrochemical biosensor as a diagnostic tool for tuberculosis. *Materials Science and Engineering: C*, vol. 74, Dec 2016.

[124] Diouani, M.F., Ouerghi, O., Refai, A., Belgacem, K., Tlili, C., Laouini, D. and Essafi, M.: Detection of ESAT-6 by a label free miniature immuno-electrochemical biosensor as a diagnostic tool for tuberculosis. *Materials Science and Engineering C*, vol. 74, pp. 465–470, May 2017. ISSN 09284931.
Available at: `https://pubmed.ncbi.nlm.nih.gov/28254318/`

[125] Kinnamon, D., Muthukumar, S., Panneer Selvam, A. and Prasad, S.: Portable Chronic Alcohol Consumption Monitor in Human Sweat through Square-Wave Voltammetry. *SLAS Technology*, vol. 23, no. 2, pp. 144–153, Apr 2018. ISSN 24726311.
Available at: `https://pubmed.ncbi.nlm.nih.gov/28954578/`

[126] Ertürk, G., Hedström, M., Tümer, M.A., Denizli, A. and Mattiasson, B.: Real-time prostate-specific antigen detection with prostate-specific antigen imprinted capacitive biosensors. *Analytica Chimica Acta*, vol. 891, pp. 120–129, Sep 2015. ISSN 18734324.
Available at: `https://pubmed.ncbi.nlm.nih.gov/26388370/`

[127] Kailashiya, J., Singh, N., Singh, S.K., Agrawal, V. and Dash, D.: Graphene oxide-based biosensor for detection of platelet-derived microparticles: A potential tool for thrombus risk identification. *Biosensors and Bioelectronics*, vol. 65, pp. 274–280, Mar 2015. ISSN 18734235.
Available at: `https://pubmed.ncbi.nlm.nih.gov/25461169/`

[128] Molecular weight and isoelectric point of various immunoglobulins.
Available at: `https://www.agrisera.com/en/info/molecular-weight-and-isoelectric-point-of-`

[129] Ho, J.a.A., ju Jou, A.F., chen Wu, L. and Hsu, S.L.: Development of an immunopredictor for the evaluation of the risk of cardiovascular diseases based on the level of soluble P-selectin. *Methods*, vol. 56, no. 2, pp. 223–229, Feb 2012. ISSN 10462023.
Available at: `https://pubmed.ncbi.nlm.nih.gov/22062957/`

[130] Singh, P., Srivastava, S., Chakrabarti, P. and Singh, S.K.: Nanosilica based electrochemical biosensor: A novel approach for the detection of platelet-derived microparticles. *Sensors and Actuators, B: Chemical*, vol. 240, pp. 322–329, Mar 2017. ISSN 09254005.

[131] Shixuan, H., Zhang, W., Liu, L., Huang, Y., He, J., Xie, W., Wu, P. and Du, C.: Baseline correction for raman spectra using improved asymmetric least squares. *Analytical methods*, vol. 6, pp. 4402–4407, Mar 2014.

[132] Jakubowska, M.: Signal processing in electrochemistry. *Electroanalysis*, vol. 23, pp. 553 – 572, Feb 2011.

[133] DeFreitas, J.M., Beck, T.W. and Stock, M.S.: Comparison of methods for removing electromagnetic noise from electromyographic signals. *Physiological Measurement*, vol. 33, no. 2, pp. 147–158, Feb 2012. ISSN 09673334.
Available at: `https://pubmed.ncbi.nlm.nih.gov/22227849/`

[134] Jakubowska, M.: Signal Processing in Electrochemistry. *Electroanalysis*, vol. 23, no. 3, pp. n/a–n/a, Feb 2011. ISSN 10400397.
Available at: `http://doi.wiley.com/10.1002/elan.201000465`

[135] Rubinsztein, D.C., Cuervo, A.M., Ravikumar, B., Sarkar, S., Korolchuk, V., Kaushik, S. and Klionsky, D.J.: In search of an "autophagomometer". Jul 2009.
Available at: `https://einstein.pure.elsevier.com/en/publications/in-search-of-an-autophag`